Design and Optimization of a FSAE Vehicle

Submitted to the Faculty of Worcester Polytechnic Institute
In partial fulfilment of the requirements for this Major Qualifying Project By:

Andrew Casella, ME	Alex Deneault, ME	Patrick Donaghey, ME
Mark Lightbody, ME	Jeffrey Robinson, ME	Cote Taylor, ME

Date:
Approved By:

Professors David Planchard	and Professor John Hall

Abstract

The purpose of this MQP was to design and optimize a formula SAE race car for use in the FSAE 2018 competition based on a frame designed and built by the 2016-2017 FSAE MQP team. The major goals for this MQP were to improve in competition and to reduce the weight of the car. The car was divided into subsystems, and the 2015-2016 car was analyzed and used a starting point for design decisions and validation. The suspension and engine subsystems were studied extensively as it was determined that these systems needed the biggest redesigns. The steering subsystem also needed to be significantly modified in order to fit in the smaller frame (compared to the 2016 frame). All of the designs in the car follow the 2018 competition rules. This report will fully detail the car and explain what worked, what didn't, and how it can be improved for next year's MQP team.

Executive Summary

The major goal for this team's MQP is to design and build a Formula style race car that will compete in the 2018 Formula SAE Competition in Michigan. The 2018 WPI Team is looking to finish the competition in a better place than the 2016 WPI Team did. The 2018 team used the methods, analysis, and takeaways from the 2016 team in order to make the best car possible. The 2016 car performed very well in the 2016 competition and thus served as a model for many of this team's designs.

The car was broken into seven main subsystems by the team in order to further progress the car and divide work. The team started this project with a frame made from last year's MQP team and designed these seven subsystems around its parameters. The team designed concepts using SolidWorks, performed FEA analysis using SolidWorks simulations and ANSYS, prototyped using 3D printers, and manufactured parts with machine mills and lathes. The final product of these methods resulted in an assembled car that will be competing in the 2018 competition.

The Drivetrain was the first major subsystem that was examined. The main component in this system is the differential. The differential in a car is designed to neutralize the distance the inner and outer part of a wheel travel when turning. Differentials are hard and time consuming to make, and therefore, the team decided not to design one in house. Additionally, there are many different types of differentials for cars, so research was done to determine the best option available. After careful consideration, the team decided to purchase a limited slip differential from Drexler Automotive.

The Engine subsystem was the next subsystem that was considered. The major component of this subsystem is the intake system. Extensive research and redesign was put into this system. The intake on the 2016 car performed well, but this year's team wanted a full redesign. FEA analysis and flow simulations were performed to determine the optimal volume of the intake. After the redesign, the team prototyped the intake system and will be testing it with a manufactured metal intake. The other component in the Engine subsystem that was mainly focused on was the fuel tank and fuel system. This was also fully redesigned as a new fuel tank shape is needed due to the new frame.

The Suspension subsystem required considerable attention immediately in the design process. The suspension was also a full redesign in this year's car. The 2016 car and earlier cars were helpful for learning experiences, but the 2018 car contained a new suspension. The a-arms, shocks, and geometry were studied and designed thoroughly.

The Steering subsystem of the car was based off of the system used in the 2016 car. The steering box was redesigned but still uses the miter gears that were used before. The mounting method was also changed to a tab based design that is more compact. The Kaz Technologies steering rack that the 2016 team had originally wanted to use was selected for this car as it is now available for purchase. The tie rods and lower steering shafts were redesigned as well. The upper steering shaft was kept the same to simplify the system.

The Brake subsystem was partially based off the 2016 car and partially redesigned. For the 2018 car, the brake calipers, master cylinders, and rotors came to be the same as the 2016 car. However, the brake pedal needed a full redesign due to a smaller frame forcing the template named Percy not to fit. A new brake pedal was designed and machined, as well as the assembly for mounting it to the frame. The floorplate was also designed and manufactured as well.

The Ergonomic subsystem was not the main focus during A and B term. The firewall and headrest were both fully redesigned. All of the ergonomic components will have to be fully

redesigned due to the new frame. In C term, the seat and body panels will be manufactured as well as the impact attenuator.

The last subsystem was Shifting. This system involved multiple designs and analyses. In order for this system to be accomplished the Mechanical Engineering team and the Electrical Engineering team had to coordinate. The end result was a 6 bar design, which was validated through FEA analysis.

In C and D term the MQP team will be validating their designs through testing. The team will also offer recommendations for the continuation of this car for next year's MQP team.

Table of Contents

Table of Figures

Table of Tables

Background Research

Engine Performance Optimization

For the 2018 competition year, one major area of interest for the team has been the issue of engine performance. Little concrete data on the subject is available from the 2015 or 2016 development cycles, but anecdotal evidence suggests that these vehicles were severely limited in maximum power output, maximum achievable RPM, and the consistency of the engine's power curve. Due to the lack of data from previous competition years, it is difficult to determine which components of the engine system, if any in particular, were the main cause of the power problem. This also made it essentially impossible to set specific design goals for the powertrain of the 2018 vehicle, so efforts made this year should be considered as a baseline for later work.

In lieu of attempting to fully characterize the performance of existing hardware from previous years, the 2018 team has decided to direct its efforts toward observing and addressing possible avenues for optimization purely with regard to the current powertrain. Due to the relatively short time available to develop a powertrain from engine up, and the limited manpower the six-person team could devote to the task, the 2018 team relied heavily on conclusions drawn from scholarly research, other FSAE teams, and industry design trends. Although rationale was provided for all design decisions through calculation or simulation, many early design decisions were made on the basis of such generalizations with the intent to narrow the scope of work to a degree manageable within the given schedule limitations.

This report section describes the design trends and possible strategies considered for the design and optimization of the powertrain. Due to an aforementioned reliance on high-level approximations, this section also includes information about some conceptual design choices. The main areas of interest identified for engine optimization were identified as: engine modification, exhaust resonance tuning, forced-air induction, and air intake design. Of these topics, air intake design received by far the greatest degree of effort and attention at the design stage, for reasons which will be addressed later.

Before discussing these areas of interest independently, it is important to note the importance of one key information source to all engine optimization efforts pursued by the 2018 WPI team. This source is a report by the Formula SAE team at California Polytechnic State University specifically regarding the optimization of their engine system for their 2010 vehicle (Ales, Mendoza, Thomas, & Vinokurov; 2010). The work discussed in this report concerns the same engine used in the 2018 WPI vehicle, albeit an earlier version, and their report thus provided much valuable information, particularly about the effects of certain modifications to this engine that would have otherwise been a complete mystery.

Engine Modification

The engine used for the 2018 WPI FSAE vehicle is a single-cylinder, 449cc displacement, four-stroke model from a 2015 Yamaha WR450F. Full specifications for this engine and its integral transmission are listed starting on page 53 (2-2) of the 2015 Yamaha WR450F Owner's Manual, which is available for free on the Yamaha website. This engine was chosen by the 2017 team largely due to its similarity to the Yamaha YFZ450R, which was used by the 2015 and 2016 WPI teams, and also due to its low cost and high performance potential. Both engines were chosen due to their high power to weight ratio despite having less power than other engines commonly used in competition. The reasoning for this was that higher powered cars could only rarely be used to their full potential in most FSAE competition events, and the greater weight implicit in a more powerful engine hindered cornering ability.

Commented [1]: citation/link

When initially discussing the powertrain, a popular potential topic of optimization was the subject of engine modification. Within the general category of modification, the team was specifically interested in the possibility of installing an aftermarket piston and camshafts into the engine. Although modifying the engine was a somewhat risky strategy due to the possibility of critically damaging the engine, the idea of installing components designed by other manufacturers was highly appealing. If it were possible to simply purchase improvements to the performance of the WR450F, even prior to discussing the design of the intake or exhaust, the time saved and performance gained would be well worth the extra expense. Brief research yielded information about the exact modifications intended to be installed, with additional information on the projected effects available from the Cal Poly report.

Figure 1: Hot Cams Intake and Exhaust Camshafts for WR450F (Hot Cams, Inc.)

The first method of modification discussed was the installation of Hot Cams, Inc. aftermarket intake and-or exhaust camshafts. According to the Cal Poly engine report and the Hot Cams website, the aftermarket camshafts would increase the duration for which the valves are open during both intake and exhaust events by 19 and 15 degrees at the crankshaft, respectively, with corresponding increases in total valve lift of 0.09" and 0.08". Hot Cams claims only vaguely that

these cams will improve mid- and top-end performance, and the Cal Poly report does not make many claims about the effect these cams had on their engine. As camshaft lift, profiles, and timing are possibly the most direct way to alter the performance of an engine, it was disappointing to find such a lack of information about a potentially crucial modification. Similarly, when the team looked into increasing the compression ratio of the WR450F with an aftermarket piston, or boring the cylinder for a larger piston, a lack of information on the expected results dampened interest.

Figure 2: High Compression Ratio Piston for WR450F (Vertex Pistons, Inc.)

According to research into high compression pistons, the most common ratios after the stock 12.3:1 seemed to be 12.8:1 and 13.5:1. The Cal Poly report includes useful information about the aftermarket piston used in their engine, which provided a 13.5:1 compression ratio, including engine test data from before and after modifying their engine. When the Cal Poly team installed the aftermarket cams and piston along with their custom intake and exhaust designs, a significant performance increase was observed over baseline results. Their engine saw increases from four to six horsepower, from 6500 to 9000 RPM, and torque by 1-2 foot pounds over the same range. However, their test data also showed that this improvement was almost entirely produced by their intake and exhaust, with negligible gains of less than 1 percent after the engine modifications were installed. Whether this was due to destructive interference between the effects of the aftermarket piston and camshafts, or simply the magnitude of power gains to be expected from these parts is left unclear.

With each camshaft costing $200, and the piston another $200, the total cost of modifying the engine would be well over $600 when accounting for shipping costs and other relevant purchases. This is a steep price for modifications when also considering the time and effort inherent in installing the parts. When the potential risks of modifying the engine are also taken into account the situation becomes even worse. The aftermarket piston and crankshafts greatly increase the probability of valve "crashes," auto ignition ("knocking"), heat damage, and other miscellaneous problems made possible by interfering with the internals of the engine. Considering on top of these detriments the less than 1 percent improvements observed by the Cal Poly team for these modifications, it became clear that modifying the WR450F would not be a worthwhile use of time. The team concluded that Yamaha had done a good enough job optimizing the WR450F engine for maximum performance, and that time should be spent instead on intake and exhaust tuning.

Air Intake

The engine air intake is generally considered to be a highly important component of any engine system when investigating potential avenues for performance improvement. In aftermarket car modification and powertrain development the intake is a frequent focus of optimization efforts as a cost effective alternative to engine modification. The air intake was selected as the primary subject of engine optimization efforts for two main reasons: the FSAE mandatory air restrictor, and the feasible degree of control over its design relative to the exhaust or engine itself. In order to determine the best methodology and design concepts for the intake, a significant amount of time was dedicated to researching the fundamental concepts that define the performance of certain components, and to see if optimization could be easily defined by formulas, ratios, or specific values.

Restricted Air Intake Theory of Operation

According to FSAE rules[RJB3] , all gasoline-powered vehicles must restrict airflow to the engine to a 20 mm diameter orifice at some point between the throttle body and cylinder, as shown in Figure 3 below. The restrictor is a key component of the intake system, and as its name suggests, it has the potential to heavily influence the performance and behavior of the engine if not carefully accounted for in the design of the intake.

Commented [2]: fix citation

Commented [3]: update

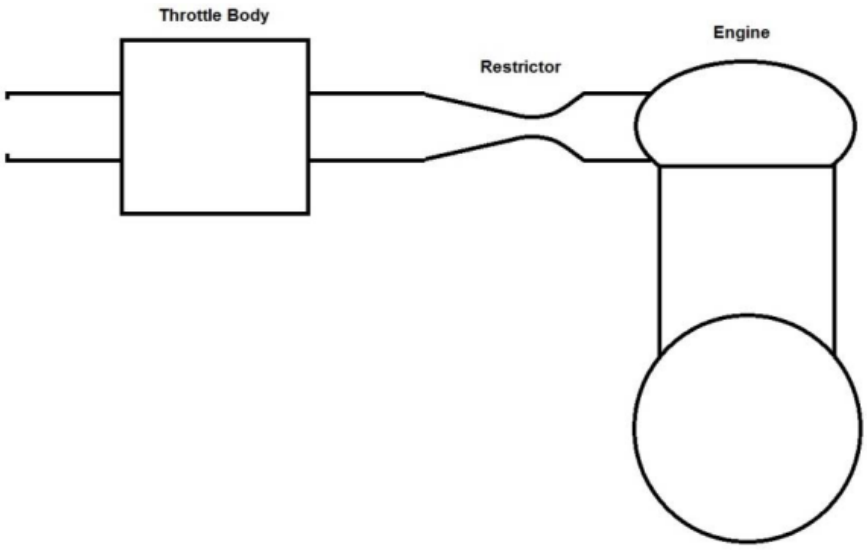

Figure 3: Intake Restrictor Location Defined by FSAE Rules

The FSAE rules state that this restriction is specifically intended to limit the maximum power output of engines in FSAE vehicles. Therefore, this is one aspect of the vehicle that demands priority over other components surrounding the engine during the design process. This is especially

important as, unlike the four-cylinder engines many other FSAE competition vehicles use, single cylinder engines like the WR450F are particularly vulnerable to the handicapping effects of the restrictor. To explain why, a description of some fundamental concepts governing the function of a restricted air intake follow is given.

Due to the cyclical nature of the internal combustion engine, the airflow through the intake of an engine will never be entirely constant, but will pulse whenever the engine is in an "intake stroke" and its intake valves are opened. In a four-stroke engine, the intake valves of each cylinder will open for roughly half of one crank rotation, every other crank rotation, during the intake stroke[RJB4] of the piston. For a single-cylinder engine, this means that in a single combustion cycle of two full crank rotations, the intake valves will only be open for roughly one quarter of the cycle. In a four-cylinder engine, in which the firing of each cylinder is staggered, at least one cylinder will thus always be in its intake stroke at any given point in the combustion cycle. This means that, for single- and four-cylinder engines of the same displacement, the flow of air through the intake is drastically different. While the single-cylinder engine must ingest its full displacement of air within only one quarter of its combustion cycle, the four-cylinder engine distributes its air ingestion relatively evenly, resulting in reduced intensity of intake pulses. The implications of this airflow distribution are significant, as the single cylinder engine is more sensitive to momentary intake airflow disturbances due to its brief intake stroke, and yet simultaneously produces more intense airflow pulses that place greater efficiency demands on the intake manifold. The intensity of airflow pulses during intake is an issue primarily due to the behavior of air itself, and derives from the functionality of the restrictor.

Commented [4]: fix citation

While the air restrictor is frequently discussed at an abstract level, the reason for its restriction is seldom described fully, and requires a brief overview of the concept of choked flow for an ideal gas. In ducted airflow, as in an intake restrictor, choked flow occurs where the cross-sectional area of the duct is at a minimum, and the velocity of air in the duct reaches the speed of sound at the "choke point," or "throat" – the sonic condition. In addition to the occurrence of the sonic condition at the duct throat, choked flow also implies, by its very name, that the mass flow rate of air through the choke point is at a maximum, i.e. that the maximum possible airflow through the duct occurs under choked flow conditions. The choked condition is initiated primarily by a pressure difference between the upstream and downstream areas of the duct around the throat, where a ratio of 0.528 is the highest at which the flow will be choked, and a ratio of 1 translates to a flow velocity of zero. One key purpose of restrictor optimization is thus to minimize pressure drop across the choke point.

The speed of sound in a gas is variable according to temperature, and is specified by the formula[RJB1] a=sqrt(k*R*T), where k is the specific heat ratio, R is the specific gas constant, and T is the temperature of the gas. For air these values are typically k=1.4, R=286 J/kg-K, and T=298 K at room temperature. The mass flow rate of an ideal gas through a frictionless nozzle at the choked condition is governed by the formula:

$$\dot{m} = \frac{APk}{\sqrt{kRT}}\sqrt{\left(\frac{2}{k+1}\right)^{\frac{k+1}{k-1}}}$$

where A is the cross-sectional area of the choke point, P is the pressure of the gas at ambient conditions upstream of the choke point, and the other variables are the same as applied above. If standard conditions are assumed, such as a sea-level atmospheric pressure of P=101325 Pa, k=1.4, and R=286 J/kg-K, this formula can be simplified for application to the restrictor:

$$\dot{m} = 3222.135 * \frac{D^2}{\sqrt{T}}$$

where D is the diameter of the restrictor in meters, and T is the ambient air temperature in Kelvin. For a restrictor of 20 mm diameter, 0.02 m, as specified in the FSAE rules, and room-temperature air, the ideal maximum mass flow rate of air through the restrictor is approximately 0.075 kg/s. Taking into account that this is an optimistic estimate, a comparison with the airflow rate the restrictor will be required to deliver is now in order.

For a single-cylinder engine, the flow rate of air demanded can be assumed to be equivalent to the displacement of the cylinder, 449 cc or 0.000449 m^3, at a rate of RPM/120 cycles per second when the four-stroke cycle is taken into account. With a standard air density of ϱ=P/RT=1.19 kg/m^3, this works out to an average of approximately 0.051 kg/s at the 11,500 RPM redline of the WR450F. Since this average mass flow rate is only 68 percent of the choked mass flow rate for the mandatory 20 mm restrictor diameter, choked flow should not occur, and the engine should behave exactly the same with the restrictor as it had without. In fact, according to this idealized formula, a 20 mm restrictor should be sufficient to support even a 750 cc engine operating at 12000 RPM, or a 1.5 L engine at 6000 RPM. However, this simplified model ignores all non-idealities of friction, turbulence, and variable flow rate in the restrictor, which combine to limit performance in practice. The latter is of particular concern here, and the pulsating flow produced by a single-cylinder engine is the primary cause for much of the difficulty of designing single-cylinder restricted air intakes.

If the airflow demanded by the engine is recalculated, taking into account the intake valve open duration, the difficulty of designing an intake for the engine becomes clear. Assuming that the intake valve is open for exactly one quarter of each four-stroke cycle, the duration of the intake stroke is 30/RPM seconds. If an air volume equivalent to the entire engine displacement is transferred into the cylinder within this time, for a volumetric efficiency of 100 percent, the average mass flow rate at redline now becomes approximately 0.205 kg/s while the intake valve is open, or 273 percent of the maximum possible mass flow rate through the restrictor. While neither the average flow scenario above, nor this worst-case scenario would be observed in practice, their contrast clarifies the rationale behind some higher-level aspects of intake design and drivetrain choice.

Returning to the earlier discussion of cylinder count, it is clear now why the four-cylinder engine has an inherent, although slightly counterintuitive advantage over the single-cylinder engine in restricted applications. An intake supplying a four-cylinder engine will experience a flow pattern similar to the averaged flow scenario, in which flow through the restrictor is induced at lower intensity and higher frequency, in turn allowing for larger engine displacements without running into the physical limitations of the restrictor. Along with the performance advantages of four-cylinder engines over single-cylinder, even at sub-one-liter displacements, this is likely a contributing factor in why some highly successful FSAE teams have been observed to use engines such as the four-

cylinder Honda CBR600. In the specific context of simplifying intake design, the team recommends that future WPI FSAE teams consider the possibility of using an engine with multiple cylinders to simplify intake design. Additionally, this issue of flow rate distribution provides the rationale for a characteristic component of most single-cylinder air intakes – the plenum.

The plenum is a component common to all vehicle air intake systems, and is key to reducing the effect of any intake restrictions on engine performance. The purpose of the plenum in ordinary cars is largely to allow for even distribution of intake air between all cylinders, and to reduce effects of turbulence and restriction caused by intake filters and tubing runs. [RJB9] As applied to a single-cylinder engine with a restrictor, the plenum instead functions mainly as an "air capacitor," a reservoir of unrestricted air for the engine to draw from during its intake stroke. During intake events the plenum provides a cushioning effect to flow at the engine and restrictor, simultaneously allowing for increased volumetric efficiency over a direct restrictor-engine system and allowing for more evenly distributed flow through the restrictor. This is due to the intermittent nature of the intake events for the single-cylinder engine, as each intake event drains the air from the plenum, and during the three-quarters of the combustion cycle during which the intake valves are closed, the plenum can refill through the restrictor. Considering its theory of operation, the ideal plenum volume is infinite, to infinitely smooth the flow through the restrictor, but in practice this is unfeasible both due to size constraints and the delayed throttle response produced by a vastly oversized plenum. The focus of intake design effort by the 2018 team was thus set on the optimization of the shape and volume of the plenum to best reduce the detrimental effects of the restrictor while balancing the similarly important concerns of packaging and throttle response.

Commented [5]: fix citation

Subdivision of Design and Concept Refinement

The design of the intake was started from scratch due to the lack of information from the WPI 2016 FSAE team. Discussion with team members involved with the intake for the 2016 vehicle revealed that there was indeed little validation done for the intake design. Due to a lack of publicly available information on intake manifold optimization for single cylinder engines with restrictors, previous applications had been designed partially according to vague and often conflicting rules of thumb. Although research articles and publicly available FSAE reports regarding intake design as a whole revealed some [RJB10] relevant papers, none addressed the specific situation aside from the Cal Poly FSAE report mentioned earlier. Most of these articles concerned four-cylinder engines, specific experimental design concepts, or efficiency rather than performance, with no discernable agreement as to the ideal end-to-end configuration of a single-cylinder restricted intake. Given the simultaneous abundance of forum posts by FSAE teams from other universities regarding intake design, initial concerns that the intake would be a complicated ordeal were confirmed. To make the design process more manageable, and to determine if scholarly research agreed on optimizations for individual components, the team broke the intake system into subsections, including the bellmouth, the restrictor, the plenum, and the runner. The bellmouth, sometimes referred to as a "velocity stack," is the first component of the intake system to interact with the air stream, and is intended to direct the airflow to the throttle as smoothly as possible. After the throttle, the restrictor is the next component of the intake system, followed by the plenum. The runner is the last component of the

Commented [6]: fix citation

intake before the cylinder head, and includes the fuel injector port. Figure XX below clarifies the positions and appearances of these components on the current 2018 intake prototype. The 2016 WPI team gave information on the restrictor and bellmouth, which served as a model for this year's design. The subsections are as follows: A is the Bellmouth, B is the Throttle Body, C is the Restrictor, D is the Plenum, E is the Runner, F is the Fuel Injector Mount, and G is the Engine Integral Runner Extension.

Commented [7]: update

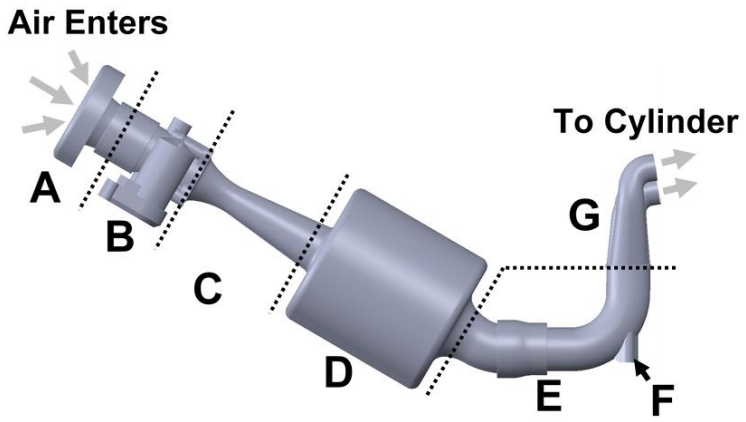

Figure 4: Subsections of Intake System

A 2006 article in Race Engine Technology Magazine describes the benefits of the bellmouth profile over a plain tube end, and the advantages of specific profiles over a simple radius. This article states that the primary benefit of a bellmouth is the elimination of turbulence and contraction caused by a sharp pipe end, a concept illustrated by Figure 5. The ideal design was specified as a series of dimensions relative to the diameter of the inlet to which the bellmouth is fitted, with an entrance area 2.13 times the inlet diameter, an axial length equal to the diameter of the inlet, a radius of 0.08 times the inlet diameter outside the entrance area, and an elliptical profile connecting the two.

Commented [8]: cite

Commented [9]: update

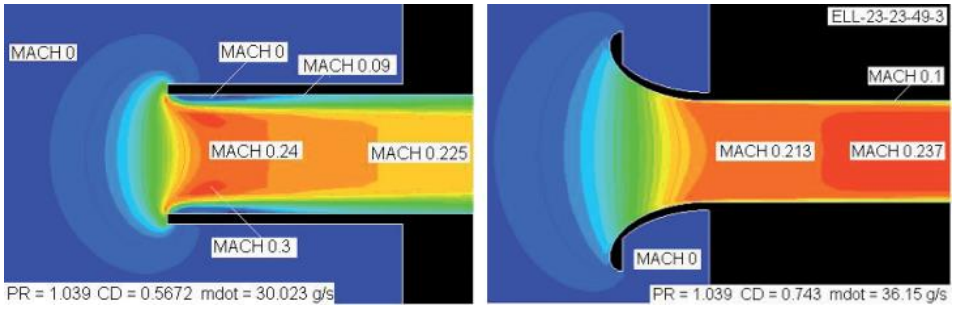

Figure 5: Airflow Entering Plain Pipe and Elliptical Bellmouth (Blair & Cahoon, 2006)

Although the article also stated that this optimized profile only has a small advantage over a simple radius in terms of discharge coefficient, the team chose to adhere to the optimal profile as one of the only optimizations that could be made with relative certainty.

For the restrictor, the article consulted compared several combinations of converging and diverging angles for some common restrictor profiles, providing pressure drop measurements between entrance and exit for each. As discussed in the theory section of this report, the pressure drop across the restrictor is possibly its most important characteristic. The promotion of minimal pressure drop delays the initiation of choked flow, and therefore the choking of the engine's air supply. According to the simulation-based study described in the report, the ideal combination of was a "De Laval" nozzle profile, an entrance angle of 16 degrees, and an exit angle of 4 degrees. The De Laval nozzle profile, when viewed as a cross section, involves a convex entrance ramp of constant radius ending tangent to a straight exit ramp, as shown in Figure 6 below.

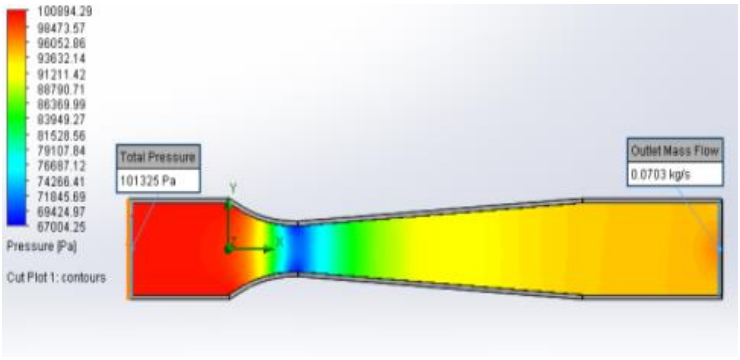

Figure 6: Pressure in 16°/4° "De Laval" Restrictor (Deshpande & Narappanawar, 2015)

The angles specified for the entrance and exit are specified with respect to the axis of the nozzle. Therefore they represent the 'half-angle' of the converging and diverging sections of the nozzle rather than the included angle. Using SolidWorks Flow Simulation and the test conditions detailed in the report, the restrictor profile was proved optimal within a reasonable degree of certainty.

In researching the runner as well, a study characterizing the effects of runner design features on intake performance in addition to the Cal Poly report referenced earlier, assisted the design decisions made. In a[RJB12] report by researchers at The Ohio State University (OSU) sponsored by Ford, various runner lengths and diameters, in combination with tapered and bellmouth runner entrance profiles, were compared through simulation and physical testing with a single cylinder and a similar 500 cc engine. This report provides a thorough overview of ideal runner design strategies, presenting specific results and conclusions about the advantages runner resonance tuning can provide, as well as the strategies required to reap these benefits.

Some important conclusions of this OSU report can be summarized by observing the magnitude and nature of power improvements produced by a selection of the designs tested. The highest efficiency runner tested in this study was made with a tapered inlet. The test engine gained

Commented [10]: cite

Commented [11]: fix citation

5.95 percent in peak power at an offset of -250 RPM from the baseline peak, with a peak volumetric efficiency increase of 3.59 percent at an offset of 625 RPM over baseline, or -125 RPM from the new peak power. These results may seem impressive at first glance, and in terms of peak power and efficiency figures they are. However, when the result data in the report is reviewed with consistency and a smoothed torque curve in mind, even the "best" runner in terms of peak figures has little to claim.

Despite the slight increases in peak power many produced, none of the runners tested by the OSU report had significant positive effects on the volumetric efficiency or power curves of the engine overall. It mainly redistributed local peaks and dips while maintaining overall trends, or in some cases worsened local dips. Although this seems to be a negative result, it did give some relief. Out of runner lengths varying from 6 cm to nearly 30 cm, none had a drastic effect on the performance of the test engine overall. While some designs caused restrictions to flow due to small entry radii or unfortunate resonances, these results were similarly small in scale to the increases reported for the "best" runners. These results showed overall that runner design is a non-critical aspect of intake design, and given an unrestricted flow path between the plenum and engine, the runner has almost no effect on performance at all. Similar results were recorded by the Cal Poly engine team in their report, although their data is more irregular and less detailed.

In addition to the relatively small increases in power provided by properly tuned runners, the complexity of ensuring proper resonance makes the intake runner a frustrating component of the intake system to optimize. The intake runner would also have packaging concerns such as avoiding conflicts with the frame members, rule-mandated exclusion zones, and the nearby exhaust. When considering all of this, the small and debatably relevant benefits of a properly designed intake runner become minimal. While it would be ideal to optimize the runner along with the rest of the intake, the optimization can be ignored in order to direct focus more productively to other components of the intake.

When researching the plenum, the conclusions made by research reports aligned with the theory on the point that increasing plenum volume resulted in increased performance. In a report specifically studying plenum volume by professors at the US Naval Academy, eight plenum volumes from two to ten times the displacement of the engine were tested with a four cylinder, 600 cc engine using a 20mm diameter intake restrictor. This study concluded that plenum volume positively correlated with power and torque, with power increasing by 17 percent from the smallest to largest plenum tested, and torque increasing by 31 percent. This report also concluded that plenum volume had only negligible effects on throttle response time up to a volume of 10 times engine displacement. This alleviated concerns from the team about this aspect of plenum design. Again, the Cal Poly report provided a similar result with lower fidelity, showing that the larger of two plenum volumes they tested produced greater power and torque throughout the speed range tested. As no ideal plenum volume was identified in either case, this research into plenum design did little to advance the team's design process, but did illustrate the degree of influence intake design can have on performance.

Commented [12]: citation

Forced Air Induction

In addition to the previously mentioned options, the possibility of including a turbocharger in the intake system to circumvent some of the challenges posed by a restricted intake was also considered. In 2015, the MQP tasked with creating the initial design of the 2016 FSAE car proposed the integration of a Honeywell MGT12 turbocharger system into the final design of the car (Moser, 2015). However, due to time constraints during the car's assembly, the system design was never completed or implemented.

In addition to the previously proposed turbocharger concept, supercharging or running ethanol fuel were also considered. In order to compare these three methods, design requirements were weighted with multiplication values between 1 and 10 by their level of importance, with 10 being the most important. Reliability and availability of parts were rated highest, as a large amount of points can be lost during any FSAE competition if a system breaks regularly or parts to repair the system are difficult to obtain. Power increase was weighed next, as the implemented system must produce nearly double the power of the current setup in order to be at a similar power level of other FSAE cars. This was followed by cost and complexity, as a large amount of points can be lost during competition due to high car production costs, and because a complex system would be less likely to be implemented due to time constraints when building the car. Efficiency and use of off the shelf parts were rated last, as the 2016 car is currently already highly efficient, and because WPI's FSAE Team has the skills and resources to manufacture any custom parts that would be needed. In order for the different designs to be directly compared a design matrix was created to weigh different methods (see Table 1). Each part was given a score from 1 to 10 for each design criteria, and this was multiplied with the weight of each design requirement. From this, it was determined that a turbocharger system aligned best with the design criteria due to its low cost from sponsorships, availability of parts, and ability to increase power.

Commented [13]: cited differently than [RBJ]

Commented [14]: RBJ is just the way word copied my citations in. they all need to be fixed to APA style or something

Commented [15]: edit number if table number below changes

Table 1: Design Matrix for Forced Induction

Design Criteria	Weight	Turbocharger	Supercharger	E85
Cost	7	7	3	8
Power Increase	8	8	6	4
Complexity	7	5	6	9
Reliability	9	7	7	9
Use of off the shelf parts	5	7	7	9
Efficiency	6	7	5	8

Availability	9	8	4	3
Score	**-**	**360**	**275**	**352**

Due to the WR450F's high compression ratio, the engine would most likely not be able to handle more than 10 psi of boost without a high risk of engine failure or pre-detonation. In addition, it was identified that if the boost pressure remained under 7psi, the implementation of an intercooler was not needed (Miller, 2008). As per FSAE rules, any intercooler must be placed between the throttle and the engine (see Figure 7), which increases throttle delay (FSAE Rules, 2017).

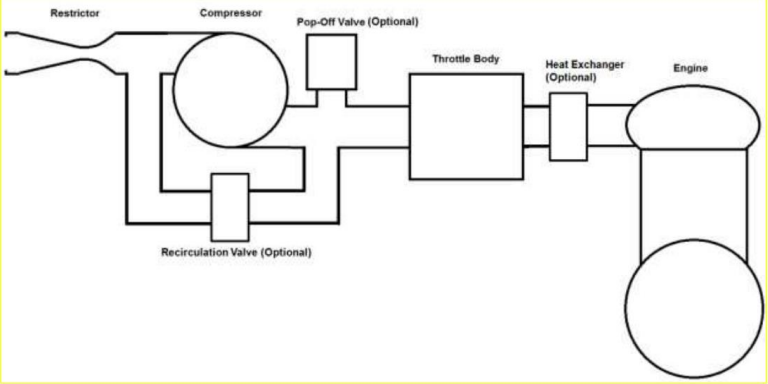

Figure 7: Required placement for intake components for Turbocharged FSAE Cars

After weighing all factors it was decided that if a turbocharger system was implemented, it should be designed around running 7 psi of boost without the use of an intercooler. In addition, an engine RPM of 8000 was chosen for optimization calculations as this was the mean RPM value of the desired powerband. For this part of the project, the volumetric efficiency of the engine was estimated to be around 90%, a reasonably conservative number for most engines. Once these values were determined, the airflow and pressure ratio were found using EQ1 and EQ2, shown below. These values were then used to compare the compressor graphs of different turbochargers to determine which ones would be best matched to the engine. The proposed MGT12 turbocharger was compared with a Garrett GT1241 turbocharger; both compressor graphs can be seen in Figures 8 and 9. Comparing these compressor graphs helped to determine if the MGT12 turbocharger recommended by the 2015 MQP was an ideal size for this application. It was found that the MGT12 turbocharger was slightly too large for this application, and that the GT1241, as well as other turbochargers, were slightly better suited. However, it was ultimately decided that for an initial design, the MGT12 turbocharger should be used as the team has two currently available.

EQ 1) Airflow=Displacement*Target RPM*VE*2.199*10^{-6}

EQ 2) Pressure Ratio=(Boost Pressure)/(Atmospheric pressure)

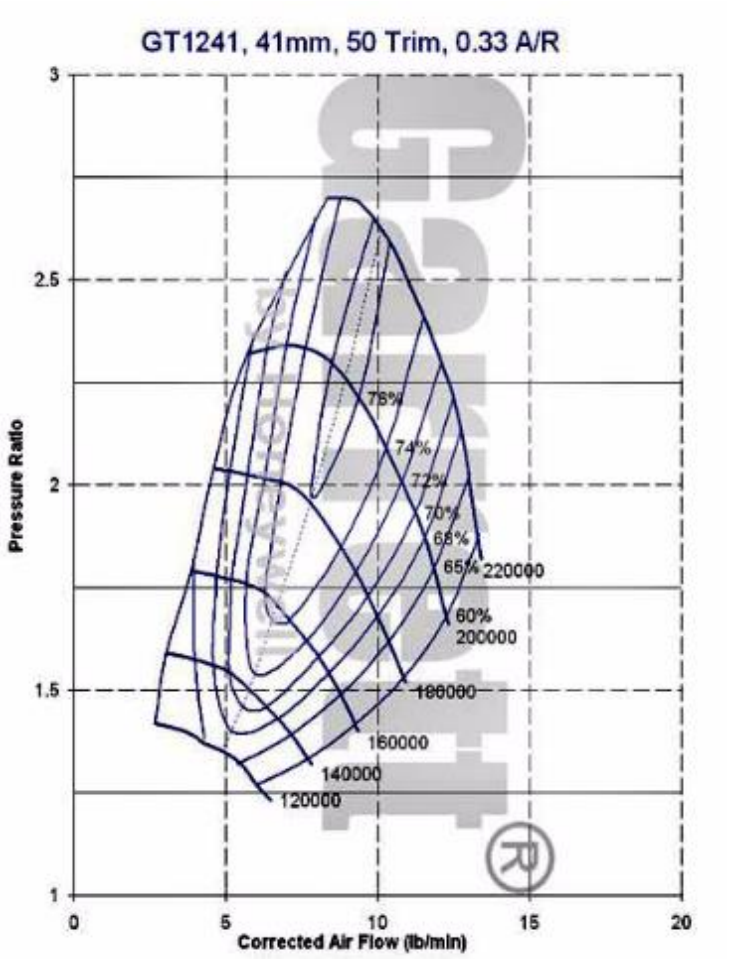

Figure 8: Compressor graph of Garrett GT1241 turbocharger

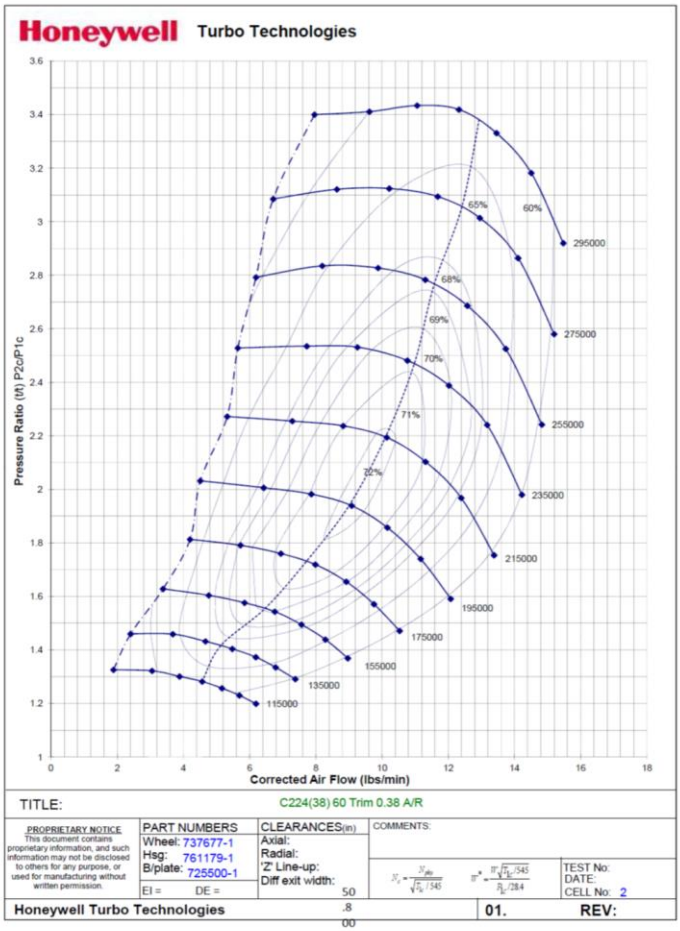

Figure 9: Compressor Graph of Honeywell MGT12 turbocharger

While this report covers some of the basic justifications and calculations for implementation of a turbocharger system, more detailed designs, including suggested turbo placement can be found in a past ISP report (on the SAE Google drive in folder titled: "SAE ISP 4430 (Turbocharger system design)").

Design Software

During research on intake design, the team found engine simulation software products, most prominently the Ricardo family of software, which promise to simplify and demystify intake and exhaust tuning, as well as engine tuning itself. These software packages were mentioned throughout the Cal Poly design report and in several others, as a reliable source of information and validation for often complex designs. The reason the 2018 team did not attempt to gain sponsorship from Ricardo, ANSYS, or others for CFD tools or engine-specific software is primarily due to the complexity of these software products and a lack of time. Due to the compressed timeline imposed by the scheduling of the FSAE MQP, the team did not have the man-hours to spend on learning an entire new software suite. Ricardo offers FSAE team sponsorships, including free software licenses, and the 2018 team insists that future WPI teams attempt to gain sponsorship from this company to hopefully streamline, or at least better inform design decisions.

Methods

This section aims to explain the design phase in detail and what methods were used to determine the current designs of all subsystems. The subsystems defined by the 2018 team include: drivetrain, engine system, suspension, steering, brakes, ergonomics, and shifting. The organization of this section aligns with the relevance of these subsystems to one another. Each subsection explains design choices, design validation methods, manufacturing strategies, and recommendations for future work regarding a single subsystem or component.

Drivetrain

Differential Selection

After the 2015 Yamaha WR450F engine was selected the next step was to decide how best to transfer the torque to the ground. The selected engine is equipped with a five speed internal gearbox and a sprocket intended for a chain drive to the rear wheel, as implemented in the OEM vehicle. Effective torque and top speed is changed by changing the final drive ratio between the engine sprocket and the sprocket attached to the rear tire. It was decided that a similar setup will be used with one large difference, the addition of a limited slip differential. The addition of a differential is the most effective way to get the power to the ground, and make the best use of both rear tires. A limited slip differential is a mechanical device that allows the two output shafts, one to each wheel, to turn at different speeds. This is needed because during high lateral acceleration turns, the inside wheel may not have the frictional force needed to transfer all the torque to the ground and accelerate the vehicle. Because of this the use of a traditional differential may cause the wheel to loose traction and spin, which would slow lap times considerably. A limited slip differential limits the difference in wheel speed between the two output shafts causing a large majority of the torque to go to the outside wheel, which has considerable more traction.

The selection of a limited slip differential was not taken lightly as an incorrect selection could have a large impact on performance. Three differentials were chosen to look at. The first was an atv differential made by Can-AM and used in many of their newer vehicles. This was most like the differential used in the 2016 formula car, so the team was already familiar with its benefits and shortcomings. The most appealing characteristic of this was the price and availability. It is a widely used part and there is a lot documentation online about them. However, because this product is a shaft driven final drive, a custom case would have to be machined, which is no small task. If this option were chosen, the axel would also have to be cut and welded to the needed length. The next option was a torsen type LSD made by Taylor Race Engineering specifically for use in a formula SAE vehicle. This option was considerably more expensive but offered more benefits. This differential is slightly adjustable by changing out internal components which allows for better tuning of the vehicle. Another benefit to this differential is the availability of drive shaft components. Taylor Race sells everything for the drive shafts individually allowing an individual to pick and choose as it wants. Also, judging from positive feedback online, both customer service and the lead time on the product are excellent. The last differential that was looked into was made by Drexler Automotive, a German engineering company that has a great reputation in the racing world. This differential is a clutch pack LSD, that offers adjustable lockup with the turn of a bolt and is by far the lightest option. Drexler also offers custom length drive shafts and will ship everything ready to be dropped into the mounts. The down side to this option would be the cost and lead time. It costs around $5,700 and has a lead time of 12 weeks. This differential is completely rebuildable and could be used in many cars to come.

Table 2: Weighted design matrix for differential selection

		ATV front Differential		**Taylor FSAE Differential**		**Drexler Differential**	
	Weight	**Score**	**Total**	**Score**	**Total**	**Score**	**Total**
Cost	5	9	45	4	20	2	10
Adjustability	8	2	16	5	40	10	80
Weight	7	4	28	8	56	8	56
Ease of implementation	8	1	8	5	40	8	64
Lead time	3	8	24	6	18	8	24
Total			**121**		**172**		**234**

The final decision on a differential was made using a weighted matrix, see Table 2. Five key characteristics were used in order to make the decision, with the first being cost. Cost was weighed in the middle because the team's defined budget would allow for the purchase of any of the options, with minor relocation of resources. A higher cost may limit freedom with other parts of the car but would not impede the team from finishing the vehicle. The next was adjustability, which was weighted highly because of a lack of knowledge of suspension and tire performance. The ability to tune the lockup easily could greatly increase the drivability of the car. The next factor was weight. This was also weighted somewhat high with weight reduction in mind. The next was ease of implementation. This was also given a high weight because of the team's limited man power and time. Spending less time on implementation would allow for more time to tune the car and focus on other areas that were lacking on the 2016 car. The last parameter was lead time. This was given a fairly low weight because the team was being proactive and thinking about this decision early in the build. Even with a long lead time the team was well prepared. As the weighted matrix clearly shows, the Drexler LSD was the best option and was purchased for implementation in the car.

Differential Mounts and Chain Guide

Along with the differential itself, the differential mounts are a crucial part of the drivetrain. In addition to holding the differential in place, they also define the chain line of the drivetrain and the angle of the half shafts. They thus not only need to be strong enough, but also must ensure the differential is properly located in all three dimensions. For this year, the team has also added the complicating factor of chain tensioning to the tasks handled by the differential mounts, in an effort to improve on the mounts designed for the 2016 WPI vehicle.

Mount Concepts

In 2016, the differential mounts attached the differential rigidly to the frame with bulky, 1/2-inch plate aluminum brackets and custom shaft collars. This design used a separate chain tensioner located near the rear engine mount, which used a torsional spring and a tensioning bolt to keep the chain from jumping off the drive sprocket. Due to the intersection of the chain line and a frame cross member supporting the rear of the engine, a delrin chain guide was made to redirect the chain. Although this mount and chain guide system functioned properly for the majority of the time, the chain guide failed on at least one occasion. It failed due to an accidental engine lock-up during dyno testing, which placed extreme loads on the drivetrain causing the tensioning bolt to snap. The team believes it is possible to make significant improvements to this system for the car.

The main goal of the differential mount design is to incorporate chain tensioning functionality into the mounts in order to reduce the complexity and weight of the system. More specifically, the team wanted to provide at least half of one chain link worth of linear adjustment in the tensioning system. Any less would risk being unable to properly tension the chain. The team also decided that the differential mounts would attach to the frame with welded tabs and shoulder bolts instead of shaft collars. This would ideally reduce the weight and complexity while increasing strength. The three main concepts the team came up with to accomplish these goals were:

- Linear tensioning with bolts in slots - held in place by torqueing bolts
- Rotational tensioner – pivot entire mount around fixture, adjust with turnbuckle
- Eccentric bearing cups – pivot diff within fixed mount, hold in place with pinch bolts

After discussing the goals for the system, and the potential advantages and disadvantages of each, designs for the latter two were made as they were more viable options. The first idea was discarded early due to the likelihood of higher system weight and the difficulty of securely fixing the mounts in place under the projected loads. However, no extensive calculation or design work was done to fully invalidate this option. After evaluating the design concepts the final drive ratio needed to be determined since the size of the driven sprocket will have a large influence on the degree of adjustment available to the chain tensioning system.

Final Drive Ratio Selection

In determining the final drive ratio, that being the ratio between the engine output sprocket and the driven sprocket at the differential, several concerns needed to be addressed, including packaging due to sprocket size, as well as performance due to the influence gearing would have on driver experience. The first step taken by the team was to review previous methodologies used for final drive determination, such as those of the 2016 WPI team, as well as the Cal Poly engine development team.

According to documentation left by the 2016 WPI FSAE team, the final drive ratio for their car was decided by tabulating road speed values according to engine RPM and gear selection. Seeking to maximize use of the full gearing range available on their closely geared YFZ450R, the team tried to adjust their final drive ratio to make the car reach its maximum desired road speed at redline in fifth gear. This resulted in a final drive ratio of 38:14, or 2.714:1. According to accounts from some current team members who drove the 2016 car, this resulted in a feeling of near constant shifting when driven on the track, as well as a mysterious lack of acceleration performance possibly related to the constant shifting. A review of the tables generated by the 2016 team showed that most gears would only keep the engine in its power band for less than 10 MPH, hence the rapid pace of shifting required to drive the car.

For the Cal Poly team, their gear ratios were narrowed down through calculations of "tractive effort," top speed, and time to speed. By completing physical testing with previously designed FSAE cars, the Cal Poly engine team was also able to observe the effects of certain final drive ratios and gear selections on acceleration. Instead of comparing the total road speed spread offered by each final drive choice, the Cal Poly team narrowed their comparisons to the specific gears each final drive ratio would use. For example, when comparing the relatively high drive ratio of 33:14 to the relatively low ratio of 48:14, they compare the two from first to third gear, and second to fourth gear, respectively. By specifying the gears they intended to use, rather than assuming all would be used, the Cal Poly team allowed themselves to more finely tune the behavior of their drivetrain to match driver preference and engine tuning. While they did not specify exactly which gear ratio they intended to use in their report, their approach to final drive selection seemed remarkably thorough.

The 2018 WPI team intended to strike a balance between these two approaches to final drive selection, since certain attributes of each method would be useful for the design of the new car. Due to a lack of information about torque and power figures for the WR450F, even at the level of conjecture, calculations of tractive effort and acceleration time would be essentially pointless, so the total speed range of each gearing option became the primary design metric. The first step of the design process was thus a determination of the limits of possible final drive choice, to narrow the field of options. After browsing through online aftermarket parts stores, front sprocket selection was limited to a range of 12-15 teeth, all using the 520 chain standard since only specific sprockets would fit the splined output shaft of the WR450F engine. With this information in mind, the frame was then examined to determine the maximum rear sprocket size that would feasibly fit. Using a guide found online, an adaptable model of a 520 sprocket was made, and its size was adjusted from 36 teeth upward to find the limit. In checking the fit of each sprocket size, the outer edge of the sprocket was kept at minimum 1/2 inch from any frame members, and less than 1/2 inch below the bottom of the frame, also keeping in mind a desired one-half link of chain length adjustment. From this exercise, the largest rear sprocket that was observed to comfortably fit into the frame was 38 teeth, since a 39 tooth sprocket did not leave enough room for the required adjustment range.

Commented [16]: http://www.gizmology.net/sprockets.htm

With this information in mind, a spreadsheet of road speed values per gear was created, in the same vein as the approach taken by the 2016 WPI team. Taking into account 20-inch diameter tires, the 2.652:1 primary drive ratio of the WR450F engine, and its five gear ratios, a table of road speeds was laid out from 500 RPM to the 11500 RPM stock redline of the WR450F, with specific fields for front and rear sprocket tooth counts. Figure 10 below is a chart of these road speeds for one of the gear ratios considered. After playing with different gear ratios, the ratios 38:12 and 36:13 began to look most appealing.

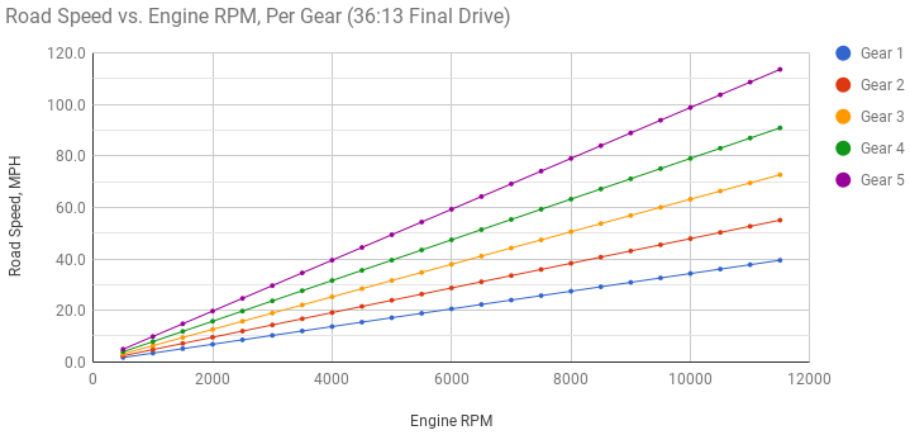

Figure 10: Chart of Road Speed vs. RPM for 36:13 Final Drive with WR450F

In addition to being the lowest gear ratio possible for the car, 38:12 would allow for full usage of all five gears, and assuming a power band of 6000-8000 RPM, would place the top speed of the vehicle at just under 70 MPH. Considering that the engine already has a 13 tooth drive sprocket attached from the factory, and the wider speed spread possible with a higher gear ratio, 36:13 is an appealing option. This higher ratio would allow for full usage of gears one through four, and would place the top speed of the car at just under 80 MPH. At this point neither gear ratio has been conclusively chosen, but for purposes of designing the differential mounts, a 38 tooth rear sprocket was assumed.

Differential Positioning and Tab Design

With a potential rear sprocket size now selected, the basic layout of the differential mounts was arranged, starting with the location of the differential, this being the point in the adjustment range of the mounts where the rear sprocket would be closest to the frame. Since the centers of the rear wheels are positioned nearly in plane with the rear of the car, setting the differential as far rearward as possible would produce the minimum possible half shaft deflection. This location was set with the differential 125 mm on center from each of the rearmost frame cross members, placing a 38 tooth 520 sprocket just under 1/2 inch away from each frame member for the smallest comfortable clearance. This location was chosen while checking the fit of different sprocket sizes, and is shown in Figure 11 below. Also note the differential and half-shaft models, which were given to the team by Drexler immediately following the confirmation of the differential order. These assemblies were clearly imported from another CAD software, and required much work to arrange into an assembly usable for packaging.

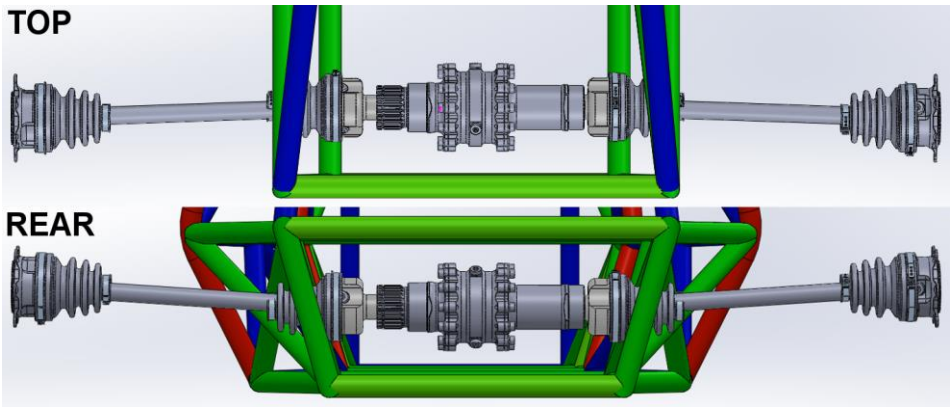

Figure 11: Differential Starting Location and Half Shaft Angles, Top and Rear Views

With the position of the differential chosen, the mounting tabs that would be welded to the frame to support the mounts were then designed. Before creating any concrete designs, a static analysis was run by hand to approximate the loading the mounts would need to withstand. For

determining the maximum load, the assumed worst-case scenario involved an engine lock-up as seen during dyno testing in 2016. For this case, the tires were assumed to break traction at 1.5 G of deceleration, with a total vehicle weight of 750 lbs including the driver. With 50/50 weight distribution, as would roughly be the case on a dynamometer, this placed 562.5 pounds-force tangentially on the rear wheels. For a tire diameter of 20 inches, assuming no compression, and a sprocket diameter of roughly 4 inches as found from the earlier model, the approximate tension force applied to the chain would be 1406 pounds. With this force applied at the drive side of the differential, and properly functioning mount bearings, the vast majority of the force would be transmitted to the mounts as a linear forward pull on the drive side mount. For a differential mount attached to the frame at both top and bottom, this 1406-pound force would split into two 703 pound forces at the mount tabs. If perfect shear is assumed, this force then splits into two 301.5 pound forces at the tabs.

Since previous WPI vehicles had experienced some issues with frame tab failure, the differential mount tabs were significantly overbuilt to ensure that the frame would be the least likely component to break in the event of any accident. To do so, 0.16-inch-thick steel was chosen for the tabs, along with 3/8-inch shoulder bolts as the mounting hardware. Early in designing the first differential concept, the length of the tabs was set at one inch from the center of the frame tubes to the center of the mount bolts, leaving a small amount of free space for different mount designs later on, if required. In hindsight, these choices produced significantly stronger tabs than required, even for an "overbuilt" configuration according to the assumed worst-case scenario, with a minimum FOS of 12 due to bearing stress in the tabs. In retrospect, the team does not think that this degree of excess is advisable for other components of the car, but for the differential mounts the additional weight added is not noticeably harmful. From here, the bearing sizes required to fit the Drexler differential were determined, those being 6211 and 6010, and work began on modeling the two potential designs for the mounts.

Design Refinement and Completion

The design of the pivoting mount concept involved attaching the differential mount to the mounting tabs on the lower of the two rear frame cross members, using separate mounts for the drive side and non-drive side of the differential. With the lower end of the mount riding on shoulder bolts, the mount would be allowed to pivot around this lower bolt to tension the chain. This pivoting would be controlled by a small turnbuckle attached between the top of the mount and the upper frame tabs. Figure 12 below shows the layout of this first completed mount assembly.

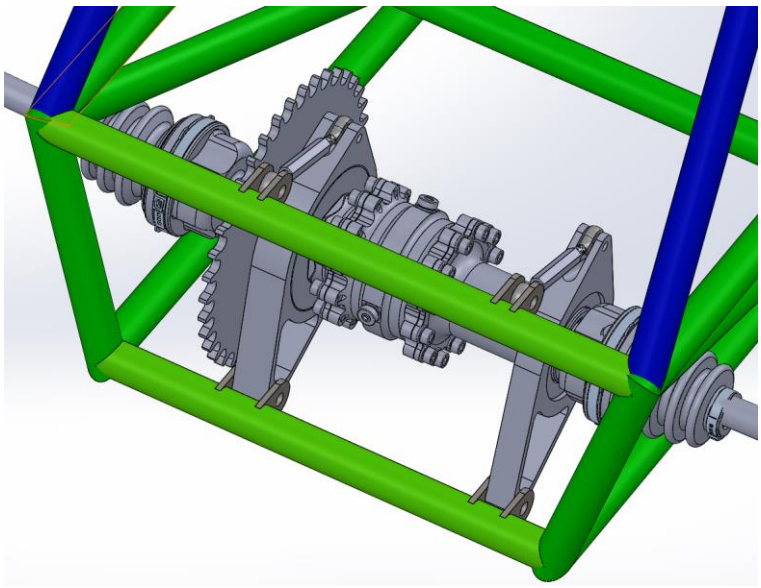

Figure 12: Pivoting Differential Mount Model in Frame

When this design was modeled in SolidWorks, a number of potential complications were noticed about this potentially simple design, primarily regarding the miniature size of the turnbuckles required for this design. Due to the small size of the mounts relative to most turnbuckles, those used on the differential mounts would be among the smallest readily available, likely requiring overall lengths of less than four inches. While these turnbuckles would certainly be capable of withstanding the worst case 700-pound axial load predicted, the mounts themselves would be somewhat more complex than was preferable, in order to provide a clevis joint for the turnbuckles to attach to. In addition to the complexity of the mounts, this first differential mount design would be difficult to adjust, since two turnbuckles would need to be adjusted to equal lengths to prevent undue torsional stress on the mounts or bearings. Due to these issues, and a general wariness about using turnbuckles as a structural component of the differential mount, the team decided to scrap this concept as well, and focus on the third of the original ideas.

The eccentric cup mount was thus the one that was carried through to completion, and was chosen over the other two competing concepts primarily for its simplicity and strength. This mount concept works by pressing each differential bearing into a cup with an outer diameter off-center from the bearing seat. The distance between the center of the bearing seat and the center of the outer diameter of the cup thus becomes the radius around which the differential is allowed to rotate. The benefit of this design is that the differential is allowed to pivot about an axis within itself, meaning that the diameter of this rotation can be finely tuned to offer the required linear displacement while requiring only a small amount of extra material and space over a rigid mount.

To suit the pitch of the 520 chain that would be used on the car, the offset of the eccentric cups was set at 7 mm, to provide a total position adjustment range of 14 mm, and thus a total chain length adjustment range of 28 mm, or just under 1 full chain link. Adjustment was limited due to the fact that a full link of adjustment would simply be cause for shortening the chain, and additional offset would make the sprocket protrude too far below the frame. For this offset, and the 100 mm diameter of the drive side bearing, the outer diameter of the eccentric cup was 122 mm. For the non-drive side bearing, which has a diameter of 80 mm, the diameter of the eccentric cup was 102 mm. With these dimensions in hand, the cups and mounts were then modeled. Figure XX shows one of the eccentric cups, which has holes in its side to aid rotation of the cup in its mount.

Commented [17]: update

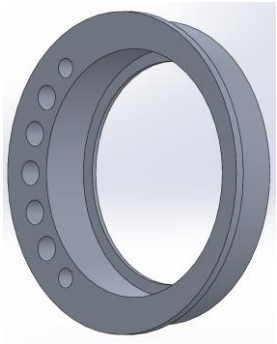

Figure 13: Eccentric Bearing Cup

For the first revision of this design, the differential mount brackets were made the same thickness as the cups, that being equal to the thickness of each bearing with a small allowance for a locating lip. This resulted in a drive side mount nearly one-inch-thick, and a non-drive side mount roughly 3/4-inch-thick, with the ends of both tapered down to 1/2 inch at the mount tabs. This design used a pinch bolt to fix the rotation of the eccentric cups, with the bolt located between the mount points. An important feature of this design was the configuration of the bearing cups, which used flanges at opposite sides of the cup to ensure that after assembly there would be no way for the bearings to slide out of place.

Since the differential mount would see a large amount of vibration, and continuous loading, it was important to consider the stability of the differential as a package. To prevent horizontal slippage, the differential included inboard flanges to locate the bearings horizontally on their seats, and the eccentric cups were designed to include matching flanges on the outboard side to lock the bearing in place between the two horizontally. This was also done for the cups themselves, with a flange on the inboard face of each cup to prevent it from sliding outward horizontally in the mount bracket. The combined effect of these flanges, when assembled, is to prevent the assembly from coming apart without removing the whole assembly from the frame tabs, thus making any additional positive locking for the bearings and cups redundant. This is illustrated by Figure 14.

Commented [18]: update

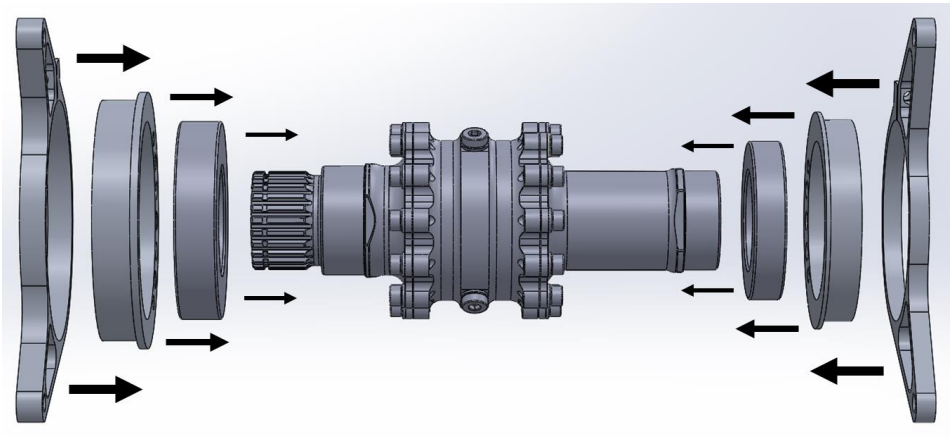

Figure 14: Sandwich Assembly of Differential Mounts

After completing the design, FEA was run on this first revision using the same 1406-pound force calculated as the worst-case scenario earlier. Figure 15 below shows the full arrangement of the FEA assembly. For this analysis, the frame tabs were attached to modeled tubes of equivalent length to the real frame members they would be welded to, and blanks of all fasteners were made to simulate the behavior of the mounts as they would be assembled in practice. A simplified model of the differential assembly was also made, with cylindrical faces substituting for the bearings and the sprocket. In the static simulation environment, the mount tabs were attached to the frame tubes with "Bonded" contact constraints, and all contacts between the mount components and differential blank were accounted for with "No Penetration" constraints. All fastener representations and the differential blank were set to behave as rigid components, to simplify their behavior and effects. The remaining components were assigned the materials they would be made of in reality, those being AL6061 for the mount brackets and cups, and 4130 chromoly steel for the tabs and frame tubes. The results of the FEA stated a minimum factor of safety of roughly 6, and minimal deformation. Although this design seemed acceptable after this simulation, a review of its design prior to beginning manufacturing revealed some serious issues with material waste due to the mount thickness, as well as difficulties with machining the pinch bolt location. This mount design was thus revised to significantly simplify the design and minimize material usage, resulting in the second version which is currently intended for manufacture.

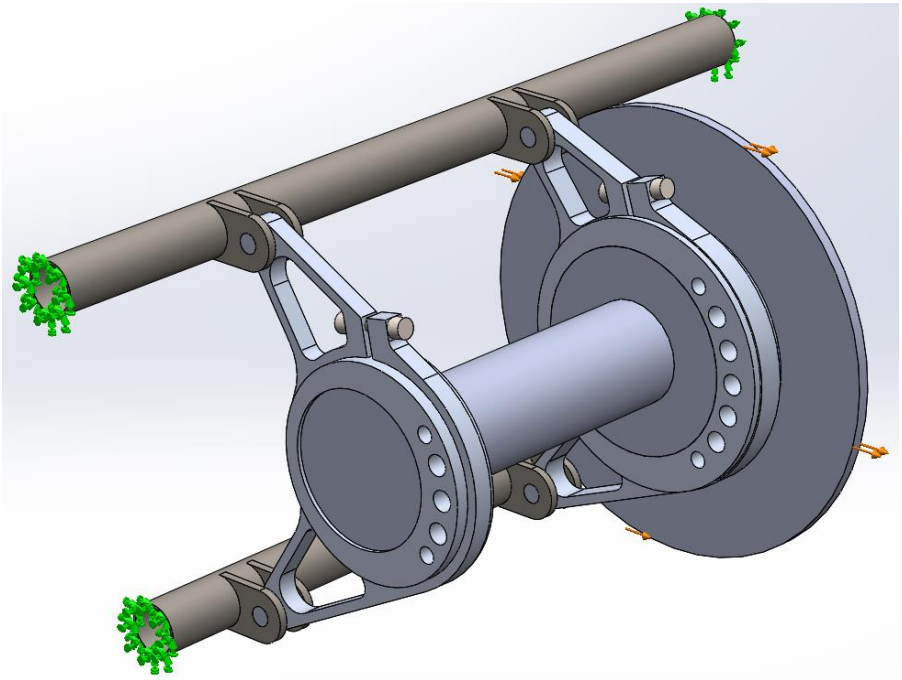

Figure 15: Differential Mount Assembly for FEA

The revised differential mount design makes significant simplifications from the first, most notably with a jump to much thinner material. For the drive side mount, 1/2-inch AL6061 plate is used in place of 1-inch plate, with 3/8-inch plate for the non-drive side mount. Since the mounting tabs had already been welded to the frame by the time this revised design was completed, the non-drive side mount will use a 1/8-inch spacer to offset it horizontally in the 1/2-inch spacing between each pair of tabs. While the eccentric cups must still be machined from thicker material, this has been deemed acceptable to properly mount the bearings, and has no effect on the functionality of the mounts. The mounts have also been made almost entirely flat, with the only machining process necessary after cutting the horizontal profiles being the drilling of the pinch bolt holes, which have been moved to the top of the mounts. This has allowed for the usage of waterjet cutting to make the differential mounts instead of the extensive milling procedures that would be required to cut thicker plate. When tested with the same FEA procedure used for the original differential mounts, the FOS of the revised mounts is 1.9, which is a safe value considering the extreme loading used for the worst case scenario. Figure 16 below shows a plot of the FOS of the mount design, and Figure 17 shows the assembly in the frame. This completed mount design has not been manufactured yet, aside from the frame tabs, but is expected to be completed at the end of B Term, or soon after.

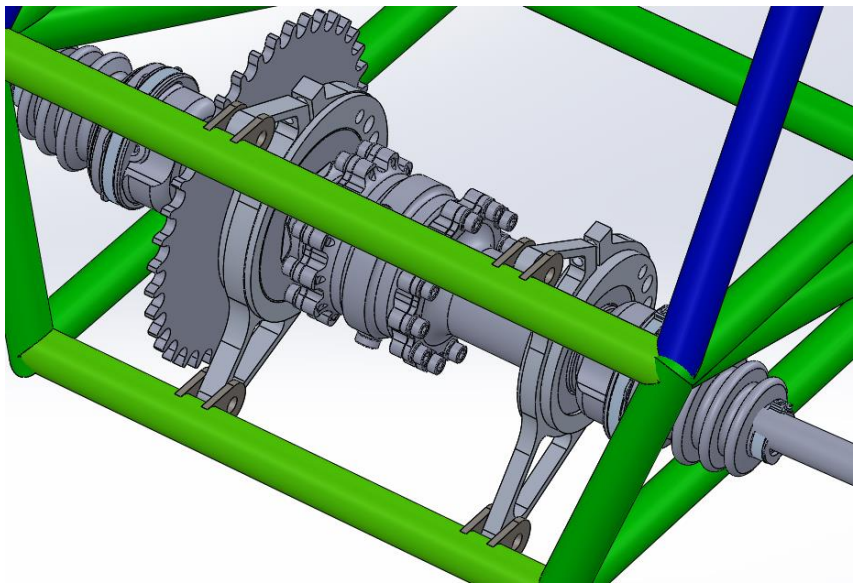

Figure 16: Completed Differential Mount Design

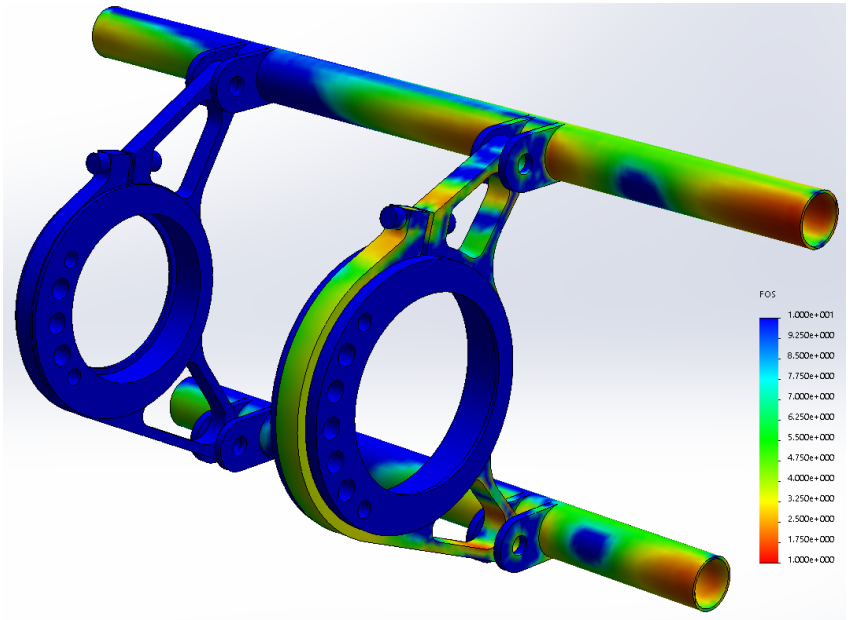

Figure 17: Factor of Safety Plot of Completed Differential Mounts

Engine Mounts

As mentioned in a previous section of this report, the frame and drivetrain were not designed in parallel, in an ideal world, the frame would have been designed with integral engine mounts, but since the frame began its design cycle, with a separate team of students, one year before the drivetrain and the rest of the car, this was not possible.

Despite the rear section of the frame remaining the same as the 2015-2016 vehicle, the slight differences between the YFZ450f of the previous year and the current WR450F along with the allocation of a brand new differential and axles warranted the design of a new set of engine mounts. When designing the mounts a few things must be taken into consideration, the engine needs to be as low in the frame as possible, without leaving the envelope of the primary structure. As the engine is one of the single heaviest components, the lower it can be mounted, the lower the vehicle's center of gravity is, which will only aid performance. The mounts must also place the enige far enough towards the rear of the vehicle to allow for clearance between the J-pipe and the firewall, butnot too far rearwards, as the differential, differential mounts, chain, chain tensioner, chain guard and shifting components all must be packaged in the frame, behind the engine.

In previous years, time has been devoted to trying to procure 3D models of the engines for mounting and packaging purposes. Last years MQP team made an attempt to get a model of the WR450F from Yamaha but was not able to succeed. Instead wasting more time on a venture that was not guaranteed to be successful, mount locations were initially measured manually, using a tape measure and threaded rod, while the engine was mounted on a stand. These measurements were used to triangulate the mounting points relative to one another

Calipers were used to measure mount hole diameters and widths, it was assumed that all mounting points were horizontally symmetrical. A tape measure was also used to approximate the location of the sprocket centerline with respect to the rear engine mounts, this will be important for finding the chain line to the differential and for creation of SolidWorks model, to be used for mount design, that will incorporate all of the measurements taken by hand.

With all of the measurements taken, some rough front engine mounts were drawn up and laser cut using spare ⅛" balsa wood that was hanging around the shop. The shape of the mount was solely based on looking at the engine and did not fit very well, however, using threaded rod extending out from the mounting points on the engine, the placement of the connections points on the mounts were verified. This allowed for the creation of a simplistic 3D model that had all the critical mounting dimensions of the engine.

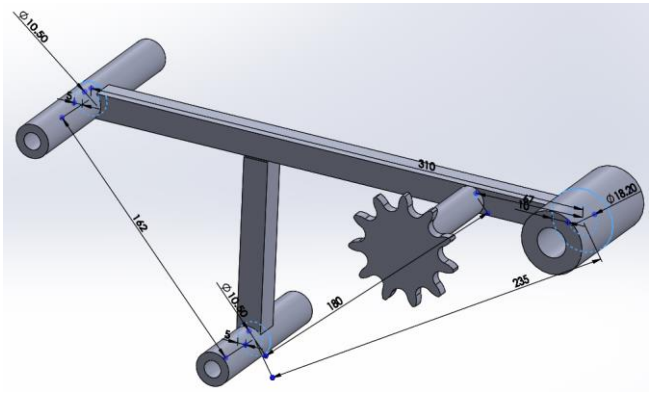

Figure 18: Engine Mounts

As evidenced by the prototyped front engine mounts, interference with the engine would be an issue when designing the final shape of the mounts, so in order to design the mounts properly it is be necessary to model the overall space that the engine will take up. In the past, MQP teams have used the Autodesk's "123d Catch" app to scan the engine and import the 3D surface into SolidWorks to use for packaging, this app was discontinued in January 2017, but got the team thinking about options for 3D scanning. Through our advisor, Professor David Planchard, we learned that WPI's Dr. Erica Stults had access to a mobile 3D scanner that should be able to produce a scan that would be good enough for our purposes. The scanner itself was mounted to an Ipad, and produced a very low quality scan, but it did a fine job defining the space that the engine occupies. Using datum planes and axes, the engine scan was mounted onto model of hand measured mounts from before, this created a full engine model of the correct size and with workable mounting geometry.


Figure 19: 3D Engine Scan

This assembly was placed in a SolidWorks model of the frame, to align the engine model laterally in the frame, the driver side face of the engine sprocket was mated coincident to the driver side face off the differential sprocket, as the differential assembly was already in the top level assembly of the entire vehicle. A datum plane was created in the engine model and was matted to the top plane of the frame to control engine height and pitch, the engine was constrained such that its lowest point was coincident with the plane created by the bottom surface of the lowest frame members. A model J-pipe was created and mated to the engine model, this was used to verify that there was space between the firewall and the exhaust, necessity for the driver's sake. All other degrees of freedom were eliminated using distance mates between the engine mount centerlines and frame tube centerlines. With the engine fully constrained, engine mounts were sketched originating at the mounting points on the engine and terminating at the nearest frame rail(s). The shape was fine-tuned to fit around the shape of the engine with rather large tolerance, in an effort to avoid unforeseen interferences come final assembly. Once the final shape was determined, holes were made to reduce the overall weight of the mounts. If issues arise during simulation, these holes and the material thickness will be the first things to be modified.

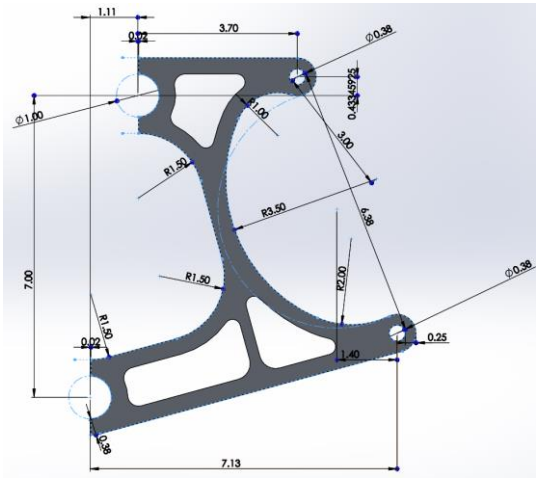

Figure 20: Engine Mount 2D Profile

In order to simplify manufacturing, the engine mounts are limited to a 2D profile with a .375" thickness, as this facilitates laser cutting or hydro cutting, which can be done by of one the team sponsors, Howe and Howe Technologies. The Mounts were also designed to mount to the frame with off-the-shelf ½" shaft collar, in an effort to reduce manufacturing time, the selected hardware would be ¼-20 bolts, standard for the selected shaft collars. Due to the design, the hardware must be threaded into the edge of the .375" aluminum plate, as there is a very minor concern that thread tear out will be a failure point for the mounts, the team will be looking into having a spare mount pull-tested on an Instron Machine in order to determine the failure load and lay rest to any concern.

Finite Element Analysis

To validate the design of the engine mounts, a static simulation was conducted in SolidWorks in order to obtain a factor of safety for all four mounts. Before the simulation could be set up, the applied loads needed to be determined. At the current stage in the design process, the engine is untested, thus the torque output is unknown. Similar to load determination used for the differential mounts, engine lockup was assumed, which results in a 1400 in-lbf torque at the engine sprocket. The engine weight was also unknown as the scale the team has easy access to tops out at 30kg (~66lbs), a conservative value of 90 lbs was assumed. Based on the target deceleration, a 1.5G engine forward force was assumed and a 1400 lbf chain tension force was used, as with the differential mounts. Two contain the engine model, three tube mimicking the tubes used for the frame construction were put into assembly preserving the orientation of the frame member that the engine mounts bolt to. The ends of these tubes were assigned fix geometry

Six models of the a ½" shaft collar were inserted into the assembly and mated to the frame tubes using a fixed-hinge boundary condition to permit rotation around the tube, but not translation. The motor mounts are attached to the shaft collars using a simulated ¼" bolted connector torqued to 100 lbf-in. The final component in the simulation is the engine model, without the engine scan, which is mated to the engine mounts, the front mounts and the engine model fully define the position of the rear mounts and shaft collars.

Commented [19]: don't remember chain tension

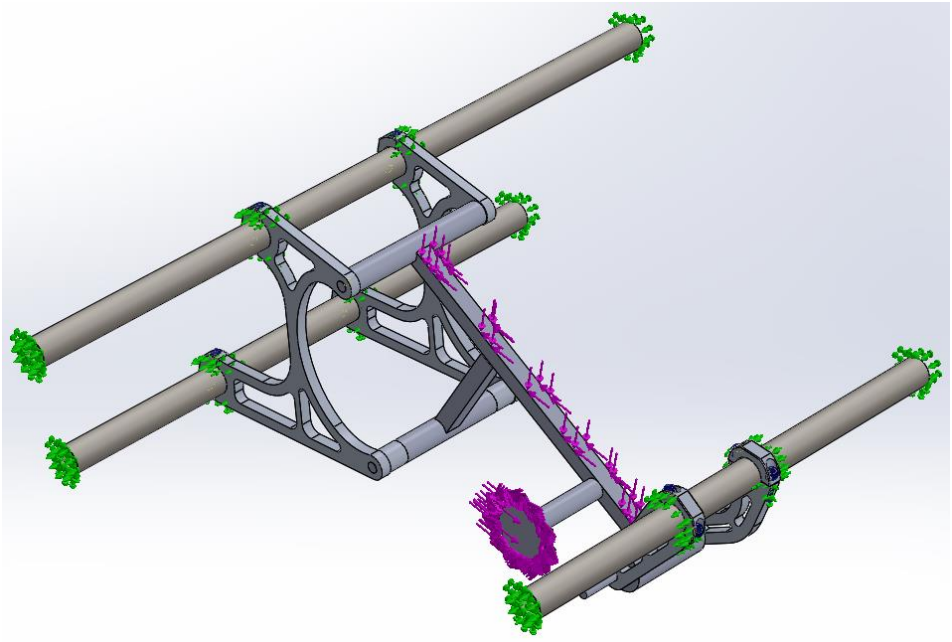

Figure 21: Engine Mount Assembly FEA

In addition to the constraints mentioned above, no penetration contact sets were used at all surface contact locations and all components except the engine mounts themselves were made rigid, serving as a path for load to travel to the mounts. The selected material was 6061-T6 aluminum due to its relatively low cost, low weight and availability. As mentioned above, the thickness of the mounts was ⅜" and with the above loading, the mounts passed the simulation with factor of safety around 1.5, so no further modifications were made.

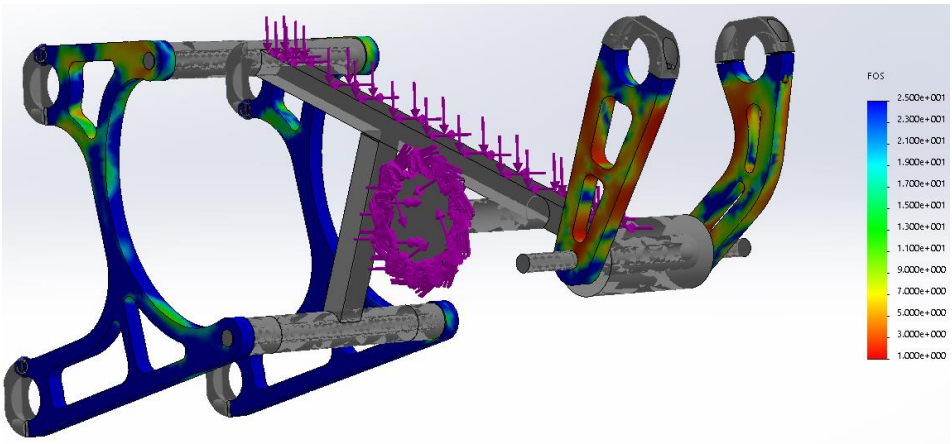

Figure 22: FOS Fringe Plot

Another simulation was done with assuming 1G side load due to cornering, and the mounts passed with a factor of safety of 3.

Engine System

Fuel system

Fuel system design was primarily based around frame packaging and engine constraints. The system was designed to be a recirculating system, as most off the shelf components that would meet our requirements are designed for this type of system (also because that is what has been used in the past, so it is what is most familiar). 5/16 ID fuel line was chosen because it had been used in the past, and obtaining fuel fuel filters and other components for that tubing size was easy. In the future, fuel hose size could most likely be reduced to save weight. A Walbro 255 Fuel pump was selected due to its reliability (also because we had used it in the past and was convenient. For the next car build, a smaller, more lightweight pump may be able to be used, as a 255LPH (liter per hour) can typically support builds over 500HP.

An Aeromotive adjustable bypass fuel pressure regulator was selected, as in the past the team has encountered issues with custom fabricated regulators. This regulator was originally selected

because it had the number of inlets and outlets needed (it was thought that we needed three total, and the regulator had 4), as well as because it was adjustable within the pressure ranges needed. However, it was later realized that less fuel inlets/outlets were needed, so in the future a smaller and lighter regulator may be able to be found.

The second portion of the fuel system design was the fuel tank. The 2016 car had roughly a one gallon capacity tank, and nearly ran out of fuel during the endurance portion of the FSAE competition. This was the basis for a new fuel capacity goal of 1.5 gallons, as this should give the car enough fuel to complete the endurance race without adding excessive weight. Due to packaging, there was limited space to achieve this, meaning that one side of the tank had to protrude backwards next to the engine (see Figure 23).

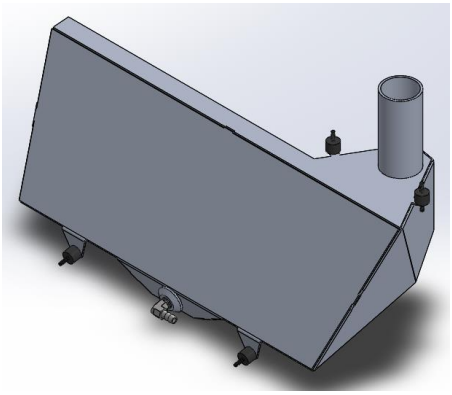

Figure 23: Fuel Tank Isometric

Additionally, the 2016 car experienced fuel starvation issues during endurance, despite having a fuel sump tasked with keeping fuel near the fuel inlet. To correct this, the new fuel tank design incorporates baffles, as well as a sloped bottom, to help ensure the fuel pickup will always be able to intake fuel (see Figure 24)

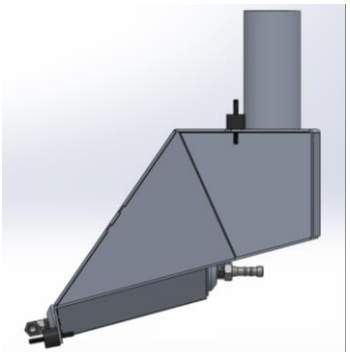

Figure 24: Fuel Tank Side View

The tank was built out of 0.09in thick 5052 Aluminum, as this was the thinnest material able to be welded (in addition, most fuel cells are made from 0.09in thick aluminum). It was important that 6061 Aluminum was not used, due to the fact that it cracks when bended (the tank is constructed out of multiple 2D pieces that are them bent and welded together).

Air Intake

During the first half of this year, the majority of work dedicated to the engine has been related to the intake. Consisting of several subsections, each with their own purpose, flow characteristics, and variety of controlling parameters, the intake has been complex and challenging to design. Since there are no simple answers for any part of the intake, iteration has been a key component of its design process, and that process has required the development of unique methodologies to match.

Intake Simulation Model

For several weeks this year, the majority of intake design effort was dedicated to the development of a time-dependent simulation model using Microsoft Excel and SolidWorks Flow Simulation (SWFS) to approximate the pressure waves generated inside the cylinder of the WR450F during intake strokes. This model was developed both to circumvent the process of acquiring a license for engine-specific CFD software, as the team already had access to SWFS, and to allow for precise control of the boundary conditions used in simulating flow through intake models.

In previous years, SWFS was used to validate intake performance prior to physical manufacturing, but only at a rudimentary level using static analysis. While this was easy to set up in the program, and was "better than nothing," the static simulation method was essentially useless for determining any numerical descriptions of intake performance, and mainly served to provide pretty pictures of flow patterns. When the 2018 team began researching intake design and decided to develop a more concrete methodology, there was little information available on the subject of transient flow simulation, and no team members were aware that it was an option in SWFS prior to this project. After some additional research to comprehend the options available for arranging transient simulation in SWFS, including some relevant YouTube videos, the appropriate flow scenarios were arranged. A simple test was set up with a model of the intake designed by the 2016 team, but no new information had been gained about how flow was incited in the real intake. Answering this question was the main purpose of the Excel component of the intake simulation methodology.

Getting Started with SolidWorks Flow Simulation

The first step of developing the intake simulation method was to determine the boundary conditions required for accurate modeling, including the numerical output method required. Since the primary purpose of a well-designed intake is to improve volumetric efficiency (VE), and therefore torque and power, volume flow rate data would need to be the primary numerical output of the simulation.

The first condition set was the entrance of the intake, which for the 2016 model was a plane across the entrance of the restrictor. To emulate ambient air conditions, this plane was set as an

"Environment Pressure" boundary with a temperature and pressure of 298 K, 101325 Pa. The next boundary condition defined was the internal surface of the intake, which was set to behave as a "Real Wall." The settings used for this condition throughout testing were a temperature equivalent to the ambient air, and a roughness value of 1 micrometer as an approximation of a smooth finished surface. Since the exit boundary condition had not yet been given any formal definition, an interim solution to get started with SWFS was to use the exit plane of the intake as a variable pressure boundary (where the intake mounted to the engine). In Excel a simple half-sine wave pressure drop was arranged as a crude approximation of the pressure pulse from the engine. For the pressure values input to the SWFS exit boundary condition, an interval of 0.000125 seconds was used for all tests, a value arbitrarily chosen to be on the same order of magnitude as the calculation time steps preferred by SWFS. To calculate the volumetric flow rate that resulted, a "Surface Goal" was used on the same face as the exit pressure boundary and set to track the volume flow rate of air into what would be the engine. Once a preliminary test was run, for the purpose of gaining familiarity with the SWFS user interface, the results were discarded and work resumed on determining the currently unknown model conditions.

The first step after this preliminary attempt was to create a SolidWorks model of the portion of intake runner integral to the cylinder head of the WR450F. Since the intake valves would form a convenient physical boundary between the intake flow handled by SWFS and the cylinder conditions imitated by the exit pressure boundary, modeling the intake runner extension would reduce the number of assumptions made in calculating the pressure pulse profile at the intake exit. Characterizing the internal geometry of the cylinder head proved quite difficult due to its complex shape and tight confines, but it was eventually approximated. What was ultimately used to dimension this integral runner was the diameter of the valve seats, which could be found from the owner's manual; the diameter of the inlet, which had been manually measured; and some rough measurements of the internal surface of the runner. Figure 25 is a picture of this integral runner, and illustrates the difficulty of measuring the cavity. Using a protractor, the angle of the inlet port was also measured relative to the square sides of the engine.

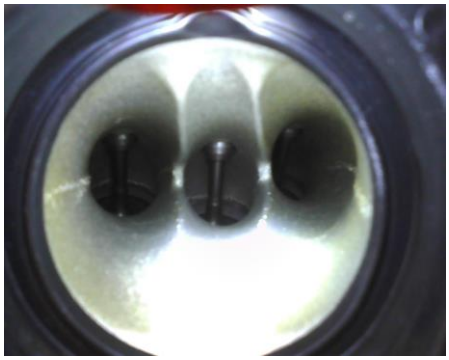

Figure 25: Integral Intake Runner Extension, and Intake Valve Stems

In SolidWorks, assembling even a skeletal model of this runner required several hours of iterative dimension adjustment, but once its form was figured out it produced a valuable result. Using a 3D sketch, the valve faces were located within an approximation of the cylinder bore, the inlet orifice was located at the origin using the angular measurements of its position relative to the engine body, and the relative positioning of the bore and inlet was determined by iteration, with the linear measurements to the valve positions as a guide. The completed 3D sketch made some approximations of the real shape, such as the assumption of coplanar valve faces when they are in fact slightly angled, and the true shapes of the runner sections leading to each valve. Where measurements could not be taken, their values were approximated from pictures, and the completed model appeared to resemble the actual integral runner to an acceptable degree. Figure 26 shows the completed integral runner model from the same angle as the above picture.

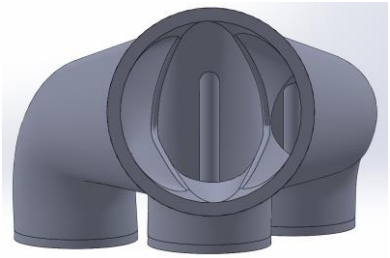

Figure 26: Interior of Model of Integral Runner Extension

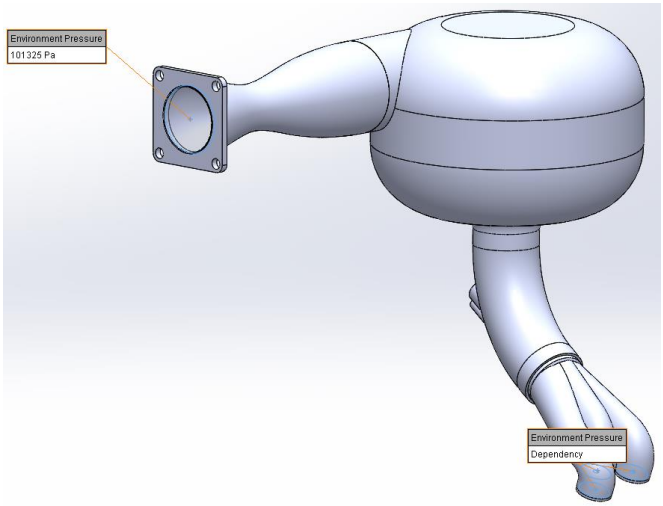

Figure 27: 2016 Intake Model with Integral Runner and SWFS Boundary Conditions Set

Once the integral runner model was mated to the outlet of the 2016 intake model, the exit pressure boundary condition was redefined to the three valve faces of the integral runner, as shown in Figure 27 After this, focus shifted to adding to the pressure wave calculation spreadsheet to

account for additional physical aspects of the situation. The spreadsheet was completed prior to any additional simulation runs in SWFS from which numerical results were collected.

Pressure Wave Simulation Spreadsheet

The completed pressure wave calculation spreadsheet is a somewhat complex set of calculations designed to approximate the static pressure at the valves of one cylinder of a four-stroke engine at a specific steady-state condition. It outputs pressure data as a function of time, with an option for user control of the output time step, and manual control of the total output time period. The spreadsheet takes in user inputs of:

- Bore and Stroke of Cylinder (millimeters)
- Compression Ratio
- Engine RPM
- Intake Valve Duration (crank degrees where lift is at or greater than 1 mm)
- Intake Valve Lift (millimeters)
- Plenum/Ambient Air Pressure (Pascals)
- Plenum/Ambient Air Temperature (Kelvin)
- Volumetric Efficiency Guess (decimal percentage)

The spreadsheet also uses some other constants and thermodynamic data that are not intended to be user-controlled:

- Universal Gas Constant R = 8.314 J/mol-K
- Exhaust Gas Initial Temperature
- Simplified Chemical Composition of Gasoline Exhaust Fumes
- Molar Mass, Specific Heat Cp of Nitrogen (N2)
- Molar Mass, Specific Heat Cp of Carbon Dioxide (CO2)
- Molar Mass, Specific Heat Cp of Water Vapor (H2O)
- Molar Mass, Specific Heat Cp of Carbon Monoxide (CO)
- Molar Mass, Specific Heats Cp and Cv of Air

These thermodynamic properties were included in some aspects of the pressure calculation process by creating curve fits of tabulated data with temperature as the independent variable.

With all of the above information entered, the spreadsheet goes through several steps of calculation to characterize the current situation, finally outputting total pressure in the cylinder. As the spreadsheet is designed to be dragged to the desired length, each column includes only a formula for its particular variable which references either specific values or values calculated in other columns. An excerpt of the pressure wave data this spreadsheet produces is shown in Figure 28. The physical characteristics taken into account, which represent the different steps of the calculation, include:

- Crank Angle of Engine – Repeats at intervals of 720 degrees, for each four-stroke combustion cycle
- Piston Position and Velocity – Determined by sinusoid functions
- Total Cylinder Volume – Displacement at current time stamp, including cylinder volume remaining at TDC due to finite compression ratio

Commented [20]: update

- Propagation (Mach) Delay Time, Delay Adjusted Stroke, and Delay Adjusted Displacement – Accounts for delay between changes in Piston Position and Velocity and response of air in intake runner
- Intake Valve Position – Percentage openness of intake valves at current time; used to control approximate air flow rate into cylinder
- Volume and Mass of Air Ingested – Assumption of some airflow into cylinder to create more realistic pressure wave profile; includes coefficient for model calibration
- Mixed Gas Temperature – Current temperature of exhaust gas and air mixture; found from mass fractions of air and exhaust gas in cylinder at current time
- Total Moles of Gas in Cylinder – Including residual exhaust gas at beginning of intake stroke and air ingested during stroke, allows static cylinder pressure calculation with Ideal Gas Laws
- Gas Mixture Density – Average density of air and exhaust gas mixture in cylinder, for determination of dynamic pressure; determined by mass proportions of exhaust gas and air in cylinder
- Dynamic Pressure at Piston – Pressure created exclusively by motion of piston
- Static Pressure in Cylinder – Pressure created by the imperfect flow of air into the cylinder; also by the cooling, and therefore volume reduction, of the residual exhaust gas in the cylinder
- Total Pressure in Cylinder – Combination of Dynamic and Static pressures in cylinder

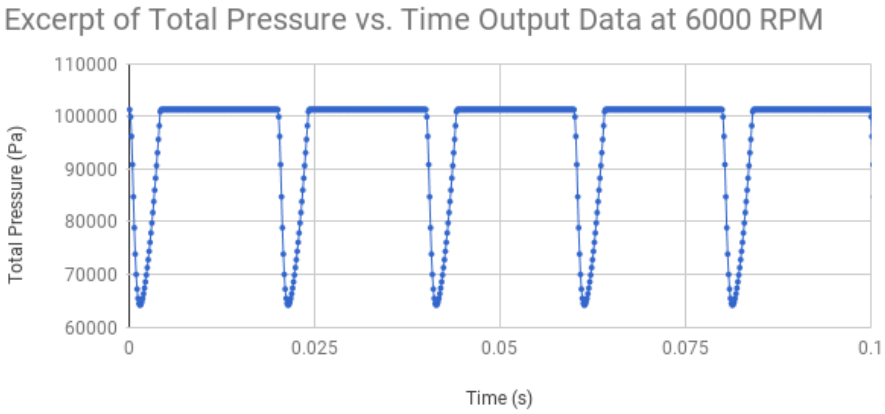

Figure 28: Excerpt of Pressure Output Data from Pressure Wave Spreadsheet

This model also makes several assumptions to simplify calculations for the available data and one-dimensional nature of spreadsheet calculations. These assumptions are acknowledged to potentially have significant effects on the output of these calculations, but have been excluded due

to a lack of information or inability to sufficiently characterize these phenomena with the current form of the simulation model. All known assumptions are listed below:

- Piston stroke follows sinusoid pattern
- Intake valves open exactly at TDC,
- As in valve duration figure, 1 mm lift is minimum for valve open
- Intake valves open and close exactly according to sinusoid (cam profile unknown)
- Airflow into cylinder is proportional to piston stroke, propagation delay only exception
- Due to the time scale of the intake stroke, propagation delay is non-negligible
- Propagation delay is primarily governed by temperature and specific heat ratio of air, not exhaust gas (to avoid circular dependency with Mixed Gas Temperature formula)
- Airflow into cylinder is restricted proportional to intake valve openness
- Heat transfer between intake air and exhaust gas is instantaneous
- Intake air density is constant for purposes of mass flow determination
- Intake air has constant specific heat (Cp) for determination of Mixed Gas Temperature
- Exhaust valves are fully closed throughout intake stroke
- Some exhaust gas remains in cylinder at beginning of intake stroke, volume equal to TDC cylinder volume
- Residual exhaust gas is at 1atm pressure, 1100K temperature (mid-high temp for exhaust gas temp sensor)[RJB1]
- Fuel injection is ignored; intake air is assumed pure
- Due to assumed flow conditions, pressure in the cylinder rises above atmospheric pressure for a non-negligible portion of the intake stroke, and our total pressure formula includes a cutoff to compensate for this and only allow cylinder pressures at or below atmospheric pressure. This has the effect of shortening the pressure pulse for certain simulation conditions.

Due to the sheer quantity of different steps involved in the pressure wave calculations, it is unfeasible to include a full description of these formulas and their interdependencies here. All formulas not related to the physical operation of engine components rely upon ideal gas laws or simple thermodynamic formulas regarding the mixture of different gases, and can be found in the textbook Fundamentals of Engineering Thermodynamics by Moran and Shapiro.

Model Calibration

Once the pressure wave calculation spreadsheet was complete, engine tuning data from the 2016 car was used to calibrate the volumetric efficiency calculation model by adjusting the pressure wave model spreadsheet. This was done using a coefficient left in the spreadsheet specifically for this purpose, named the "Volume Air Moved Coefficient" (VAM). This coefficient is included in the formula for "Volume Air Moved," which determines the rate at which air is drawn into the cylinder, and due to its placement in the formula essentially scales the volumetric efficiency guess to compensate for errors in the calculation method. Since the determination of cylinder pressure is a complicated problem, and requires the assumption of many characteristics of the flow entering the

cylinder, this coefficient was included in the spreadsheet as a simple way to scale the pressure response as necessary. The VAM Coefficient was calibrated by comparing the volumetric efficiency calculated by the simulation method to the values calculated for the 2016 intake, the only test item that had been set up to test in SWFS at that point.

The data file used for comparison was a spreadsheet of engine tuning data left by the 2016 team. This data seemed to have been exported from the ECU controller software, and included calculated values for volumetric efficiency determined by sensor readings during dynamic engine testing. Team members present around the time this data would have been taken were contacted, and they confirmed that this data file does correspond to tuning data from the 2016 intake.

To gather comparable data from the simulation results, data was exported using the Surface Goals set to monitor the simulated airflow into the cylinder. Using the "Goal Plot" function in SolidWorks, volume flow rate data was exported from the Surface Goals to Excel. On opening the data files, it was noted that charts of volume flow rate across the target surfaces showed continuous flow throughout the simulated time span rather than intermittent flow only when the intake valves would be open, as shown by Figure 29.

Commented [21]: update

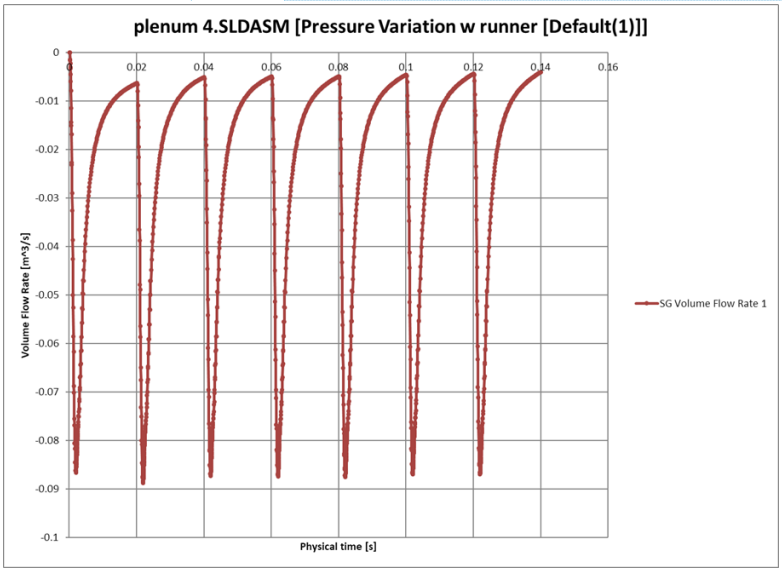

Figure 29: Goal Plot Result for a 6000 RPM Calibration Run

Research into the problem found that it was impossible to temporarily block pressure boundaries in SWFS, making it impossible for the simulation to match the behavior of a real intake valve. Although this issue may have affected the accuracy of the simulated volumetric efficiency results throughout calibration and testing due to the effects of valve closure on airflow, the calibration process should have compensated for any such error. As the volumetric efficiency output by this model is also used for comparison rather than specific values, this issue should ultimately have little effect on the validity of the model for its intended purpose.

To extract volumetric efficiency data from the exported volume flow rate data, simple Excel formulas were used to numerically integrate the total volume transferred into the cylinder over the simulation period. Using formulas used prior to determine valve openness in the pressure wave spreadsheet, periods when the intake valves would be closed were excluded. The first cycle of the data was then manually removed to exclude any startup transients, as well as the last cycle if it was incomplete. The number of complete combustion cycles in the simulation period was then manually counted by observing the result graphs, and was used to find the average volume flow per intake stroke. This average volume transfer per cycle was then divided by the displacement of the engine to determine the volumetric efficiency of the simulated intake. If this simulated volumetric efficiency differed from the Volumetric Efficiency Guess entered into the pressure wave calculation spreadsheet by more than two percent, the Guess value in the spreadsheet was changed to the average of the previous Guess and simulated values. This process was repeated until the results converged on one Volumetric Efficiency, which was then compared to the corresponding value for that RPM from the 2016 tuning data. If the two differed by more than two percent, the VAM Coefficient was adjusted, and iterative testing was repeated until the modeled result matched the physically estimated value.

This lengthy process of simulation, comparison, and convergence was repeated for 2000, 4000, 6000, 8000, and 10000 RPM, to provide five VAM Coefficients across the RPM range that would later be used for intake design testing. For the many simulation runs required, time was a key constraint, so a time period of 0.14 seconds was used for all runs during the calibration process aside from the 2000 RPM runs, which used a period of 0.25 seconds. Despite their brevity, these periods were deemed acceptable as simulated volumetric efficiency was averaged over four combustion cycles for the 4000 RPM runs, or three cycles for the 2000 RPM runs, which was adequate for the degree of accuracy sought. Additionally, for the 2000 and 4000 RPM test runs, the resulting data varied little between cycles, so the averaging aspect of the calculation method was not essential to the accuracy of the resulting volumetric efficiency figure. For the 8000 and 10000 RPM tests, the volume transferred in each cycle varied more, but the large number of cycles simulated countered this issue. With these time periods, each simulation run took between 20 and 40 minutes to run.

Once values were determined for the VAM Coefficient for the five RPM levels tested, the curve fitting function in Excel was used to create a polynomial fit, and this formula was then entered into the cell in the spreadsheet where VAM coefficient had previously been entered manually. With this step, the volumetric efficiency simulation model was considered complete and calibrated from 2000 to 10000 RPM. The behavior of the model between the calibrated RPM values has not been characterized, but calibrating the model at finer intervals would take an excessive amount of time, and allowing for the use of intermediate RPM values should provide additional opportunities for simulation comparison. The team also acknowledge the fact that the accuracy of this method may not hold for intake models other than that of the 2016 car, as the one it was calibrated for. Based on the results observed during testing, this simulation model seems to produce error within plus or minus two percent with the intake it was calibrated for, so it should produce data well within a usable degree of accuracy for comparisons of different intake designs at the same RPM.

Prototype Intake Design

Now that the simulation method for comparing the volumetric efficiency of different air intake designs had been completed, the process of designing the first prototype intake could begin. At this point in the development process, the team had almost fully prepared the engine for benchtop testing, so the prototype intake had to be designed and manufactured on a tight time budget. To make this possible, only two major designs were modeled and simulation tested, with specific RPM ranges in mind and a heavy reliance on "ideal" component proportions derived from earlier research.

The first component modeled after completing the simulation model was the throttle body, an electronically controlled Bosch unit with a 40mm throttle blade diameter. A technical drawing of this throttle was found online after some brief searching, and once the part number and some of the dimensions were confirmed, the model was designed according to this drawing. On the technical drawing found, nearly complete dimensions were given for the components of the throttle in the direct path of airflow, but only general dimensions were provided for the external portion of the body. The shape of these external components was approximated beyond the given dimensions allow for precise packaging, if necessary.

This throttle model was completed in two pieces, the body and the vane, to allow for simple adjustment of throttle vane angle via an assembly constraint if desired during flow simulation testing. After checking the effect of the throttle vane on flow conditions with some test runs, and finding its effect to be negligible when over 60 degrees open, the angle adjustment functionality has not yet been used again, with all testing simulating "wide open throttle" (WOT). When testing the 2016 intake, the throttle body had not yet been modeled due to negligence of its potential to affect flow patterns in the intake, but after seeing this result confidence in the simulation model was renewed.

After completing the model of the throttle body the bellmouth was modeled next, following the "optimized" profile found in research. Since the throttle body had no bolt holes, only a small lip on its inlet side, likely intended for the direct attachment of air filters, the team decided to attach the bellmouth with a silicone tubing coupler and some hose clamps. To adjust its design for this purpose, the outer profile of the bellmouth exit was made to match the end of the throttle body, adding a 10 mm straight section after the elliptical profile as well as a rounded lip to improve traction on the silicone coupler.

After completing the bellmouth, the restrictor was modeled next, again using the optimized values found during earlier research. While modeling the restrictor, some of the angular dimensions mentioned in the restrictor design report were unclear, but after comparing images from the report to the profile of the modeled restrictor, they seemed to match. There was also some confusion when choosing an exit diameter for the restrictor as, unlike the entrance which mates to the throttle body, the exit of the restrictor does not need a specific exit diameter since it vents directly into the plenum. A diameter of 41mm was chosen for the restrictor exit to match the measured diameter of the integral intake runner, and to thus allow the restrictor to be directly attached to the integral runner to test the effect of zero plenum volume on volumetric efficiency (63% at 6000 RPM, 46% at 8000 RPM).

Since no conclusive evidence had been found for the advantages of any particular plenum shape, it was difficult to decide where to begin with the plenum design. In previous years the WPI team had used several different plenum shapes and volumes, and due to their varying success no trends could be easily determined. In the absence of any clear idea for how to proceed, plenum design began with the two simplest shapes that came to mind; a sphere and a cylinder. For each of these shapes, plenum volumes of 1, 5, and 10 times the displacement of the engine were modeled. Each plenum included a bellmouth leading to the runner for each using the same optimized elliptical profile as for the entrance bellmouth. For the spherical plenum, this meant tapering from the runner and restrictor until the bell profile became tangent to the sphere. For the cylindrical plenum, the elliptical profile was raised into the plenum volume slightly to include the radius on the outside of the bellmouth entrance, as research had shown that this slight alteration could offer additional benefits to airflow through the plenum. The cylindrical plenum was also given a protruding radius where the restrictor entered, to hopefully smooth the entrance of air into the plenum in a similar way. These design choices were made primarily through arbitrary intuition about what looked "streamlined" due to the total lack of information about what makes a "good" plenum design. All plenum designs were also given a "zero-length runner" by directly attaching the elliptical bell taper at their exit to the integral runner model, since there was not yet a clear concept for the shape the runner would need to be to package the intake properly on the car. Figure 30 shows cross sections of the spherical and cylindrical plenum designs a 5x displacement volume.

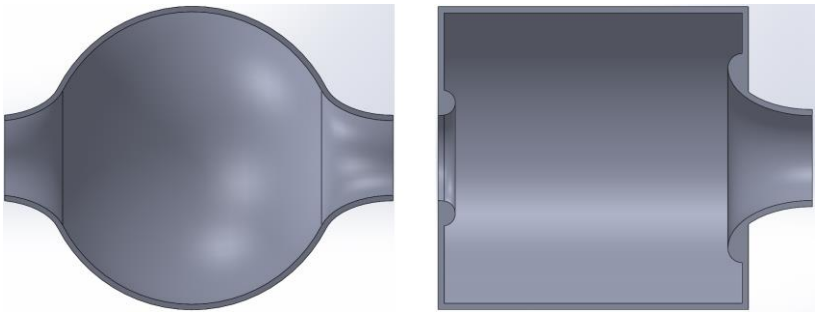

Figure 30: Plenum Prototype Design Cross Sections, 5x Engine Displacement Volume

To vary the volume of the spherical plenum, a model was made to represent the volume contained by the plenum, and the SolidWorks "Mass Properties" tool was used to check the volume as the radius of the spherical portion was varied. For the cylindrical plenum a similar process was followed, but only the length of the cylinder was varied to change its volume.

In addition to these components, another model was made of an arbitrarily shaped volume to place around the intake bellmouth. In SFWS, the inside surface of this volume was set as an environment pressure boundary to simulate unrestricted airflow from the atmosphere. Setting this surface as the entrance pressure boundary instead of a plane across the entrance of the intake is the only major difference between the SWFS setup for plenum testing relative to the configuration used

for model calibration. Figure 31 shows the SWFS test configuration for plenum design, including the free air bubble.

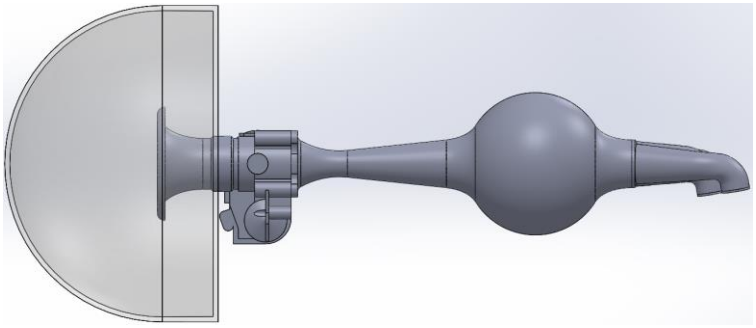

Figure 31: Plenum Design Simulation Assembly, Including Free Air Bubble

After these components were assembled into a continuous intake, simulations were run for all configurations at 6000 RPM, beginning with the 1x displacement spherical plenum and continuing through to the 10x displacement cylindrical plenum. The results observed for the volumetric efficiencies of these configurations proved somewhat confusing, as the spherical plenum design remained nearly constant at 60 percent efficiency for all volumes tested, and the cylindrical plenum produced volumetric efficiencies of 70 percent, 67 percent, and 64 percent for the 1x, 5x, and 10x volumes, respectively. After re-running simulations for the cylindrical plenum designs, the results were confirmed – the smallest of the cylindrical plenum designs was the most efficient. While the conclusions of research on the subject had shown that a larger plenum volume was preferable for volumetric efficiency, the simulation results had shown the opposite, with proportionally equivalent drops in efficiency from the 1x to 5x displacement volumes, and from the 5x to 10x volumes. Testing the cylindrical plenums again at 8000 RPM only confirmed these results, with volumetric efficiencies of 66 percent, 60 percent, and 58 percent for the 1x, 5x, and 10x volumes. Above all, it was clear that the spherical plenum design was not competitive, with consistently low efficiencies for all volumes, but the team was still hesitant to follow through with a plenum design that ran counter to the theoretical and research-corroborated trends, even at a prototype level.

Modification and Manufacturing

At this point in the design process time was running out, and a prototype intake was needed as quickly as possible to allow engine testing to begin, so the cylindrical plenum design was chosen for manufacturing. The team chose to build both 1x and 5x displacement versions of the cylindrical plenum due to uncertainty about the accuracy of the simulation model, and the higher overall efficiency the cylindrical design had shown relative to the spherical version. As further testing in SWFS would have been preferable before choosing a prototype design, the team intends to take extra time in C and/or D Term to determine if a better, feasible plenum design exists, especially if the existing prototype designs perform notably more poorly during engine tuning than designs from previous years.

To ensure the intake designs would be completed as quickly as possible, 3D printing was chosen as the means for making the prototype intakes. Brief consideration was given to the possibility of machining some of these parts from aluminum, or molding them from fiberglass, but due to the complexity of these processes, 3D printing would likely be the simplest and fastest way to build prototypes. To make sure the parts would fit into the build volume of the printers that would be used, those being the Ultimaker 3 and MakerBot Replicator 2, the intake prototypes were broken down into 7 parts, which would later be rejoined by couplers and epoxy resin:

- External Bellmouth
- Restrictor Top Half (from bolt flange for throttle body, to just past the choke point)
- Restrictor Bottom Half (exit cone)
- Plenum Top
- Plenum Body and Bottom
- Runner Bellmouth
- Additional Runner

The first six of these components were produced by modifying and segmenting existing parts used for simulation testing. As it was preferable to attach a standard air filter over the bellmouth entrance instead of constructing a filter, a 15 mm cylindrical extension was added to the radius at the bellmouth entrance, to provide space for the cylindrical flange and hose clamp of a standard filter shape. Although it was not initially intended for the bellmouth to have an outer diameter consistent with conventional air filter flange diameters, the optimized profile happened to produce a diameter of almost exactly 4.375 inches, making it easy to find a matching K&N air filter (model RC-9890).

To allow it to be printed standing upright, and thereby increase the accuracy of the print, the restrictor was split into two pieces with a flanged joint between the two. The bolt flange to attach it to the throttle was increased in thickness, and at the plenum end a cylindrical extension was added to allow for a stronger joint with the top of the plenum.

The plenum was split into top and bottom, with both parts gaining thicker walls for reinforcement against the pressure waves they would experience, as well as another flanged joint to locate the top and bottom together. Two versions of the plenum bottom piece were modeled, one for each of the two volumes made.

The internal bellmouth leading from plenum to runner was also made into a separate part from the plenum body, with its end receiving a similar cylindrical joint to the plenum end of the restrictor. This joint was deliberately made loose to allow for some variation in the part dimensions due to shrinkage during printing. The end of the bellmouth that had previously attached directly to the integral runner was replaced by an extension with a 30-degree angle, and a rounded lip identical to that on the external bellmouth and throttle body. Attached to this extension by way of another silicone coupler is the only portion of the intake not 3D printed, that being the lower runner section.

Compared to the rest of the intake, the lower portion of the runner, which makes the last 90-degree bend to enter the intake port of the engine, is far closer to both the engine and the exhaust, and it must also include the fuel injector mount. Due to the fragility of 3D printed plastic when faced with the chemical and thermal stresses this part would face, it made more sense to

construct this lower portion of the intake runner out of thick-wall aluminum tubing, and to weld the fuel injector mount in place. Thick-wall tubing was chosen to ensure a better fit in the existing intake connection fitting on the engine, and to reduce the chance of accidentally melting through the tube while welding the injector mount in place. The injector mount was designed similarly to the design used in previous years, with a hole for the injector and two parallel threaded holes for small bolts to hold the injector in place.

With the full intake assembly modeled in SolidWorks prior to manufacturing, an additional set of SWFS simulations was run to verify that the changes made to the design for manufacturing, particularly regarding the runner extension, would not significantly alter the volumetric efficiency of the plenum design. Simulation runs were done for 6000 and 8000 RPM, resulting in volumetric efficiencies of 77 percent and 72 percent, respectively. Despite still not having any simple way to verify the results of the simulation model, these results seem reasonable relative to each other, with higher RPM reducing the efficiency of the intake similarly to earlier tests. Overall, the team is pleased with these results, and if they are proven correct during engine tuning this will represent a significant improvement in intake design over the 2016 vehicle, both due to the slight improvement in efficiency and the significantly smaller physical volume occupied by the intake.

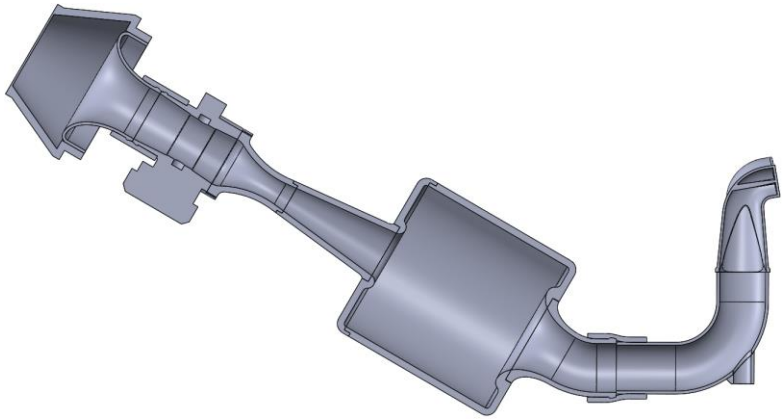

Figure 32: Cross Section of Complete Prototype Intake with 5x Volume Plenum

Exhaust Tuning

Exhaust tuning was the third avenue for optimization discussed, and one eventually deemed as similarly important to intake design. As with the intake, exhaust tuning has the potential to greatly impact engine performance due to airflow concerns, and like the intake it faces issues of restriction. Outside the realm of FSAE, many high performance vehicle designs use large diameter exhaust pipes and cleverly shaped headers to minimize the physical confinement of exhaust gases, and the back pressure at the exhaust valves as a result. As addressed in the Cal Poly engine development report, reduction of back pressure due to exhaust gas stagnation is a key contributor to improved engine performance. Similarly to the intake runner, resonance tuning is one way that exhaust

efficiency is typically increased, and some companies such as FMF have built a business around providing precisely engineered exhaust headers for to improve the performance of motorcycle engines. Once the team learned that professionally designed aftermarket exhaust headers were available for the WR450F, one was ordered almost immediately. Purchasing this pre-made part significantly reduced the design and manufacturing demands placed on the team, thus halting research into exhaust tuning to allow the team to allocate manpower elsewhere.

Suspension

The purpose of a vehicle's suspension is to maintain each tires maximum contact patch with the ground over bumps and during cornering. For road going vehicles, both driver comfort and vehicle performance need to be considered, meaning that all road cars are a compromise between a soft comfortable suspension, and a firm and responsive suspension. In order for a suspension system to achieve this, suspension geometry, along with spring and damper rates, need to be optimized (1). Additionally, parameters such as vehicle weight, center of gravity, tire selection, and road surface must be considered.

For road racing applications, such as in this project, driver comfort is only marginally considered, and only to the extent as to mitigate driver fatigue while racing. Additionally, as road racing usually occurs on smooth surfaces, large ground clearances and soft, bump absorbing suspension are not needed. Aerodynamic factors also play an important role in suspension design, as under trays must remain as close to the ground as possible without bottoming out, and because increased downforce will change the effective weight applied to the suspension.

Design Parameters

In order to design a well performing suspension, one must determine the conditions that the suspension will be subject to, as well as the key characteristics you would suspension to exhibit. Suspension design is often a balancing act, as if one changes a parameter to increase one set of characteristics (ex. Steering feel) it can negatively affect another characteristic (instability under breaking). By listing the most important characteristics, and the factors that affect them, it will allow for a better understanding of the ideal way to set up the suspension. Furthermore, in an ideal case, suspension design should happen in parallel with the vehicle's frame design, as were the suspension mounts to the frame is extremely important. Figure 33 shows the differences in frame designed in parallel with the suspension and all other car components, and a frame that was not.

Commented [22]: change if below figure # changes

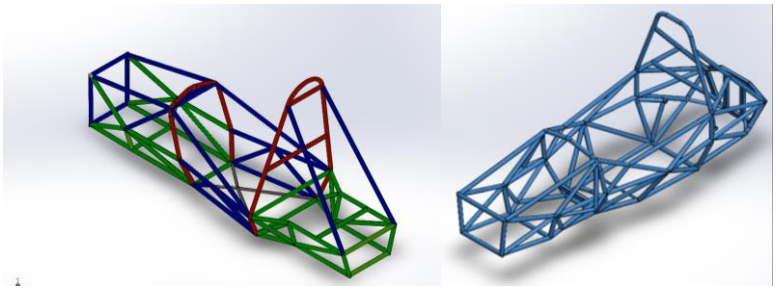

Figure 33: WPI Frame before Suspension (left), and with Suspension (right)

The WPI frame is easier to manufacture, and is simple and lightweight. However, in order to attach the differential, engine and other components, more complicated and heavy mounts needed to be manufactured. For future redesigns, wheel size, suspension type, differential, etc. should be chosen before the frame is designed, and all assembles should be designed in parallel.

Determining Suspension Geometry

Since each suspension parameter affects multiple aspects of the suspension geometry, it is often beneficial to start a suspension design using key parameters to define suspension geometry. For this project, multiple 3D sketches were created in SolidWorks to determine suspension geometry based off of specified parameters (see Figure 34). While this project was to design an unequal length double wishbone suspension, the same principles can be applied to any kind of suspension setup.

Commented [23]: change if below figure # changes

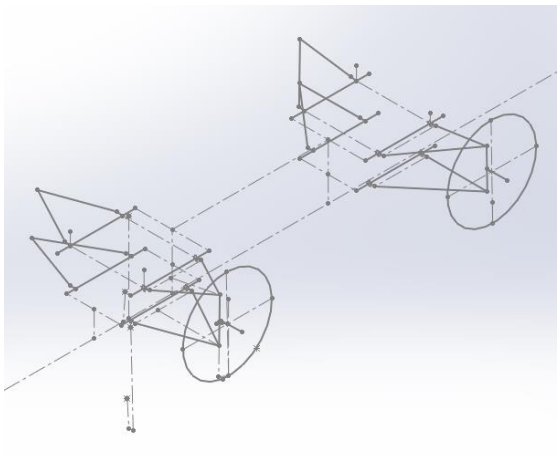

Figure 34: Wireframe model of suspension geometry

The most difficult part of suspension design is choosing which parameters or characteristics are ideal. The key is to keep this one thing in mind:

The suspensions job is to give each tire the maximum amount of grip possible in any scenario (braking, turning, accelerating, corner turn in, slaloms, etc)

While this is much easier said than done, it always needs to be kept in mind during the entire design process. For Formula SAE, the place to start is **TIRE DATA** from Milliken Research Associates (Milliken, 2001). Without tire data there is no way of knowing what half of the suspension values should be (besides comparing to past years and using general rules of thumb). Without this data, the suspension will be entirely guesswork and validating designs to the judges will be very difficult. On top of this, the suspension will most likely not be an ideal design, and skid pad scores will show this.

This suspension was designed without tire data due to time constraints, and so all values chosen should be checked over and optimized using the appropriate tire data.

As noted before, the vehicle frame and suspension should be designed in parallel. This will allow the suspension mounts to be placed in more ideal locations, and the frame can be designed to comply with all rules at an ideal ride height. This was not done for this project, hence the suspension mount points were for the most part already determined. Additionally, ride height was determined as well, due to FSAE rule T3.24.3, which forced our car to have an excessive ride height of 5.3in. Since the frame was already designed, the first step in this project was to create a 3D sketch of the suspension mounting bars on the frame, and determine where on these bars the suspension should mount, shown in Figure 35 below.

Commented [24]: change if below figure # changes

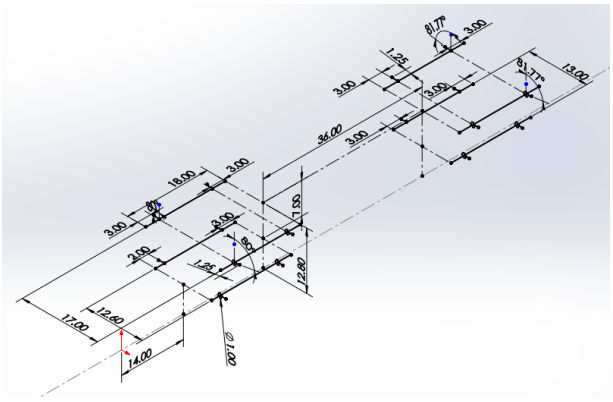

Figure 35: Suspension mounting bars with tab locations

At this stage, any mount locations were not necessarily final, as things like wheel clearance during cornering and A-Arm forces could cause these locations to change. As an initial location, mounts were placed close to the ends of the suspension mounting tubes to ensure that the tubes would flex as little as possible when loaded by the suspension. In addition, the mount length, shown

in Figure 36 below, was initially guessed at, but was chosen to be 1.25in so that any A-Arm mounting that was used (rod ends, weld cups, etc.) would not contact the frame.

Commented [25]: change if below figure # changes

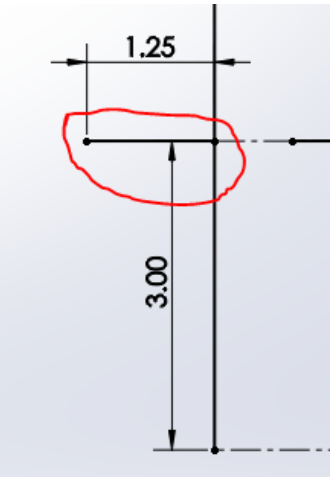

Figure 36: Wireframe sketch of suspension mount point on frame (mount is circled in red)

Once mount points were defined, a 3D "static suspension" sketch was created for the left front and left rear suspension (the final sketch was mirrored to the Right side). At this point a rough suspension shape was defined (see Figure 37), which included A-Arms, Uprights, and wheels (diameter of wheels circled in purple, with a line normal to the wheel diameter to denote the location of the outer wheel face).

Commented [26]: change if below figure # changes

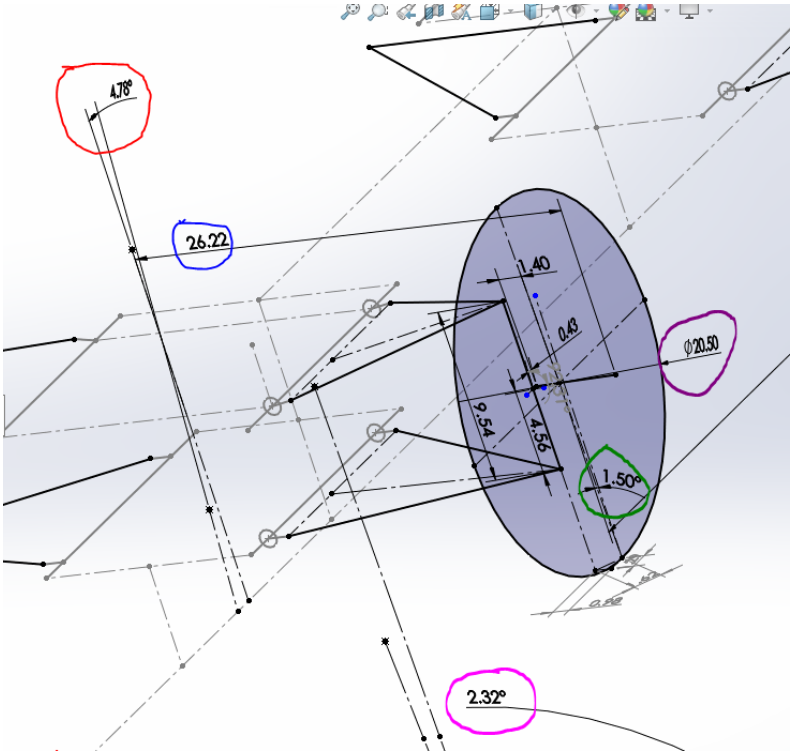

Figure 37: Front suspension wire frame

(Track Width Circled in Blue, Static camber circled in Green, caster angle circled in red, kingpin inclination circled in pink, wheel diameter circled in purple)

From there, reference lines were created to make dimensioning easier, and any known dimensions were added (wheelbase, wheel/tire diameter, wheel width, upright height, and track width). Wheelbase was chosen as 61 inches (close to last year), as this would allow for the shortest car possible (the FSAE rules specifies a wheelbase of 60 inches or more). The reasons for wanting the shortest car possible is that it allows for a tighter turning radius compared to a longer car with an identical maximum front turning angle. Additionally, a shorter car will allow for the rear wheels to follow the front wheels more closely, meaning that the car will have to turn less to get around a cone during competition. One downside of a short wheelbase is that it will make the car more twitchy, and oversteer will be more sudden (think of the speed of a long pendulum compared to a short one). Track width was chosen to be 26.22in (rolled over from 2016), with the justification being that it is as wide as possible while still fitting into our shop and into the back of a standard pickup truck bed. A wide car is beneficial because it means the car will roll less during cornering (less weight transfer from left to right), making the car more stable and allowing the tires to maintain maximum

contact patch. However, the wider a car is, the more it will have to move left to right in a slalom, and will not be able to move side to side on course to maximize corner radius. Rim diameter selection is mainly chosen due to packaging. The rims currently used are 13in diameter by 7in wide and the tires are 20.5in tall and 7in wide (same as last year as it is what is available). This was rolled over from 2016 as our packaging constraints would be similar. Aside from packaging and insuring that the car's brakes are big enough to stop the car, the smaller the rim the better. Smaller rims and tires mean less unsprung weight and less rotational inertia (less unsprung weight and rotational inertia is more important than less sprung weight because unsprung weight means the suspension will be slower to react due to increased inertia, as well as because it can change how a suspension will act compared to an ideal case. Less rotational inertia means the engine will have to work less to accelerate the rotating drivetrain components and can work on accelerating the car.), and also means that the tires will heat up to the ideal temperature faster as there is less surface area to heat up. Upright height was directly taken from 2016, and was chosen due to packaging and time constraints.

From there, variables such as kingpin inclination, rim offset, spindle (hub) length (from steering axis), and caster angle were defined (see Figure 37 above). These variables affect multiple suspension parameters, and so their final variables will result in a balancing act that will create an optimized suspension. Rim offset (see Figure 38) was 22mm, as that was the available offset for OZ racing magnesium wheels. These wheels were chosen because they were thought to be the nearly the same as the OZ racing aluminum wheels (used on the 2016 car) from a packaging standpoint (but with an 8 mm offset difference), while being 2 pounds lighter per wheel (reducing both unsprung mass and rotational inertia).

Commented [27]: change if above figure # changes

Commented [28]: change if below figure # changes

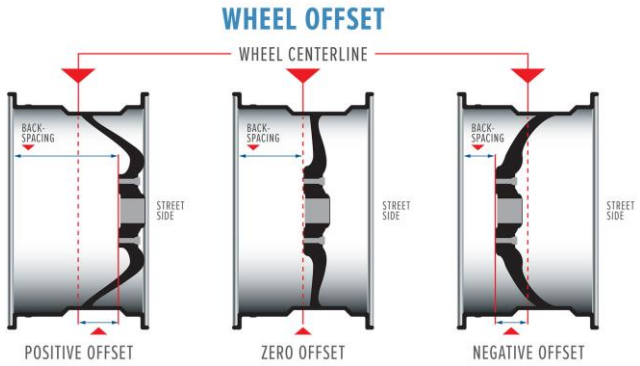

Figure 38: Wheel offset

After purchase it was realized that the magnesium spokes were thicker than on the aluminum wheels, and even with a spacer to make the two offsets identical, the Magnesium wheels would not clear the front brake calipers on the 2016 car. After some design meetings it was determined that brakes would remain the same, and an additional 15 mm would be added to the hub compared to the 2016 car (see Figure 39).

Commented [29]: change if below figure # changes

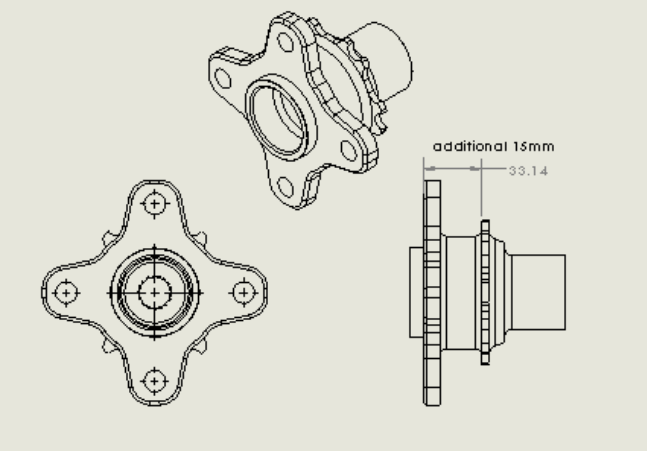

Figure 39: Modified Hub Dimension

Kingpin inclination was set as 2.32 degrees, and caster angle was set at 4.78 degrees (see Figure 37 for dimensions, and figure 6 for definitions). These values were based off research and driver feedback from the 2016 car.

Commented [30]: change if image 3 images above changes #

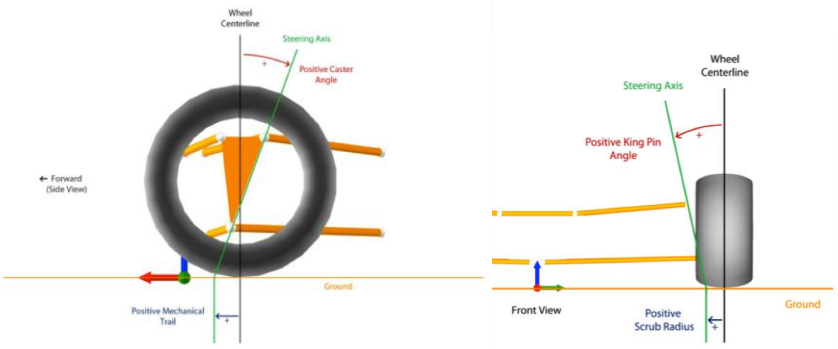

Figure 40: Caster angle and mechanical trail (left), Kingpin inclination and scrub radius (Right)

Both caster angle and kingpin inclination effect steering feel and steering effort (mainly due to scrub radius but also due to other factors) (Kojima, 2011). As the 2016 car was very easy to turn, but had minimal steering feel, it was decided that steering feel should try to be increased at the cost of increased steering effort. Additionally, increased kingpin inclination will result in increased positive camber gain on the cars outside wheel (bad), and increased caster angle will result in

negative camber gain on the cars outside wheel (good to an extent). There are also other factors that are affected (Kojima, 2011). Tire data will make it easier to choose these variables, as the best camber gain for the tires used will be clearer.

Once these variables are roughly defined, reference dimensions were created to show dependent variables such as static camber, scrub radius, roll centers, etc. to help with the selection of the best suspension parameters. Static camber is important for initial corner turn in, and for high speed corners where there is minimal steering induced camber gain, however it will reduce straight line traction as the tire contact patch is reduced (especially important for rear wheels as traction while accelerating is important). Static front camber is 1.5 degrees, and static rear camber is 1 degree. The rear static camber is lower than the front, but in the future the rear static camber should be further minimized (may reduce turn in grip) and replaced with more camber gain due to suspension compression (depending on tire data). Scrub radius (see Figure 6) is a function of kingpin angle, and wheel center point relative to the steering axis when viewed from the front plane. The bigger (more positive) the scrub radius, the more steering effort but the more stability and steering feel. You do not want negative scrub radius as it gives very little steering feel.

Mechanical Trail is a function of caster angle and wheel center point relative to the steering axis. The bigger (more Negative) the scrub radius, the more steering effort and reactiveness to any lateral forces, but the more self-centering and steering feel. Positive scrub radius is bad as it makes the car want to wander and will not self-center.

Once the static suspension sketch is fully defined, a "dynamic suspension" 3d sketch can be created that will allow suspension parameters to be looked at through the suspensions range of motion, such as camber gain due to suspension movement. Additionally, a "dynamic steering" sketch can be created, that allows the front wheels to turn (see Figure 41). This will allow for parameters such as camber gain through turning to be determined.

Commented [31]: change if Figure # below changes

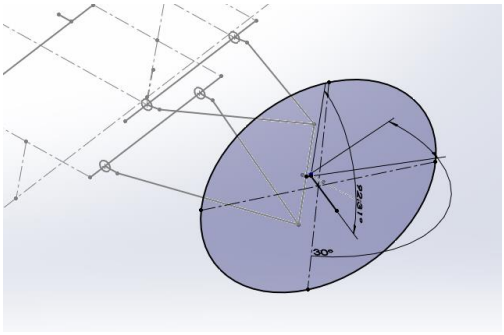

Figure 41: Dynamic Steering and Suspension Sketches

At this point in the design, once the suspension was roughly defined, the "suspension mockup" part, containing all the suspension sketches, can be inserted into an assembly, and wheels, uprights, etc. can be mated to the dynamic suspension and steering sketches to ensure that there are no collisions with any parts (see figure 42).

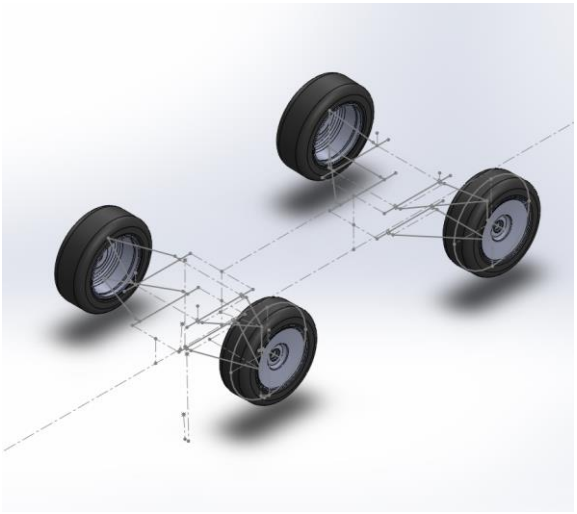

Figure 42: Suspension assembly with "suspension mockup" and "wheel" parts

Once all suspension has been nearly finalized, an "A-Arm tube" sketch can be created that references the static suspension sketch (in some cases the new sketch isn't necessary, but in this case they were needed to make the A-Arms line up properly with the mounting method chosen) (see Figure 43).

Commented [32]: change if Figure # below changes

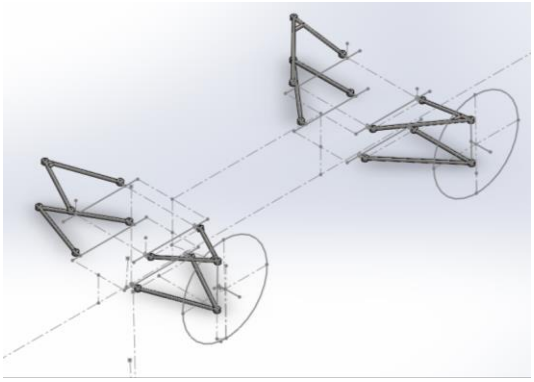

Figure 43: A-arm tube profiles in "suspension mockup" part

A-Arm Design

A-Arm design involved both figuring out geometry and determining needed strength properties. By using the design process outlined in the above section, the geometry portion of A-Arm design was already mostly finished, however there are a few factors that still needed to be determined.

The first step in A-Arm design was determining what type of spring and damper actuation would be used (Pullrod, Pushrod, Direct acting, ect.). It was decided that a pullrod design would be ideal as it would allow for the weight to be lower down than a comparable pushrod design (also because it was used on the 2016 car and worked well). A direct acting suspension was not chosen, as when it had been used in the past the long rod connecting the spring to the A-Arm created a bending moment that fatigued the threads in the end of the damper (see Figure 44).

Commented [33]: change if Figure # below changes

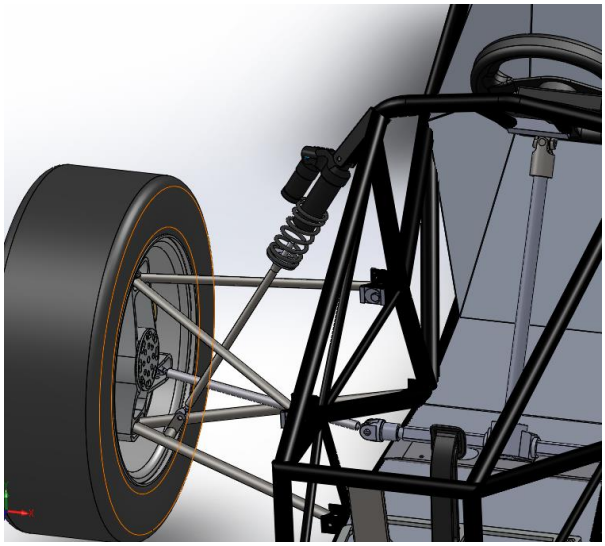

Figure 44: 2015 Front Suspension

(long pushrod created bending moment and wore out shock absorber)

Once this was determined, it was clear that a pullrod tab needed to be mounted to the upper A-Arms. The easiest way to mount the tab was with a crossbar across the A-Arm, which was made as short as possible (while still allowing for it to be easy to weld) to make the bending moment applied to the A-Arm as small as possible (see Figure 45).

Commented [34]: change if Figure # below changes

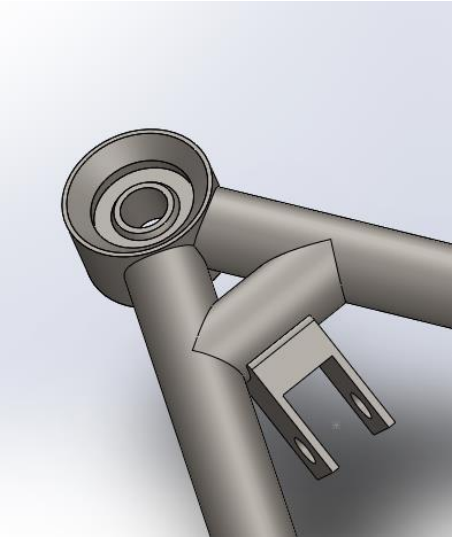

Figure 45: Pullrod Tab and Crossbar (front suspension)

Once this was done, the forces that would be applied during use needed to be calculated, including forces due to Braking, accelerating, cornering, and bump effects. Most teams use 1.5G for the braking, acceleration, and cornering forces, and 3G for a bump force. To calculate A-Arm forces, weight transfer was determined for the 1.5G forces to determine the force on each wheel. From there, the force on each A-Arm where it attaches to the upright was calculated (simple statics problem). Additionally, forces applied due to the pullrod can be calculated (also simple statics problem).

The material for the A-Arms was then chosen to be 4130 steel tubing (carbon fiber tubes would have been ideal, but were too expensive. They were also ruled out as attaching them to the metal threaded ends can be difficult to do correctly, causing them to fail). 4130 tubing was chosen because of its high strength to weight properties, and because tubing has a high resistance to bending. Once the material was determined, we had to determine how they would be made. For tube profiling we chose VR3 engineering, which restricted our tube selection to the sizes offered by VR3. To determine an appropriate tube size, the proposed design of the A-Arms were modeled in SolidWorks. This was done by first creating an A-Arm sketch in the "suspension mockup" part file, creating extrusions to recreate weld cup placement, and then using custom weldments to create the A-Arm tubes. Each A-Arm was exported to a new part file by selecting the tubes and extrusions for each A-Arm, right clicking, and then selecting "EXPORT INTO NEW PART" (see Figure 46). Once each A-Arm has been exported to its own part, FEA was run using the forces calculated previously by hand. The Frame side of the A-Arms are fixed with SPHERICAL FIXTURES (see Figure 47), and the crossbar was fixed from translating in the Y direction (see Figure 48). The forces calculated are applied to the upright side of the A-Arm (see Figure 49).

Commented [35]: change if Figure #s below change

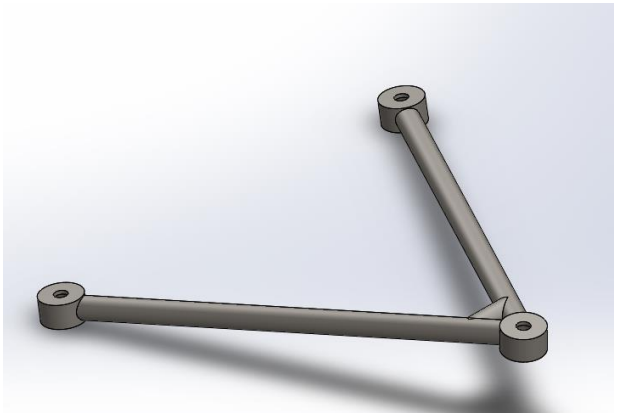

Figure 46: A-Arm part

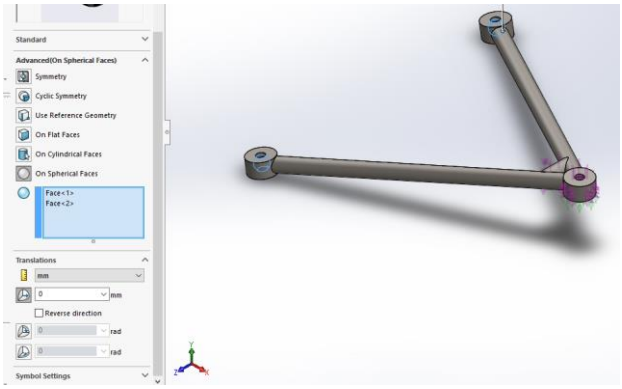

Figure 47: Spherical A-Arm fixtures

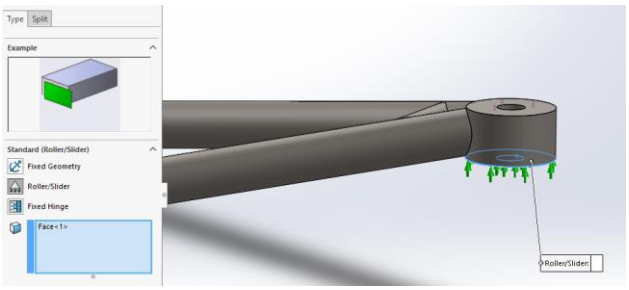

Figure 48: Slider A-Arm Fixture

Figure 49: Forces applied to A-Arm

Tube selection was a trial and error procedure, with the goal to find the lightest tube size that would have a factor of safety of 2 or higher. Ultimately, a tube size of 0.625OD x 0.058Wall was chosen, as it seemed to be a good compromise between strength and weight (was also a slightly smaller size than the 2016 car). Running the FEA was especially difficult, as the tube profiles had issues meshing. To solve this the mesh element size was made very small (.1057in for the front, and for the rear), and a Blended curvature mesh type was used for the front, and a standard mesh was used for the rear (see Figure 50).

Commented [36]: change if Figure # below changes

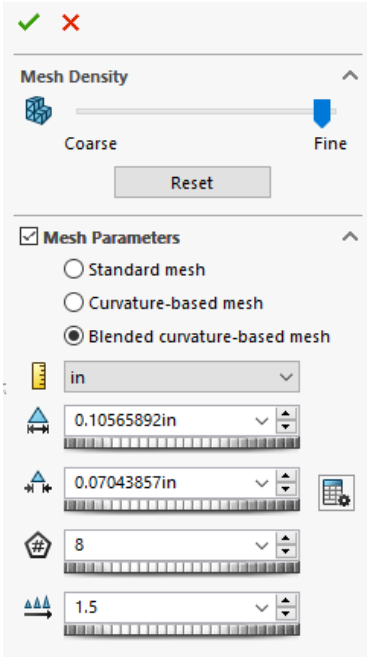

Figure 50: Mesh Parameters for Rear A-Arm

In the future this meshing should be validated for accuracy, as the results may have a large error. Another issue that was encountered was that there were a few points where the stress seemed to be unreasonably high. After looking it over and looking more into stress concentrations, it was decided that the high stress must be an error in the FEA, and so would be ignored (however we did choose a slightly thicker tube size than our FOS goal required to account for potential errors in our FEA analysis).

Rocker Design

The goal of the rocker is to translate the motion of the spring and damper into movement of the wheel. This can be done in a multitude of ways, but the two primary styles are pullrod type and pushrod type (see Figure 51). Pushrod actuated rockers, as the name implies, are actuated by a rod that is pushed by the suspension as it compresses, actuating the rocker and spring. Pushrod designs are usually simple, and linear, however the rockers are usually placed above the suspension, meaning that the majority of the systems weight is placed relatively high up on the car. Pullrod actuated rockers are similar to pushrod activated, except as the suspension compresses it pulls the pullrod, rotating the rocker and compressing the spring. The benefits of this style of actuation is that because the suspension pulls the pullrod, the rocker and spring are usually below the suspension, meaning the majority of the systems weight is near the bottom of the car.

Commented [37]: change if Figure # below changes

For this project, the rocker was designed such that all motion was as linear as possible. This was done because the rocker design for the 2016 (see Figure 52) car had binding issues, as the rockers were not loaded linearly throughout suspension travel.

Commented [38]: change if Figure # 2 below changes

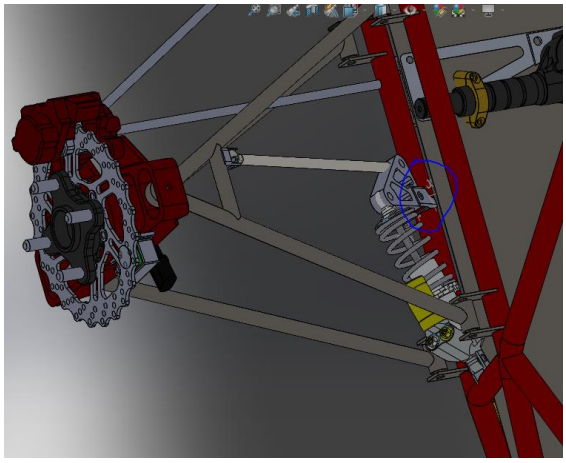

Figure 51: 2016 Front suspension

(Experienced binding and excessive tab wear at tab circled in blue)

The initial design was purely linear, with the frame, damper, and pullrod mounts all being on the same plane (see Figure 52)

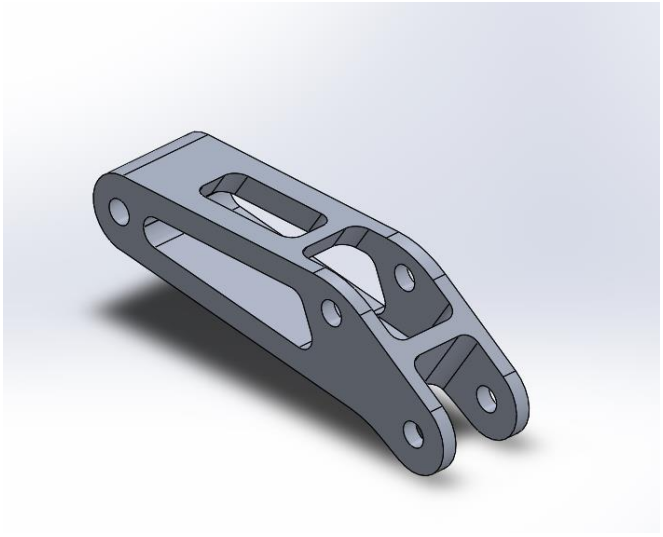

Figure 52: First Iteration of Rocker Design

However, the chosen shock absorbers had 2in of travel, which was also the amount of wheel travel desired. Because of this, the initial rocker idea was discarded, as it would provide 4in of wheel travel or more depending upon the geometry. A new design was created, that allowed the pullrod to be mounted closer to the frame than the spring and damper (see Figure 53).

Commented [39]: change if Figure # below changes

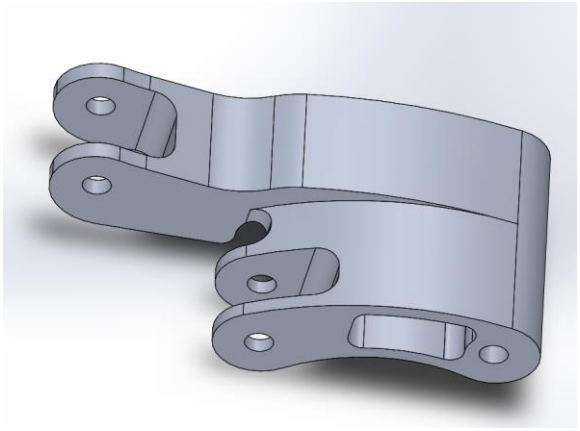

Figure 53: Final Rocker Design

One downside to this design were that because the frame, damper, and pullrod mounts are not in line, creating a moment that could increase the chance of binding. Additionally, this rocker design is slightly heavier than the 2016 rockers.

Steering

The steering system of any vehicle is extremely important because it controls changes in direction of the vehicle. This is useful because there's almost no point during the competition that the car will not need to turn. Weight transfer is another important function of the steering system as well as other car systems.

To be able to optimize the performance of our car at competition, there were a few design parameters that had to be considered. These parameters included steering weight and feel as well as steering wheel angle and tire and rim angles.

The steering system itself is composed of many different parts from the driver input to the movement of the wheels. The steering wheel is the portion that the driver touches and moves to provide input. This then turns the upper steering shaft into the steering box. The purpose of the steering box is to change the direction of the force from nearly horizontal to nearly vertical. From the steering box comes the lower steering shaft which sends force down to the steering rack. The steering rack chances rotational motion into linear motion. The ends of each side of the steering rack are connected to the uprights inside each wheel via a tie rod. The uprights make the wheels and tires turn, thus turning the car.

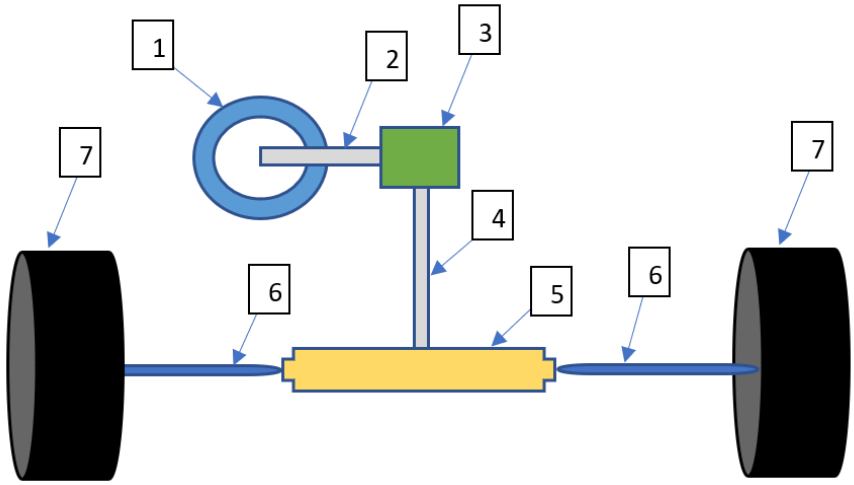

Figure 54: Simplified steering system diagram.

(Steering wheel (1), upper steering shaft (2), steering box (3), lower steering shaft (4), steering rack (5), tie rods (6), wheels/tires (7).)

The steering wheel, being the part that is touched by the driver, is a very important part of the steering system. There are a few parts that were incorporated into the steering wheel because of the rules of the competition as well as making the car easier to use. The first component is the quick release spline on the back of the wheel. This is required to meet the competition rules as having a detachable wheel makes it much easier to get out of the car quickly in case of an emergency. Another design that was incorporated are the pogo pins inside of the quick release spline. These pins are used to connect the electronics in the steering wheel to the rest of the car. The electronics on the wheel include the shifting buttons and a gear number indicator. Besides these components, some other considerations for the steering wheel are the size and shape. The conventional shape of a steering wheel is a circle but a more common shape for racing purposes is an oval or a circle with a flat bottom. These shapes save on vertical size when the wheel is in the straight position as well as providing more space under the wheel for driver legs.

From the steering wheel there is a steering shaft into the steering box. This shaft has a few features that are needed for it to function properly. The first part is the spline on the steering wheel side so it can connect to the wheel. After the spline there is a washer welded on that will help keep the roller bearing in. moving towards the center of the box, there is a keyway cut in to allow the connection of a gear.

Figure 55: Steering shaft from the steering wheel to the steering box.

The steering box is the portion of the system that redirects the rotational motion from the steering wheel down towards the steering rack. The way that the steering box works is with a set of spiral miter gears that are made to transfer motion 90 degrees.

The design of the steering box in the previous car was good but had a lot of room to improve. Overall it was quite complicated, and seemed overbuilt for the forces that it would be facing. There were some portions that were able to be kept though.

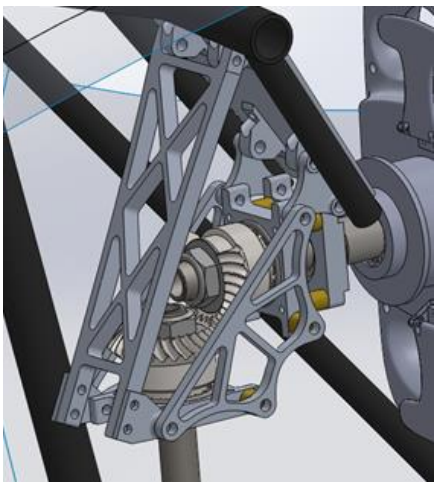

Figure 56: Old Steering Box Design

The miter gears that were used in the previous design were one of the strongest parts of the previous design. While most teams use universal joints, and have success with those, using miter gears gives much less play in the overall system and is also much stronger. Regular miter gears had been shown, in the previous design process, not to have smooth operation as well as having a lot of backlash. The gears that were used before and will be used in this car are spiral miter gears. The spiral cuts allow for much smoother operation as well as backlash mitigation.

Figure 57: Miter gears

Along with the gears, the bearings used in the previous car will also work well in the new design. The tapered roller bearings that had been selected were chosen to handle the axial and radial forces applied to the steering system during the use of the steering system. The bearings that were used before had no issues, so the same ones will be used again.

Figure 58: Roller Bearings

Because we will be using an overall similar steering box design, the pieces that hold the bearings can remain very similar to the way they were in the previous car. The only change that has been made to them has been making them one eighth*check* inch wider to avoid the need for spacers on the side. The reason for getting rid of the spacers is to reduce the number of overall pieces in the system.

Figure 59: The new side panel design

While there were a few good parts of the old version of the steering box, there are also many things wrong with it. The most prevalent is that the overall design is too complex. There are many pieces that are not really needed. There are spacers on each side that add unnecessary pieces as well as a cover plate that is not really justified. As well as being too complex, the mounting points are quite spread out. While this was not a problem for the previous car because of the higher roll hoop, the new car does not have space for spread out mounting points.

The first problem that was addressed while redesigning the steering box was the height relative to the front roll hoop. In the old car, the steering box hung quite far below the roll hoop. Because the roll hoop is lower in the new car, the steering box needed to be raised as much as possible. This was first done by changing the setup of the mounting points from using a top cover with high mounting points to close mounting points on the front most bearing mount. This alone was not enough to pass the template through as it needed. To move the steering box even higher up, the gears had to be flipped over.

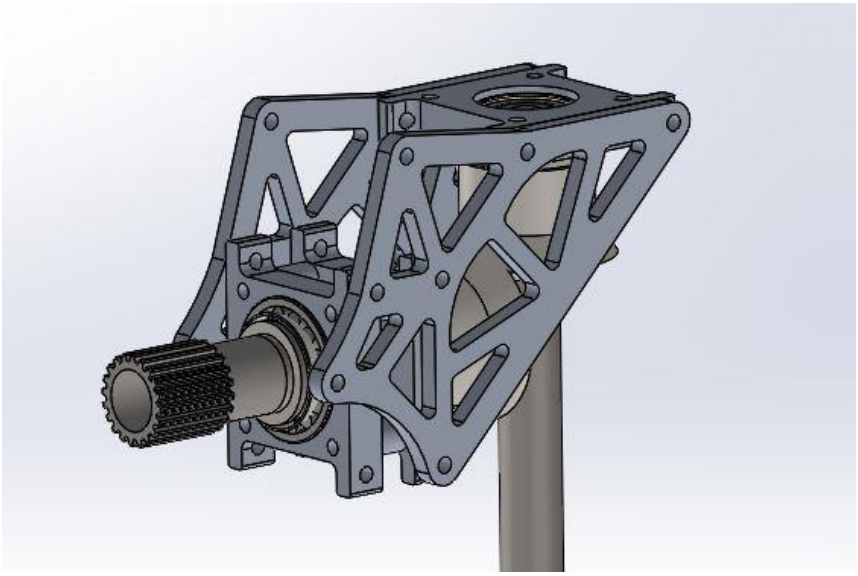

Figure 60: SolidWorks model of the new steering box design

Flipping the gears allowed the template to pass through under the box and still have the steering wheel be below the front roll hoop.

As mentioned before, the steering box of the previous car was overcomplicated. To simplify the box, the sides were completely simplified to be only one piece. There are cuts to allow for screws as well as larger ones to save weight where possible. The sides are ¼ inch thick aluminum. This flat piece was possible because of the widening of the bearing mounts. This extra width negated the need for spacers on the sides.

Another major change to the steering box was the method of mounting to the frame itself. The old steering box mounted to the frame using pipes welded on with a sheet of steel in between. The box mounted via screws through this steel sheet. The new way that the steering box was attached was with vertically oriented steel tabs. These tabs were positioned so the steering box fits nicely in between them and mounts with screws to the side plate. The reason this mounting style was chosen over the previous method was because the previous method was too wide to work with the lower roll hoop. The template that must pass forward through the car has a small cutout in the

top that allows for things that are hanging down. The pipes would have to be much wider than the steering box itself. This caused interference in this template and our car would not have passed.

The steering box with the new mounting style and simplified sides was much simpler to machine. There were only three different parts that had to be made. There were the two side plates, the three bearing mounts, and the spacers between the two front bearing mounts. The two side plates were able to be laser cut because they are only a 2d design. They are also made of quite thin material. The finish on the edges was not very good after getting cut so they had to be gone over with a deburring tool. The bearing mounts were CNC machined because they were a more complex design with 3d features. These parts also needed to have a high level of precision to ensure a pressed fit of the bearing cups into the mounts themselves. To make sure this was the case. The bearing mounts were not machined until after the bearings came in to confirm the dimensions of the parts.

Figure 61: Old bearing mount

The steering column, the shaft from the steering box to the steering rack, will be composed of three welded segments. The topmost portion will be one inch of 3/8*** inch thick steel tubing. This section will have the threads cut into it for the securing bolt as well as the keyway for the gear. The middle section will be a thinner walled tube (1/16). This middle portion is thinner because there are no cuts in it and some weight can be saved with this lighter shaft. The bottom piece is the splined piece to connect to the steering rack. This bottom piece has only two parts. The splined portion as well as a cylindrical portion that the thin shaft will fit into.

The steering rack was a very important decision for the car. The rack that was used in the previous car was the second choice for the team and was only used because the KAZ steering rack was unavailable at the time. Luckily the KAZ was available for purchase for the new car. The KAZ was decided upon using a decision matrix. The matrix from the previous car is shown below. This matrix was used again this year. It was re looked over and was the same as it had been.

Table 3: Steering rack specifications

	Kaz Technologies	Pro-Werks Stiletto
Specification	**Value**	**Value**
Weight	3 lbs	2.74 lbs
Materials	Gear: Steel, Case: Aluminum	Gear: Steel, Case: Aluminum
Rack Travel	3.25 in	4.5 in
Pinion Rotation	246 degrees	315 degrees
Rack Travel/Rotation	4.75 in/rotation	5.14 in/rotation
Mounting System	Outboard Collar Mounts	Inboard Bolt Holes
Sensor Integration	Yes	No
Cost	$670	$328

Table 4: Steering rack decision matrix

		Kaz Technologies		Pro-Werks Stiletto	
Decision Factor	**Weight**	**Score**	**Value**	**Score**	**Value**
Steering Range (Angular)	7	10	70	8	56
Linear Motion Range	9	6	54	8	72
Cost	8	4	32	9	72
Durability	10	10	100	4	40

Weight	4	7	28	10	40
Totals			**284**		**280**

Figure 62: Kaz Technologies steering rack

The tie rods are the link between the steering rack and the uprights. They need to be strong enough to not break yet remain light to keep the total weight of the car down. Hollow steel tubing was selected to fulfill this role. On the ends, there are nuts welded on to allow connection to the tie rod ends as well as providing adjustability. The ends closest to the uprights will have left hand threaded hardware to allow the tube itself to be rotated to adjust the toe angle of the wheels. The rod end on the upright side is an aluminum spherical bearing and the end closest to the rack is an inline booted ball joint. Both ends will be secured in their position on the threads with jam nuts.

Once a steering rack and implementation method had been chosen, it was necessary to determine the max output angle needed at the tires to be able to effectively navigate the course. The FSAE rules state that the minimum radius for the outside of a corner will be no less than 14.75ft through an angle of no more than 135 degrees. Figure 63 is taken from the 2015 FSAE MQP report and shows that when optimized for the best driving line the minimum turning radius needed is 16.5ft. The minimum designed turning radius of the 2015 was set to 15ft. With this in mind and driver feedback from the last car it was determined to that a goal of 14ft would be set for this year.

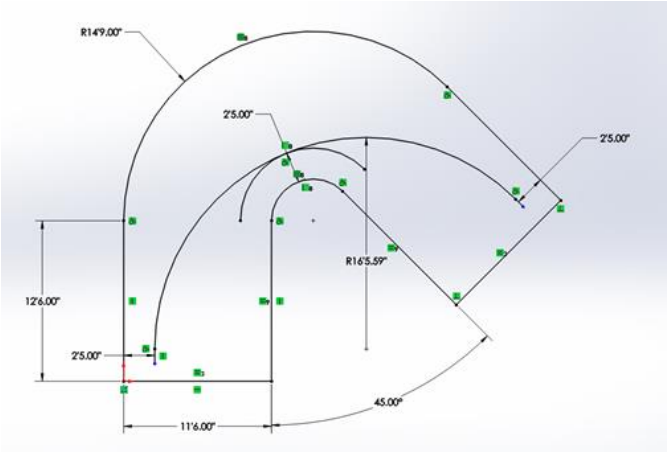

Figure 63: Optimized driver line through minimum radius corner

The next step was to determine the maximum steering angle of both the inside and outside wheel. From the model of the suspension and wheel assembly, it was determined that the maximum turning angle of the wheels with clearing was 27 deg for the inside wheel and 33 for the outside wheel.

Implementation of Ackerman Geometry

When going around a corner the inside and outside tire travel different paths around the same axis of rotation. These paths have different radiuses and require different amounts of angle for the wheels to travel these paths. When the steering wheel is turned both tires don't turn the same amount. For example in you where going around a left hand corner your inside tire could be turned 22deg while your outside tire will only have to be turned 18deg. This is displayed in figure XX. The amount of different in the two angle is determined by your track width, wheelbase and desired radius of curvature.

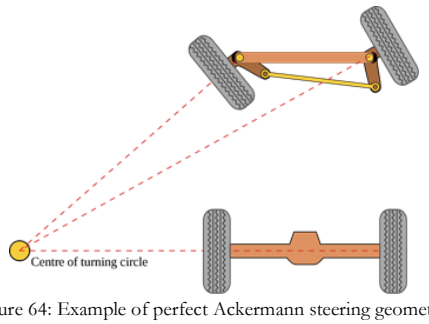

Figure 64: Example of perfect Ackermann steering geometry

However full Ackermann steering is best used in low speed, high grip corners because it eliminated tire scrub reducing rolling resistance. This changes significantly in high lateral acceleration corners, because there is already a significant amount of wheel scrub. In a high speed corner with ackermann steering the inside tire has a minimal load and is forced to a much higher slip angle than effective, creating drag and slowing the car. Parallel steering geometry is when both tires turn the same amount, in this scenario the inside tire is turning less thus leading to less drag. A lack of tire data makes it hard to tell exactly how much slip angle is needed on the inside tire to achieve maximum cornering force, because of this the decision was made to have an adjustable ackermann setup. With driver experience from the 2015 car, which ran 90% ackermann for the majority of its driving, and the recommendation from the book Race Car Vehicle Dynamics the two positions that were chosen where parallel steering and 50% ackermann.

After the decision was made for parallel and 50% Ackerman geometry, the uprights had to be redesigned in order to implement this. Some other considerations when redesigning the front uprights where, manufacturability and weight. The resign started by determining where relative to the steering axis the connection point for the uprights should be. This was done by using a simple sketch of the vehicle characteristics with the know parameters. The KaZ rack has a total travel of 1.63 in either side from center, it is 15.25in long and is placed 3.53in behind the steering axis. These parameters are shown in red in figure 65 below. With these parameters determined values were chosen for trail, shown in black and offset shown in green. The output angle of the inside and out wheel was then determined, show in blue. In order for perfect parallel steering, it was determined, that the trail should be 3.53in and the offset should be 0. For 50% Ackerman steering it was determined that the trail should again be 3.53in and the offset should be 0.65in.

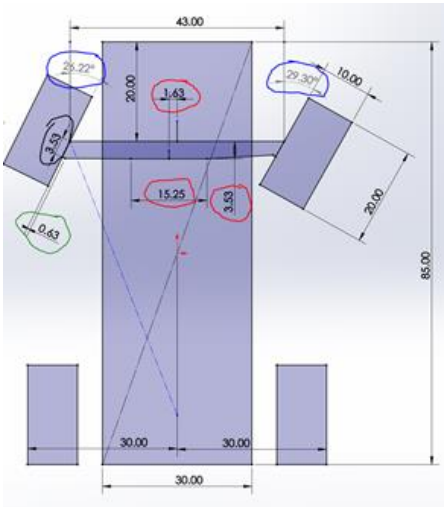

Figure 65: Sketch used to determine steering geometry

Once these values were determined, the first step to redesigning the old front uprights was to delete the original steering pickup, and plot the location of the two points needed. Then create a boss that could easily support this location, while being easier to manufacture. Figure XX shows the redesigned front upright.

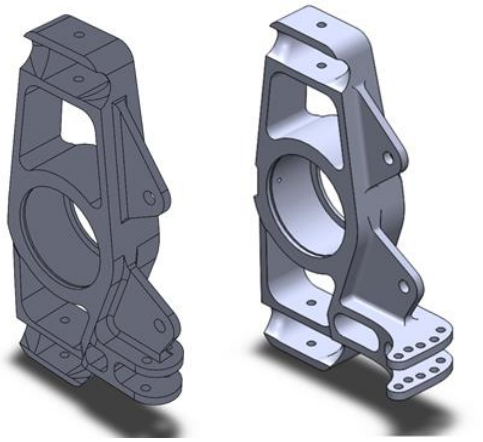

Figure 66: Redesigned front upright (left) next to old upright (right)

Brakes

Brake Components

The braking subsystem is one of the most important subsystems in the car. The braking subsystem needs to work in all conditions to ensure the drivers complete safety. This subsystem will be scrutinized during the dynamic competition events and specifically the skid pad event. The major task examined during that event is that the wheels must all lock at the same time when the car is coming to a stop.

The main components that drive the brakes are the calipers, the front and rear master cylinders, and the rotors. In the 2016 Formula SAE car, the team used Wilwood Billet Dynalite Single Calipers for the front and Wilwood PS-1 Calipers for the rear. The team also used Compact Remote Flange Mount master cylinders with a bore diameter of 3/4 in^2 for the front and 7/8 in^2 for the rear. The master cylinders have reservoirs that are filled with fluid. When the brake pedal is pushed the fluid compresses forcing a pressure on the calipers to squeeze together on the rotors. The rotors are then locked causing the wheels to stop rotating and the car to stop.

As stated earlier, one of the goals for this year's car is for it to be lighter. With this in mind, the team bought new OZ Racing Formula Student Magnesium wheels for the car, which are much

lighter than the old OZ Racing Formula Student Aluminum ones. The magnesium wheels weigh 3.4 kg and have a 22 millimeter offset, while the Aluminum ones weigh 2.45 kg and have a 30 millimeter offset. The approximate weight reduction would then be 0.95kg, which is about 2 pounds per wheel, totaling 8 pounds in weight loss for the car.

The brake subsystem in the 2016 car performed and was designed very well. Therefore it served as a model for this current design. The first design choice was to keep the same calipers and master cylinders as the 2016 car, but change the wheels. However, an oversight when buying the wheels was not knowing the width. The manufacturer would not provide the entire dimensions of the wheel so the width was unknown. When research on the brake calipers was conducted, it was found that the wheels would not properly fit on the car due to interference with the hubs and calipers. The width of the magnesium wheel is slightly larger than the previous aluminum wheel causing it not to fit. Additionally, the offset on the magnesium wheels was 8 millimeters greater than the old aluminum wheels meaning there was less room. Since the new magnesium wheels interfered with the brake calipers, the two options were to change the offset of the hubs or get new calipers and redesign the brake subsystem to cooperate with them.

The hubs were redesigned around both the suspension and the brakes. They originally could not have a big offset due to the suspension parameters. The designed offset was 8 millimeters to match the difference between the 30 millimeter offset of the magnesium and the 22 millimeter offset of the aluminum wheels. This offset was in accordance with the suspension parameters and could not increase any more. Since the width of the magnesium wheels was causing interference there needed to be another 6 millimeters of offset. The hubs could not have a larger offset, so therefore the calipers needed to be smaller.

After examining the hubs and determining that offset cannot be changed, different calipers were explored. As previously mentioned the old calipers were Wilwood Billet Dynalite Single Calipers on the front and Wilwood PS-1 Calipers on the rear. The front calipers were now too big, so smaller ones were needed about 6 millimeters thinner. The following assumptions and equations were used to determine the best calipers and master cylinders to use.

Assumptions:
W_{total} = Total weight of the car including a person = 650 pounds
H_{CG} = Center of gravity height = 14 inches
$F_{braking}$ = Intended Brake Deceleration/ Designed stopping force = 1.5 g's
$L_{wheelbase}$ = Wheel base distance = 60.5 inches

$$W_{transfer} = \frac{W_{Total} * H_{CG} * F_{braking}}{L_{wheelbase}}$$

Brake pedal lever ratio, master cylinder pressure, caliper force, clamping force, and brake pad friction were used to solve for the rotor torque. As shown in the appendix, an excel sheet was used to calculate these values. Once again, the 2016 car was utilized as a model for the design and calculations. In the 2016 car, the front wheel rotor torque was about 558 ft*lbs, and the rear wheel

rotor torque was about 135 ft*lbs. While trying to keep the 80%-20% distribution, different master cylinder areas and different front calipers were experimented with.

Using the above equation on an excel sheet, calipers with different areas were explored. The main goal was to have the ideal 80% to 20% brake torque ratio front to rear and to keep similar values as the 2016 car. The excel sheet was used as the template for exploring different master cylinders and calipers, as it always displayed the above values. When a different master cylinder area was imputed the affected equations would automatically update. This way the torque front to rear ratio was always known.

The first iteration in attempting to solve the interference was to change the calipers but keep the master cylinders the same. The current rear calipers fit on the car with no interference so those would remain the same. Research on smaller front calipers that had smaller widths was then conducted. However, there were no calipers that had a smaller width with the same area. The same area is important to keep the same brake torque ratio. Calipers with different areas were then explored but different rear calipers must also be adjusted to keep the 80-20 ratio. After many different calipers were investigated, no calipers met the requirement without having to change the master cylinders as well. The decision was then to pick both new calipers and master cylinders that would not interfere with the wheels and keep the same brake torque ratio. After many iterations the best option was to change the front calipers to Wilwood PS-1's with an area of 0.99 in^2 and to change the front master cylinder from a 3/4" bore diameter to 5/8" and the rear master cylinder from 7/8" to 1+1/8". This would give a distribution of 81%-19% while allowing the front calipers to properly fit. However, the rotor torque on the front would then be very low at 327 ft*lbs compared the 2016 value of 558 ft*lbs and the rear would be 82 ft*lbs compared 135 ft*lbs. This became the first design iteration and because the rotor torques were significantly lower, other design options were considered.

The next design iteration had a considerable problem. During one of the team meetings it was discovered that the template of Percy would not fit into the car. The frame from the current car is smaller and shorter than the 2016 car, so this was overlooked. Percy's leg was interfering with the brake pedal. This meant that the position of the brake pedal and master cylinders would have to change, or a redesign must be completed. The solution was to redesign the brake pedal and use smaller master cylinders. Changing the current Compact Remote Flange Mount master cylinders to GS Compact Remote master cylinders along with a new brake pedal design allowed Percy to fit. For the size of the master cylinders, the best option was to keep the front bore diameter of 5/8", but change the rear to 13/16". The rear caliper would also have to change in order to keep the ratio. The current PS-1 caliper with an area of 0.77 in^2 needed to have a slightly larger area, so it was changed to a Wilwood SC3 Single Piston caliper with and area of 0.87 in^2. The reason for changing the caliper is because when the front caliper was changed, one of the only options that would fit under the wheel size restriction was the DH4 Dual Hydraulic caliper with an area of 1.77 in^2. However, that caliper has floating mounts instead of traditional lug mounts, which were used on the 2016 car. Therefore, the reasoning was to have the rear calipers also be floating mounts and the SC3 Single Piston is the best option for the size with floating mounts.

The advantages and disadvantages of floating mounts on calipers were then examined. Floating calipers work by having pistons on one side of the disk brakes that move in and out on the bushings like a clamp. When the brakes are applied, the piston forces the inner brake pad against the rotor, while the caliper slides and clamps the outside pad against the rotor. Some of the advantages are the packaging sizes are much smaller, the cost can be lower, and it is easy to build. The size advantage is really important for the team because the old calipers do not fit, and some of the only small enough calipers are floating calipers. The lower cost is also important because the team has a budget and saving money on the brakes allows an increase of funds for other subsystems. Floating calipers can also be easier to build because they have fewer parts. The calipers will be bought pre-assembled, however, fewer parts generally means fewer points of failure.

One of the big disadvantages, however, is that the floating calipers allow a degree of flexibility in the assembly. The brake pads can start to wear over time due to this issue, which means they will need to be replaced more often. This may also change the feel of the pedal when braking.

After reviewing both the advantages and disadvantages the team decided that it is best to purchase the floating calipers. Other FSAE teams use floating calipers, so it is not out of the ordinary and an unreasonable decision. The final components selected were the Wilwood DH4 Dual Hydraulic Calipers for the front and Wilwood SC3 Calipers for the rear. The master cylinders would also be changed the Wilwood GS Compact Remote Master Cylinders with a bore diameter of 5/8" for the front and 13/16" for the rear. Using these parts, the car would have a rotor torque of 585 ft*lb in the front, and 171 ft*lb in the rear. This results in about a 77-23% distribution, which is very close to last year's car. This can be seen in the appendix as well as all the values used to find the distribution.

Even though this was mostly finalized the team decided to abandon this idea after a team discussion. The brake assembly on the 2016 car performed very well and the team was very satisfied with the design. Therefore, this year's team wanted to follow a very similar design. The original plan was to add a spacer to the hub to gain more offset. This would make zero interference between the caliper and the new wheel. However, this would affect the suspension parameters such as camber gain, kingpin angle, and scrub radius. Therefore, the team decided to explore the option of getting new calipers. After iterating and finding a solution, the team determined that it might be just as effective to add a spacer for more offset. The suspension was redesigned and as a result, adding more offset was proved to not greatly negatively affect the suspension. Adding an extra 15 millimeters to the hub would decrease the camber gain, which is already very high, and will not greatly increase steering effort. Therefore the team added a spacer of 15 millimeters to the hub. This made no interference between the wheels. The suspension was already redesigned and made sure that adding the additional offset was not an issue. This was the final decision on the brakes and the team was able to order two Wilwood Billet Dynalite Single Calipers with a piston area of 2.4 in^2 for the front, two Wilwood PS-1 Calipers with a piston area of 0.79 in^2 for the rear, a Wilwood Compact Remote Flange Mount Master Cylinder with a bore diameter of 3/4" for the front and 7/8" for the rear, and four RCV 220 rotors that fit with the brake calipers. Shown below are the front and rear calipers.

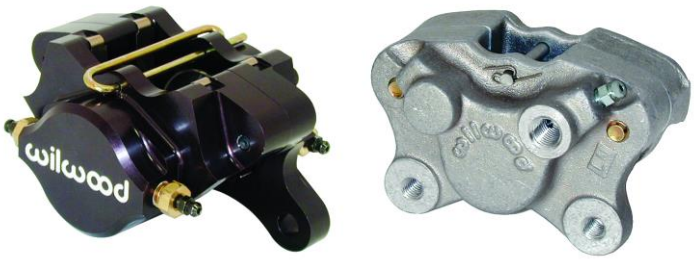

Figure 67: Wilwood Billet Dynalite Single, on the right, and Wilwood PS-1, on the left

Pedal Assembly

Background Information

In a Formula SAE car, the brake and throttle pedal assemblies must be designed for ease of use by the driver, to be lightweight, package easily and allow the for the placement of a template representing the relative size of a 95th percentile male into the cockpit of the vehicle, the size of the template is shown below in Figure 68.

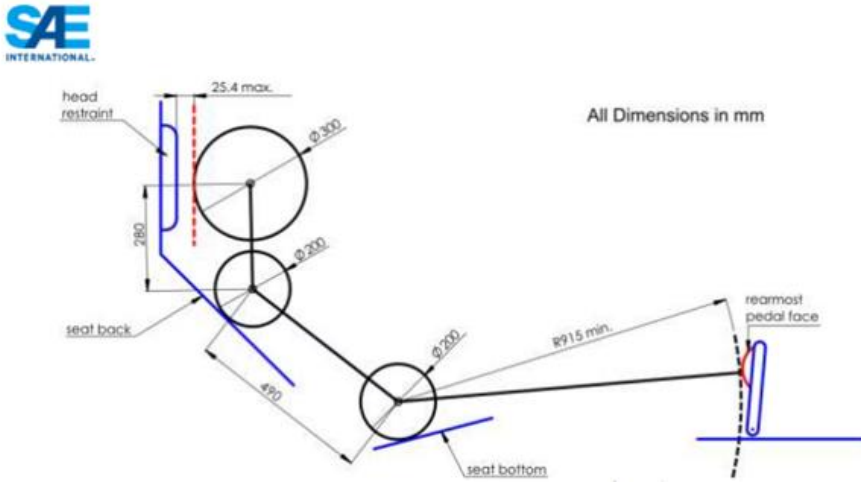

Figure 68: 95th Percentile Male Template Dimensions

As seen above, pedal placement is critical to the fitment of this template in the chassis of the vehicle, there can be a minimum radius of 915mm between the "torso" of the template, which rests in the seat bottom and the rear most pedal face. Failure to meet this minimum requirement or any

other requirement related to the template results in failure of technical inspection, thus the vehicle will not be allowed to complete in any dynamic events.

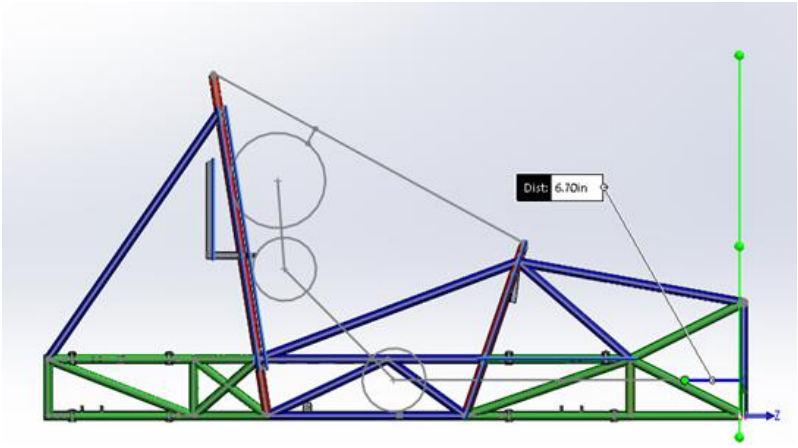

Figure 69: Sketch of 95th Percentile Male Template place in 2017-2018 Frame

Figure 69 above shows the frame design for this upcoming competition, with a sketch of the 95th percentile male template, aptly nicknamed "Percy". Between the end of Percy's foot and the plane defined by the rearmost surface of the tubes constructing the front bulkhead, there is but 6.7" of space to fit the entire pedal box.

Design Process

In the previous two cars built by WPI, for the 2016 FSAE competition and the 2014 FSAE competition, a Wilwood brake pedal/master cylinder assembly has been used. This assembly packaged both master cylinders, the pedal and a balance bar in a relatively small space, with four simply spaced mounting points. This assembly traditionally gets mounted to a large aluminum pedal plate, which also serves as a mount for the throttle pedal, the Wilwood assembly is shown below in f**igure xx**

Figure 70: Wilwood Brake Pedal Assembly used in Previous Years

Initially, the same brake pedal assembly was to be used, it is relatively inexpensive, easy to source and requires no validation as it is a pre-designed component; the only task is to package the assembly in the front of the vehicle. After some searching on FSAE forums, it was determined that would be advantageous to have an adjustable (fore and aft) pedal assembly, instead of changing seat inserts based on the driver, which has been done in the past. The pedal assembly weighs much less than a fully outfitted driver, moving the pedals a few inches fore or aft would have much less of an effect on vehicle C.G. versus moving the driver. A pedal plate, like that of previous years was designed and mounted on sliding rail system in the frame (in SolidWorks) as a proof of concept, this first iteration of a pedal box is shown below in Figure 71.

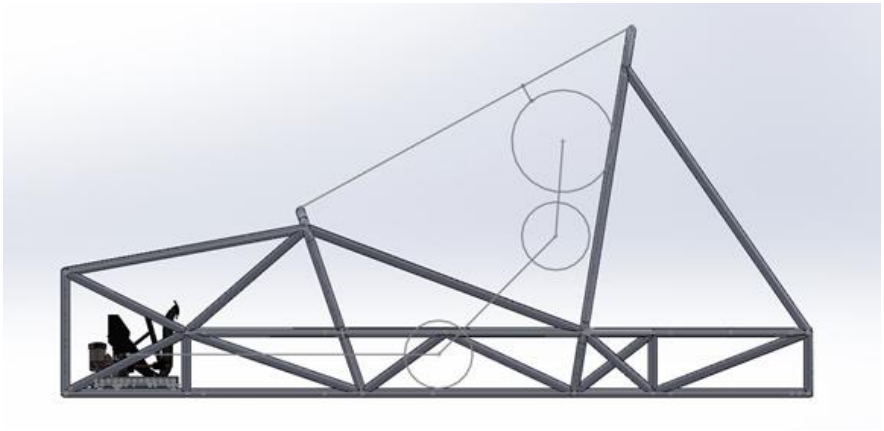

Figure 71: First Pedal Box Iteration

Difficulties arose due the front section of the frame tapering towards the front of the vehicle, this made it difficult to prototype mounting tabs because any tab would have to mount at a specific point on the tapered frame tubes. As seen above, with the Wilwood assembly mounted on the adjustable plate, even in its most forwards position, the template for the 95th percentile male interfered with the entire system.

At this point two options were considered, shorten the Wilwood bracket by 1.25in, which would still allow for the function of the adjustable pedal tray. Or source a reverse mount hanging pedal assembly shown in Figure 72, where the master cylinders mount rearward of the pedal and its associated mounts

Figure 72: Wilwood Hanging Pedal Assembly

The issue with shortening the Wilwood bracket is that it moves the pedal much closer to the master cylinders, which means the master cylinder pushrods must deal with more vertical misalignment as the pedal is in motion. That, and this would also have to be and entirely custom/complicated piece that would require a significant amount of machine time. The hanging pedal option also came with its own set of issues, due to the required pedal length to achieve a 5:1 mechanical advantage (used for braking torque calculations), the whole assembly would have to mount to the top of the frame, putting the master cylinders and reservoirs outside the envelope of the frame, undesirable in a rollover situation and against the rules, the hanging pedal also did not allow for and adjustable pedal tray.

In a team meeting, someone suggested that the master cylinders might be able to mount underneath the floor. The idea was to lay the master cylinders on their side, mount them underneath the floor, behind the brake pedal and design a custom brake pedal and mounting arrangement. The pivot point for the pedal would have to be above the connection point to the master cylinder pushrods so that as the driver pushes on the pedal, the pushrods are compressed into the master cylinders. Although this would eliminate the possibility of an adjustable pedal assembly, it was seen as the best option as the team has considerable experience with using removable seat inserts based on the driver.

The master cylinders would be mounted to a bracket traveling across the length of the frame, another similar bracket would be mounted forward of the rear bracket. The distance between

the two brackets was determined from the uncompressed length of the master cylinders and the Wilwood brake balance bar that we would be using, in the end, 6.125" ended up being the optimal distance between the two. The front bracket was placed in the model first, as close to the front of the frame as possible, then the rear 6.125" behind it, the arrangement is shown below in Figure 73.

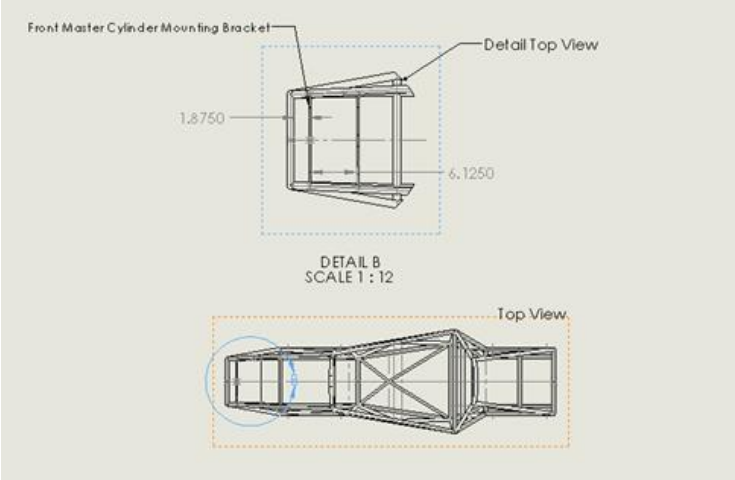

Figure 73: Placement of Master Cylinder Mounting Brackets in Frame

Initially, shaft collars would have been the method of attachment for the mounting brackets, but due to the proximity of the front bracket to a node on the frame, there might be interference between the welds around the node and the shaft collar, so welding was chosen as the preferred method of attachment. This meant that the brackets would need to be made of AISI/SAE 4130 steel, the same material as the frame tubes. To start, .25" was chosen the initial bracket thickness and the bracket height would be fixed at 1.75", the width of the mounting face of the Wilwood master cylinders we will be using. A bolt pattern was created on the rear bracket and the previously created models of the Wilwood GS remote master cylinders were placed in assembly with the pushrods located such that the overall length of the master cylinders was the uncompressed length of 7.99". Next a model of the Wilwood balance bar was inserted into the assembly and mated to both master cylinder pushrods, this ideally should place the balance bar in the general location where it will rest with the brakes bled and without any input from the driver (of course the pushrods thread into clevises on the balance bar so there will be some fore and aft adjustment.

The master cylinders were placed favoring the left side of the frame, as to keep the brake pedal to the left of the centerline of the car, the left master cylinder was placed as close to the frame rail as possible, while still allowing room for the hard brake line and the soft line to the reservoir. The master cylinders were initially placed as close together as possible, but had to be moved to 3.75'' centerline to centerline, the reasoning is explained below.

Using the sketch of the 95th percentile male template in the model of the frame in SolidWorks, we opted to place our pedal face 1 inch forward of the template (1.75" rearward of the vertical centerline extending through the balance bar, which should provide a buffer in case of any manufacturing inaccuracies or differences between the model and physical frame; Due to the style of clevis on the balance bar, the pedal can be further moved forward by threading in the master cylinder pushrods. The pedal face was angled back 10 degrees (80 from horizontal ccw) and based on physical measurements taken of a size 10 human foot, the center of the pedal face should be about 7.5" above the pivot point. In our brake calculation spreadsheet, a 5:1 mechanical advantage for the pedal was assumed when doing all relevant braking force calculations, with the pivot point 1.375in above the centerline of the balance bar, the mechanical advantage ended up being 5.45:1. The pivot point was moved .39 rearward of the vertical centerline traveling through the balance bar, this is an arbitrary number, further refinement could be done to determine an optimal location.

With all the critical points placed, the next step was to sketch a pedal shape, again the shape was arbitrary, the profile was loosely based off a Wilwood pedal, a few profiles were created, the final one, which fulfills all the critical dimensions listed above is shown below in Figure 74.

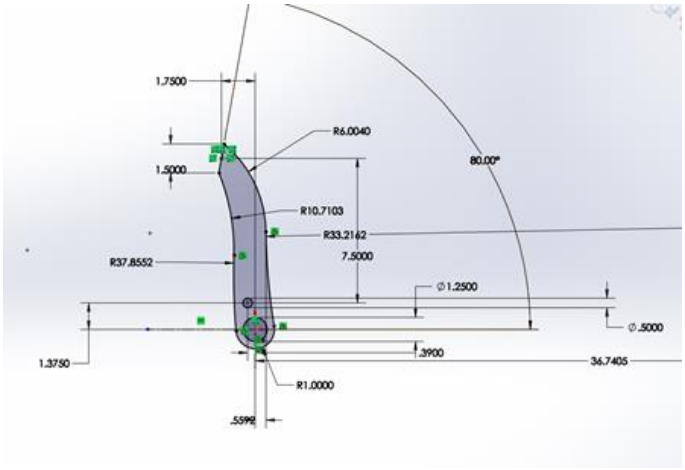

Figure 74: Sketch of Final Pedal Profile

The pedal thickness was chosen to be 1.5", this is the width of the mounting surface for the Willwood balance bar that we will be using and it will be machined out of 6061-T6 aluminum due to its availability, strength and low weight.

The next step was to create the bracket that the pedal mounted to, initially, the only constraints were a 6.125" overall length, a bolt pattern on both ends that was the same as the bolt pattern between the two master cylinders, a hole corresponding with the pivot point on the brake pedal and a slot that the brake balance bar would be able to travel inside. As a starting point, the thickness of the bracket was chosen to be .75", half of the thickness of the pedal. Because the master cylinders were mounted so close together, it was not possible to fit any hardware with a positive locking mechanism, thus the master cylinders were moved to 3.75" from centerline to

centerline to allows the use of 3/8-24 hardware in conjunction with nylock nuts to attach the pedal mount bracket, the mounting face is .25" thick. The initial pedal bracket was 2.25"x1.75"x6.125" with C-channel style cutouts to allow the use of the above hardware, this was placed in the assembly with the steel mounting brackets, master cylinders, balance bar and pedals. In the assembly, the 1.5" slot and profile for the upper part of the bracket, provision for mounting of the pedal at the pivot point, were sketched and later fully defined in the context of the singular part. The O.D. of the balance bar is 1.25", so the 1.5" slot allows for plenty of fore and aft travel of the pedal, though there should be very little with a properly bled hydraulic system.

On either side of the pedal mount bracket are two brackets that provide additional support to the assembly, they share the same mounting geometry as the pedal mount bracket and share the same outer bolt holes the master cylinders. They are also shaped like a piece of C-channel to allow for the use of a positive locking fastener and are .25" all the way around, the final assembly is shown below in Figure 75. As with the pedal, all three supporting brackets will be manufactured from 6061-T6 aluminum because there was stock available on site.

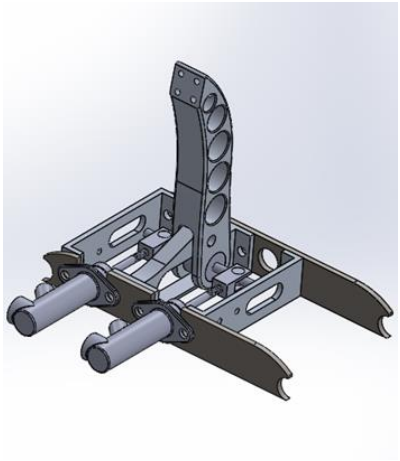

Figure 75: Final Pedal Assembly

Finite Element Analysis

Per the FSAE 2017-2018 rules, section T7.1.8 states, "The brake pedal must be designed to withstand a force of 2000 N without any failure of the brake system or pedal box. This may be tested by pressing the pedal with the maximum force that can be exerted by any official when seated normally." Initially, finite element analysis was going to be conducted on each part, using forces resolved by hand from the 2000N (450lb) pedal force, but as the assembly is statically indeterminate, conducting a simulation of the entire assembly would save time, the selected software was SolidWorks 2017.

Assumption and Modifications to the Assembly

It was assumed that the pedal box would not fail due to the Wildwood components, as they are designed and tested too perform in some of the toughest automotive racing applications, thus these were taken out of the equation. The master cylinders were removed altogether and replaced with two supports that mount in the same location, they extend to the clevises on the balance bar. These two supports were made rigid, so their only job is transfer load from the pedal to the mounts. The balance bar itself was not removed, however it was also made rigid, again to just transfer load. Finally, a simple ½" pin was created and placed in the assembly to mount the pedal to its mounting bracket, the modified assembly is shown below in Figure 76.

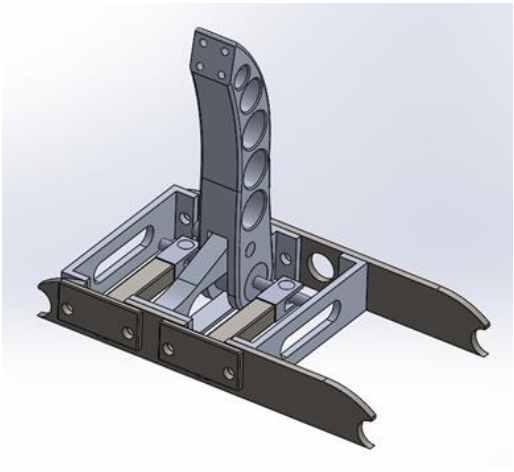

Figure 76: Pedal Assembly Brackets

Fixtures and Loads

The only fixed geometry in the entire assembly are the surfaces where the two steel mounts would be welded to the frame, shown below in Figure 77. The only load on the assembly was a 2000N force applied normal to the pedal face, shown below on the right

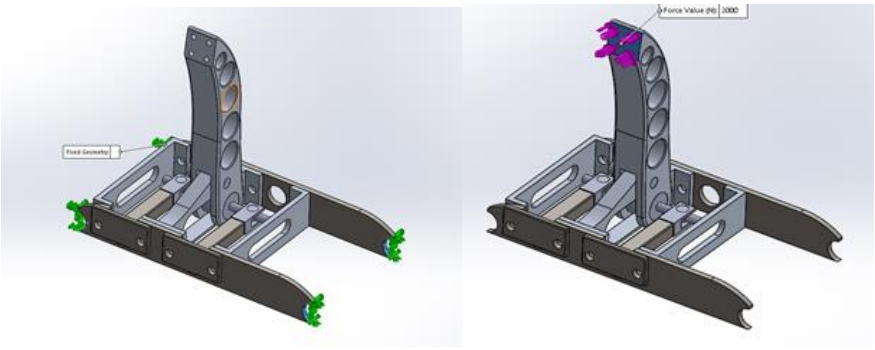

Figure 77: Pedal Assembly Brackets FEA

Connectors and Contact Sets

A simulated bolt was used in all places where an actual bolt would be used, a circular edge must be selected for both the head of the bolt and the nut. The simulate hardware size was 3/8, with a 25 ft*lb preload, the parameters are shown below in Figures 78 and 79

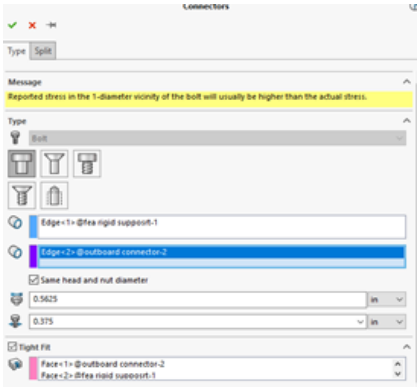

Figure 78: Pedal Assembly Brackets FEA Setup

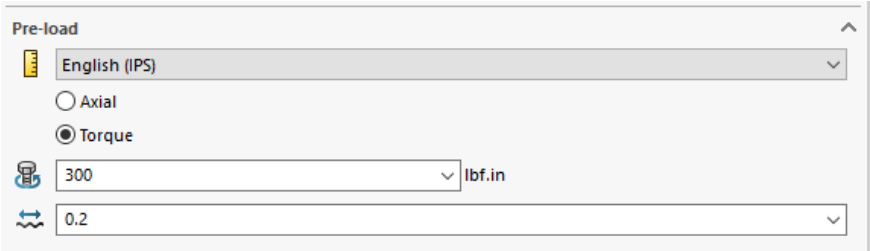

Figure 79: Pedal Assembly Brackets FEA Preload

A no-penetration contact set was used where there was coincident contact between components. This contact set essentially defines a barrier between two surfaces, such that they cannot occupy the same space during the simulation. The other type of contact set is a bonded contact, which is also between two components with coincident contact, this type of contact set permanently bonds the two touching surfaces with a "perfect glue." The only place bonded contact sets were used was between the supports and the clevises on the balance bar, to keep the two components in contact during the simulation. To assign a contact set, either bonded or no-penetration, the two coincident faces on the corresponding components must be selected individually, shown below in Figure 80, which is the contact set between the pedal mounting pin and bracket.

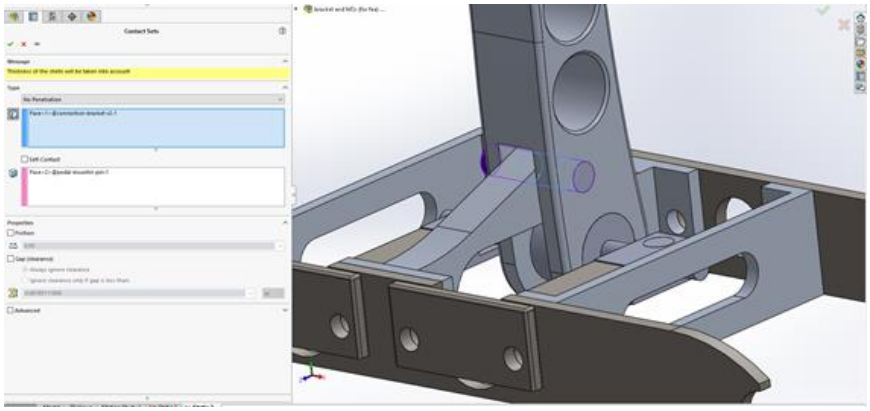

Figure 80: Pedal Assembly Brackets FEA Contact Sets

Because both components contact on faces, it does not matter which is selected first, however it would matter if there was contact between an edge or vertices and a face. It is important to define a contact set between very component that contacts another, without a defined contact set, the simulation will fail because the program will not know how to simulate component behavior relative to one another.

Mesh

To allow SolidWorks to conduct a finite element analysis on the assembly, a mesh must be created. The mesh is essentially a web connecting all nodes of each element in a part/assembly. In the early days of FEA, meshing a part was a huge undertaking, now most CAD programs with simulation packages include an automesh function that will import the part geometry and automatically create the mesh (Norton, 519). For this analysis, this function in SolidWorks was utilized. The user interface for this function is refined to the point where the end user simply must select from a course or fine mesh on a gradient, shown below in Figure 81.

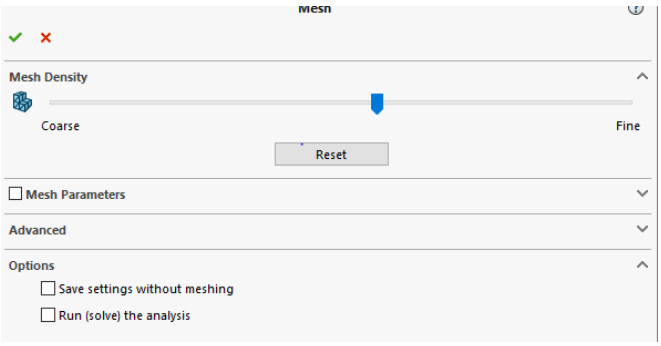

Figure 81: Pedal Assembly Brackets FEA Mesh

A course mesh will yield a faster computation time but may not be able to accurately analyze a high stress gradient, a fine mesh will quickly increase computation time, but will also yield the best results, and the key is to find the balance between the two. For this analysis, the best mesh density corresponds the gradient above. A less dense mesh had trouble around some of the complex curves around the pockets in the pedal and a very fine mesh was causing infinite computing time and multiple software crashes.

Results

After a few failed simulations, due to missing contact sets, the first successful simulation yielded the first design issue. The web shown below, indicated by the red arrow in Figure 82, was far too thin, about .125" and was yielding under load, the solution was to increase the radius of the sketch curve that joins the two extrusions that create the part. The radius was extended all the way to the rear edge of the part, resulting in a minimum web thickness of .37" increasing the factor of safety to 4 in that region.

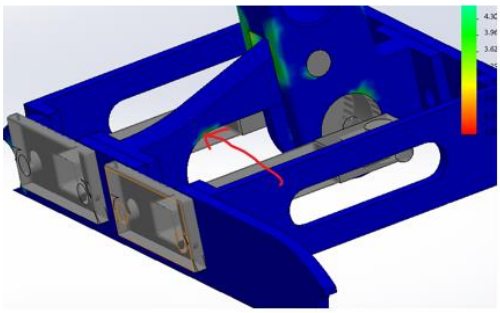

Figure 82: Pedal Assembly Brackets FEA Results 1

As expected, the highest stress in the assembly was in the steel mounting brackets, around the bolt holes where the master cylinders' mount, as they transfer all the load from the pedal to the surrounding bracketry.

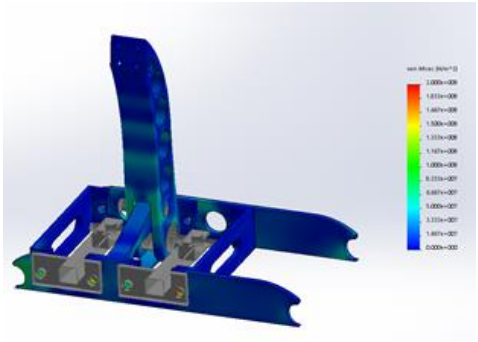

Figure 83: Pedal Assembly Brackets FEA Results 2

Figure 83 above shows the fringe plot of the von Mises effective stress, the maximum stress in the part was 2e+8 Pa, which in AISI/SAE 4130 steel, yields a lowest factor of safety of ~1.9, as shown below in Figure 84.

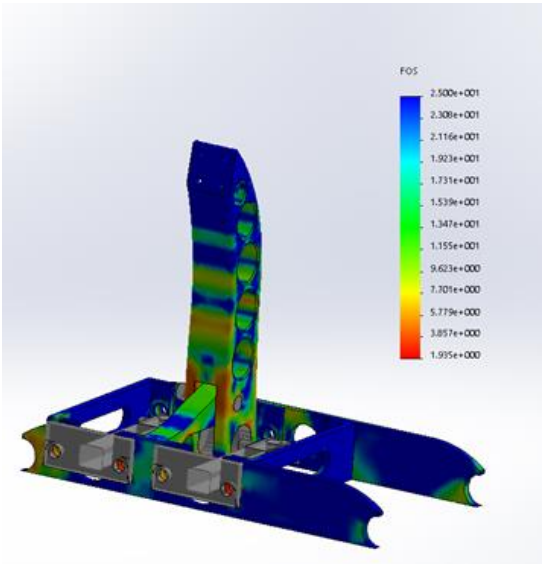

Figure 84: Pedal Assembly Brackets FEA Factor of Safety

As the minimum factor of safety in the steel brackets was ~2, and their height and width were defined by the master cylinders and frame respectively, no further changes were made. A

simulation was run where the thickness of the outer support brackets was reduced to .125", however this resulted in safety factors lower than 1.5 around their mounting holes, so to err on the side of caution, the thickness was kept at .25". At this point a considerable amount of time had been dedicated to the design an analysis of the assembly, and with plenty more to do to achieve performing vehicle in 28 weeks, the design was locked and moved to the manufacturing stage.

Post-Manufacturing Design Modifications

After the pedal was manufactured, it was decided that the weight needed to be reduced to be competitive with the weight of pedal assemblies in previous years. Initially, the pedal had 3 pockets on either side that were 1" in diameter and only .5" deep. Due to the way the pedal was machined, there was only one way to fixture the finished product in the vise, meaning all operations must be done on one side of the pedal. The solution ended up being an increase in the diameter of the 3 existing pockets, to 1.25", the addition of two smaller pockets towards the top of the pedal and making it such that all pockets cut through the entire pedal, this would reduce the weight from 2lbs to just a little bit over 1lb.

Because so much material was removed from the pedal, there was concern that the factor of safety would no longer be above 1. A new simulation was done to confirm or deny this theory. This time around the only component in the assembly was the pedal, it was fixtured using fixed geometry in the mounting holes, on the sides that would be forced against the mounting hardware during the loading situation, the fixturing is shown below in Figure 85

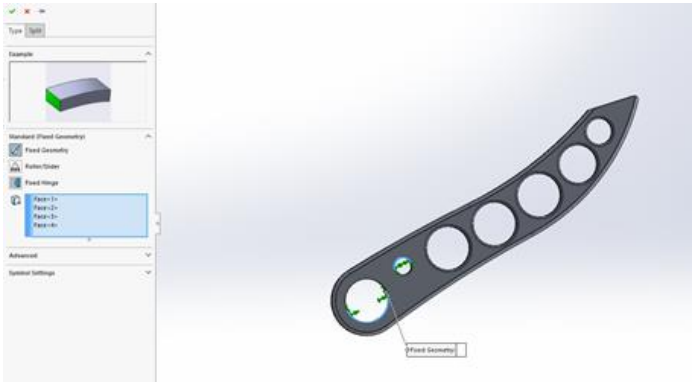

Figure 85: Pedal FEA Setup

With the same load as the previous simulation applied to the face of the pedal, the minimum factor of safety was ~2.8 as shown below in Figure 86. The ideal way to reduce the weight of the pedal would have been to pocket out both sides to form an I-beam shape, but this would've required the manufacturing of another set of jaws for the vise to hold the pedal. It was determined that the further weight savings would not be worth the added machine time, so the design was finalized and the pedal went in for its final machining operation.

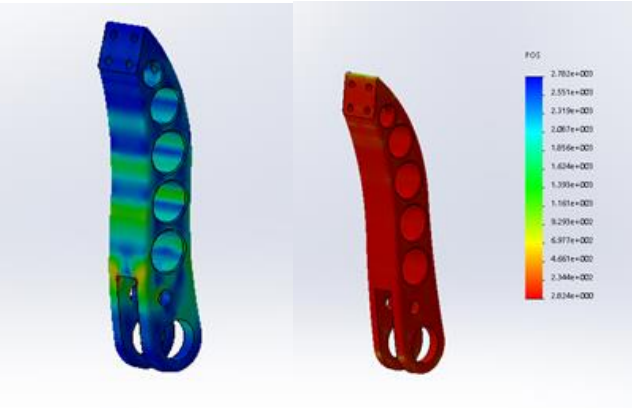

Figure 86: Pedal FEA Results

After the pedal mount bracket was manufactured, and pedal was test fit, there was a noticeable amount of binding during pedal motion due to the aluminum to aluminum contact. To alleviate this binding, .005" was taken of the face of the pedal mounting bracket, indicated by the red arrow shown below in Figure 87, and the corresponding face on the opposite side. Also, a .0625" deep slot with a 1" OD, indicated by the blue arrow, was milled around the mounting point for the pedal on both sides of the bracket, to allow for the installation of bronze thrust bearings, which should also help to minimize any binding between the pedal and mounting bracket as the pedal is in motion.

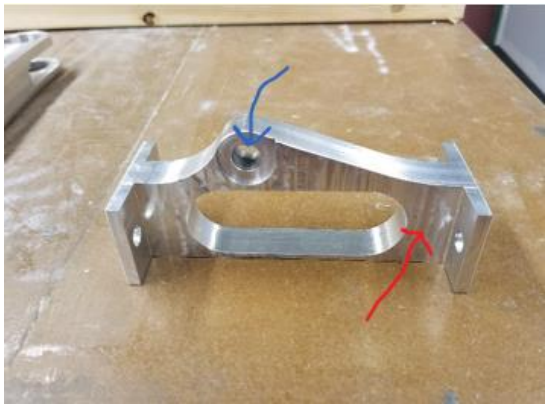

Figure 87: Pedal Bracket

Optimization Recommendations

In theory, when conducting finite element analysis, the mesh size and type should be changed over the course of multiple simulations until the stress gradient converges to one maximum

stress value, or at least a very small range (Norton, 520). Due to time constraints, the mesh for this assembly was for the most part kept constant during every simulation, with more time, the mesh could be fine-tuned for each individual part in the assembly, allowing the size/shape and thickness of each individual part to be optimized to further reduce the weight of the entire assembly. Of course, in the future, if a new frame is manufactured that is but 1.5" longer than the existing frame, the need for this custom brake pedal assembly could be eliminated and the team could revert to using the pre-packaged Wilwood assembly, which could free up time for the re-design/optimization of much more critical systems in the vehicle.

Throttle Pedal Mounting and Placement

The mounting of the throttle pedal is far less critical than the mounting of the brake pedal as the driver will not be frantically applying force to the throttle pedal in the event of a panicked driving situation. The pedal that will be used for competition is an OEM BMW part, part number (insert part number here) and is pictured below in Figure 88.

Figure 88: BMW Brake Pedal

Based on the design of the brake pedal assembly, the easiest way to mount the throttle pedal is a bracket extending from the rightmost aluminum support bracket to the bottom right frame tube in the front section of the frame, the initial design is shown below in Figure 89. The bracket would be bolted to the aluminum support with small hardware and attach to the frame with shaft collars using 6-32 machine screws.

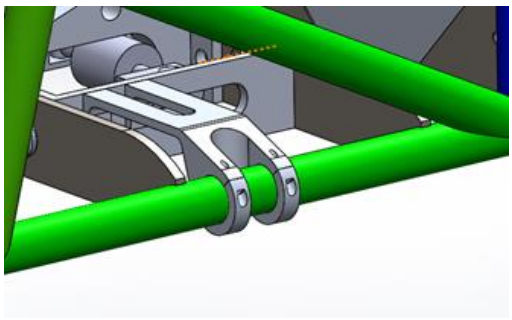

Figure 89: Brake Assembly Bracket

The pedal has an overall length of about 8.5" and having the back of the pedal rest up against the impact attenuator anti intrusion plate put the pedal face in the optimal position with respect to the brake pedal face and the "foot" of the 95th percentile male template. However, Section T3.22 of the 2017-2018 FSAE rules states that "all non-crushable objects (eg. batteries, master cylinders, hydraulic reservoirs) inside the primary structure must have 25mm (1") of clearance to the rear face of the impact attenuator anti-intrusion plate." Based on the above definition, the team assumed that the throttle pedal was a crushable object and the bracket was sent off to be manufactured, however, a later rules clarification revealed that the throttle pedal is in fact a non-crushable object, thus it would have to be moved 1" rearward in the car, luckily the mounting holes have not been drilled in the aluminum support bracket, so this task will be easily achieved. Another rules clarification submitted on FSAE online verified that if the throttle pedal is the rear most pedal, the "foot" of the 95th percentile male template is placed on the pedal face where the actual driver's foot would make contact, meaning that the pedal would still fit in the allotted space.

The manufacturing of the throttle pedal mounting bracket and associated shaft collars was outsourced to one of our team sponsors, Forgione Engineering, located in Lowell, Massachusetts. They can 3D print using a carbon fiber filament, as the bracket is a small component, it would make a good first test piece to gauge the print quality and strength of this type of rapid prototyping. As the material properties of a 3D printed part are hard to quantify, the bracket will be physically tested once the throttle pedal is mounted in the chassis, in the event of a failure, a machined aluminum bracket will take its place for competition use.

Ergonomics

Firewall and headrest

The two main components for the ergonomics of the car are the firewall and the headrest. The seat and the body panels are the other major components but those will be manufactured during C term. According to the FSAE competition rules, the firewall must act as a divider between the driver and the fuel tank system. The driver should not be in contact with the fuel, oil, cooling system, or any electrical hardware with high voltage. Four inches above the bottom of the tallest

drivers helmet must also not be in direct line of the fuel, oil, or cooling systems. There also may be no holes allowed for the seatbelt to pass through.

The firewall is made of 20 gage 6061 aluminum sheet metal. The design started with the floor pan flat on the bottom of the frame. Then it was bent upwards 45 deg, as shown in Figure XX, in order to make room for the fuel tank. The fuel tank will extend the length of the firewall tucked underneath in the triangular prism. Once the firewall reaches the back of the frame it will be bent up 36 deg more to be flush with the frame. Lastly, the top of the firewall will be bent to sit over the middle bar in the back of the frame. Two holes are cut out and folded out to create space for the seatbelt tabs. A hole is then made in each of those firewall tabs, so it can be bolted to the tabs that are welded to the frame. Four tabs are welded to the frame, which correspond with the same hole locations as the holes cut in the firewall. This allows the firewall to be rigidly mounted to the frame. Six cutouts along the sides of the firewall, shown below in Figure 90.

Commented [40]: fix

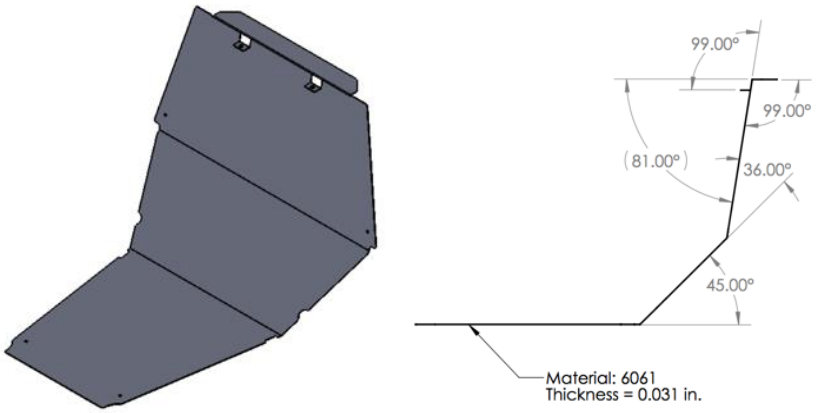

Figure 90: Firewall Sheet Metal

The headrest is the second major component in the ergonomic subsystem. The headrest serves the purpose of constraining the driver's head and not allowing it to move backwards. The same material as the firewall, 20 gage 6061 aluminum, was used for the headrest as well. The headrest had three bends, shown in the figure below, to make it flush with the frame. The top flap in the firewall will bend over the bottom of the headrest. This will help mount the headrest to the frame.

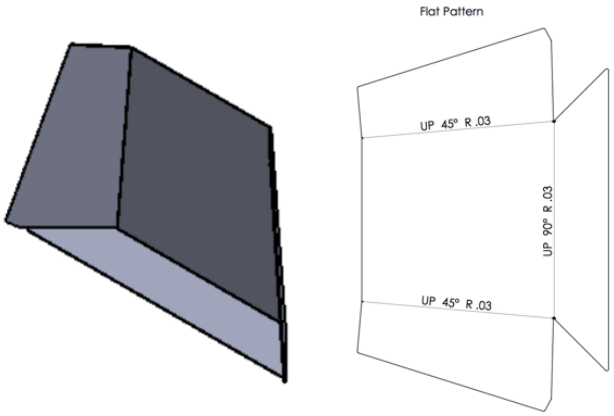

Figure 91: Headrest Sheet Metal

As stated earlier the seat and body panels will be manufactured C term. Fiberglass was laid over a leather seat in order to create a mold. Due to the leather in the seat, the mold had many wrinkles and was not smooth. The decision was to then use bondo to fill in the wrinkles and gaps to smooth the mold. Once the mold is smooth and hardened, carbon fiber will be laid over the mold to create a carbon fiber seat. This will then be used as the car's seat. Expanding foam will then be used behind the seat in order to properly mount it in the car. Wooden molds bought from a previous MQP team are being used to make the body panels for this year. These molds need to be sanded and epoxied multiple times for a smooth surface finish. Carbon fiber will also be laid over these molds and used for the body panels. The product panels of the mold will then be bent over the frame for the proper shape. This will be accomplished during C term.

Shifting

Design Considerations

In previous years, the WPI Formula SAE vehicle has utilized a variety of engine/transmission combinations for competition. Four years ago, an odd fire two-cylinder engine from a Yamaha snowmobile was mated to a continuously variable transmission, which requires no outside input from the driver to work. Two years ago, a 450cc single cylinder engine sourced from a YFZ 450f ATV was the used, integrated into the YFZ 450f engine case is a sequential 1-down-4-up 5 speed manual transmission that uses a wet clutch. The manual transmission requires input from the driver, however a pneumatic shifting system was designed for this vehicle. It uses three pneumatic actuator, one for upshifts, one for downshifts, and one for clutch disengagement when shifting between gears. The pneumatic cylinders were all fed from one supply tank kept pressurized

by a small compressor. The whole system was controlled separate from the engine control unit, using a custom-built PCB and a series of microcontrollers. The shifts were initiated by the driver using two momentary buttons mounted on the steering wheel. This system was heavy and took up a lot of space behind the firewall and in the engine bay. The goal for this year's vehicle is to drastically reduce the weight of the whole system as well as the amount of space the subsystem occupies. As stated previously, the competition engine will be a four stroke, 449cc single cylinder sourced from a 2015 Yamaha WR450F dirt bike. Like the YFZ450f of the previous years, this engine has an integral 5 speed sequential gearbox that also utilizes a wet clutch.

A significant portion of new teams, or teams with short build cycles often settle for manually shifting, it puts all the control in the hands of the driver, and although significantly slower than a pneumatic or electro-mechanical system, has very few failure points. Although there was one advocate for this option, the team opted for the design of a new electro-mechanical system, knowing that the pneumatic system could be pillaged from the older vehicle, due to engine similarities, in the event of a complete design failure. Shifting will still be initiated by the driver via buttons on a steering wheel, however instead of controlling a pneumatic system, the buttons will activate an electric motor that will initiate upshifts and downshifts. The most critical component of this system is the electric motor, it must produce enough torque to initiate a shift, and it ideally should have controllable position due to the way the gearbox is shifted.

A 1-down-4-up transmission in a dirt bike application is shifted via the riders left foot using a lever attached to a splined input shaft on the transmission, circled below in Figure 92.

Figure 92: Transmission Lever

The lever position does not correspond to the gear that the transmission is in, instead the shifter has a "home" that it returns to every time a gear is selected. When the transmission starts in neutral, the lever is depressed downward to engage first gear, when the force no longer being applied to the lever, it springs back up into its "home" position. To engage second gear, the lever is pulled upward, and when the force is removed, it springs back down to the same home position. All subsequent upshifts work the same as the 1-2 shift and neutral is a half shift between 1 and 2. The

angular displacement of the splined input on the transmission is a finite value between each full gear shift, hence the importance of positional control of the electric motor. From experimentation with the engine on the engine stand, it was determined that the required angular displacement of the splined input for either an upshift or downshift was ~17 degrees and the torque required to initiate a shift without the engine running was ~8 lb-ft.

The desire for positional control led to the search for a servo motor, as their angular position can be controlled rather precisely, and a large angular displacement is not required for this application. The search for the motor was headed by a member of the ECE side of the MQP as they had considerably more experience working with electric motors. In the end, a servo could not be found at a reasonable price with the required torque output, however, he was able to source regular 12VDC motor that produces double the required torque (16.6 lb-ft) at a free speed of 75 rpm, weighed only 2 lbs and came with a hall effect encoder for position control. The motor was soured from AndyMark.com, a popular supplier for FRC and FTC teams, and is sold as the PG71 Gearmotor, 10mm round output with a 775 Motor (part number: am-2971). It was assumed the hall effect encoder would work for all angular displacements, but upon reading the fine print, discovered that it only output seven pulse per revolution, or one pulse every ~51 degrees, which does not work for this application as the total angular displacement of the motor would be 34 degrees. At this point, the options were to continue looking for a motor, or purchase the PG71 and implement a mechanical stop to prevent the motor from holding a torque on the splined input, which if done continually, will damage the shift forks in the transmission. Because our design timeline is rather compressed, and we wanted to be testing the system by the end of B-term, we opted to purchase this motor, we also purchased a 10mm key hub (am-095a) and machine key (am-1249) for attaching components to the motor. The CAD files and technical drawings for all three components were available for download directly from the website, which expedited the next step of the process.

The question then became, mount the motor first and design a shifting mechanism around the placement of the motor? Or design a mechanism and hope that the motor could be mounted in such a way to maintain the functionality of the mechanism? The first option seemed like the wisest given the timeframe. Although the rear engine mounts had already been designed, they had not yet been manufactured so instead of making a separate mount for the electric motor, both mounts will be incorporated in one two-dimensional piece. It would have been possible to tuck the electric motor up under the engine, but this would drastically limit the space to package a shifting mechanism, also there was a concern that the electric motor would become heat-soaked, affecting its operability. The radius between the centerline of the motor output and the centerline of the splined input on the transmission was chosen to be 4.5", as this placed the motor away from engine, with enough space to design either a linkage or an interlocking fork for torque transfer.

Figure 93: Key Hub

Figure 93 above shows the electric motor and key hub mounted in their final positions, the mounts were simply sketched on the previously design engine mounts, extruded and the two bodies merged. The driver side mount contains a 4-bolt pattern to fasten the motor with M3 screws, the passenger side mount incorporates a cradle to minimize vibration as the engine when the engine is running.

Initial Mechanism Designs

The first mechanism that was designed to transfer motion from the electric motor to the transmission input was a pair of interlocking forks, the very basic concept is shown below in Figure 94, where the left fork attached to the transmission input and the right fork attached to the electric motor.

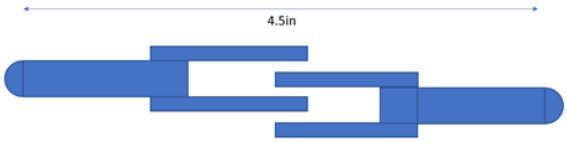

Figure 94: Interlocking Forks

Essentially, as the electric motor rotates, either clockwise or counterclockwise, the right fork will contact the left fork, causing it to rotate in the opposite direction, initiating a shift. This

mechanism is very rudimentary, imprecise and would cause a momentary delay before a shift, as the forks are not always in contact. This idea was quickly scrapped in favor of something slightly more refined.

Figure 95: Key Hub Concept 2

Figure 95 above shows the next iteration of the design, the concept is the same as the interlocking forks, however, the fork on the electric motor side is replace with an actuating arm that would be bolted to the key hub and the fork in the transmission side is designed so the actuating arm is always in contact with the internal profile of the fork, like a cam and follower, which would eliminate any delay between electric motor movement and shift initiation. As stated above, the motor selected was a regular 12VDC unit so some kind of mechanical stop is required, this is accomplished by the contact between a flat face in the internal profile of the fork and a flat face on the actuating arm, the stopped position is shown in the figure on the previous page.

This design was also scrapped relatively quickly, before and analysis was done, due to the lack of adjustability. As the mechanism is pictured above, it is designed for 17 degrees of angular displacement, clockwise or counterclockwise, at the transmission input. If for some reason this parameter needed to change, all new parts would have to be designed, manufactured and installed, putting a stop to all dynamic testing of the vehicle as it would be undriveable.

6 Bar Linkage

At the start of the design phase for the shifting subsystem, the plan was to use a 4-bar linkage in conjunction with a servo motor, after deciding on the use of a regular 12VDC motor and exploring other methods of motion transfer, the final design ends up being a 6 bar linkage, shown below in Figure 96.

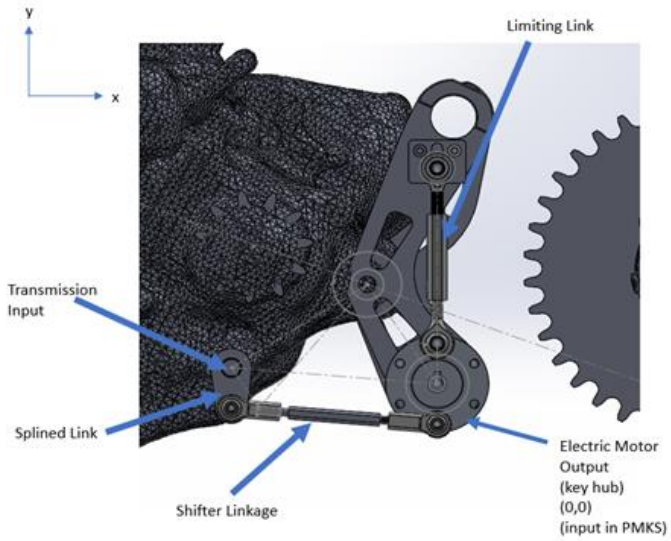

Figure 96: Key Hub 6 Bar

A simple 4-bar linkage consists of an input link, a coupler, a follower and the ground link, depending on the task at hand, either the coupler or the follower can be the output link. In the mechanism depicted above, the key hub, driven by the electric motor is the input, the shifting link is the coupler and the splined link on the transmission input shaft is the follower as well as the output link. As there is no control over the exact position of the motor, another link, the limiting link needed to be added to the mechanism, this link rides in a slotted boss attached to the motor mount and is mounted opposite the shifter linkage on the key hub. When the shifter is in its "home" position as described in the previous section, this limiting link is vertical, as the key hub rotates, either clockwise or counterclockwise, the link travels downward in the slot, once it bottoms out, planar motion stops and a shift is completed. Ideally, we will be able to time everything such that as soon as the limiting link bottoms out, power to the motor is cut and the splined input shaft on the transmission will back-drive the linkage to its home position in time for the next shift.

Both the shifter link and the limiting link are constructed from rod ends and turnbuckle style connects sourced from McMaster-Carr, the parts are listed below in Table 5, and pictured in Figure 97. The shifter link uses the 10-32 hardware and the limiting link uses the ¼-28 hardware, as this was the only size available for the required turnbuckle

Table 5: McMaster Hardware

Item	Part number (Mcmaster-Carr)

Lightweight Corrosion-Resistant Ball Joint Rod End (RH Thread) (10-32)	60685k311
Lightweight Corrosion-Resistant Ball Joint Rod End (LH Thread) (10-32)	60685k312
Lightweight Corrosion-Resistant Ball Joint Rod End (LH) (¼-28)	60685k722
Lightweight Corrosion-Resistant Ball Joint Rod End (RH) (¼-28)	60685k721
Turnbuckle Style Connecting Rod (10-32)	8420k11
Turnbuckle Style Connecting Rod (1/4-28)	8419k11

Figure 97: Connecting Rods

The turnbuckle connecting rods will allow the length of each link to be adjusted, which is especially important for the limiting link, as adjusting the length of this link will set the mechanical stopping point of the mechanism.

Kinematic Analysis

As the electric motor chosen produces double the required torque to initiate a shift, no mechanical advantage is required of the linkage; because no mechanical advantage is required, the input link and follower link are designed to have the same length between their joints, which is the radius of the bolt circle on the key hub, .9375". In theory, because these two links have the same length, that angular displacement of the input should correspond directly to the angular displacement of the follower, to verify this, a kinematic analysis was done using PMKS (planar kinematic simulator).

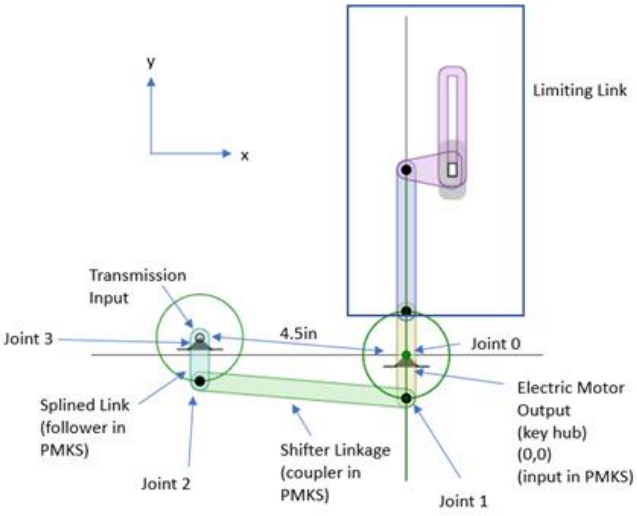

Figure 98: Planar Mechanism

Table 6: Planar Mechanism

PMKS: Planar Mechanism Kinematic Simulator — introduction + instructions

Open File | Save Configuration | Export Kinematic Data | Get as URL | Edit Commands

Target Shape = Enter Target Shape Stream Here.

Input	Links	Type of Joint	X Pos.	Y Pos.	Angle	P	V	A
◉	ground,input	R	0.000	0.000	0.000			
○	input,coupler	R	0.000	-0.938	0.000	☑	☐	☐
○	coupler,follower	R	-4.480	-0.568	0.000	☑	☐	☐
○	follower,ground	R	-4.480	0.370	0.000			
○	input,slider	R	0.000	0.938	0.000	☑	☐	☐
○	slider,stop	R	0.000	4.000	0.000	☑	☐	☐
○	stop,ground	P	1.000	4.000	90.000			

Remove Row | Clear All Rows | DOF = 1

Shown above in Figure 98 and Table 6 are the planar mechanism model and starting coordinates respectively, which were taken directly from measurements in the SolidWorks model. When using this simulator, the following assumptions are made; all revolute and prismatic joints are frictionless and the links are weightless, thus gravity has no effect on the linkage.

Commented [41]: update

For the simulation, the input rpm was set to 75, the free speed of the motor we would be using. Ideally, the slider length would have been limited to represent the motion the actual linkage will be restricted to, however this is not available in PMKS, thus the whole system can rotate 360 degrees. However, since the linkage in the vehicle will be limited to a 34-degree total swing, only data from time steps -.0444s to .0444s were analyzed, as these time steps correspond to a 20-degree swing in either direction from the initial position. A sample of the data collected for joints 0 and 1 is shown below in Table 7.

Table 7: Data for Joints 1 and 2

TimeSteps	x_0	y_0	Vx_0	Vy_0	Ax_0	Ay_0	x_1	y_1	Vx_1	Vy_1	Ax_1	Ay_1
-0.044444444	0	0	0	0	0	0	-0.32081	-0.88143	6.922748	-2.51967	19.78948	54.37114
-0.033333333	0	0	0	0	0	0	-0.24277	-0.90604	7.116009	-1.90673	14.97541	55.88901
-0.022222222	0	0	0	0	0	0	-0.16288	-0.92375	7.255113	-1.27927	10.04738	56.98152
-0.011111111	0	0	0	0	0	0	-0.08175	-0.93443	7.339001	-0.64208	5.04288	57.64038
0	0	0	0	0	0	0	0	-0.938	7.367035	0	1.03E-07	57.86056
0.011111111	0	0	0	0	0	0	0.081752	-0.93443	7.339001	0.642079	-5.04288	57.64038
0.022222222	0	0	0	0	0	0	0.162882	-0.92375	7.255113	1.279272	-10.0474	56.98152
0.033333333	0	0	0	0	0	0	0.242772	-0.90604	7.116009	1.906729	-14.9754	55.88901
0.044444444	0	0	0	0	0	0	0.320815	-0.88143	6.922748	2.519674	-19.7895	54.37114

The position data for joints one and two were graphed on a single scatter plot and are shown below in Figure 99. This plot shows the path that both joints travel during -.0444s to .0444s and is a visual verification that the linkage is functioning as expected.

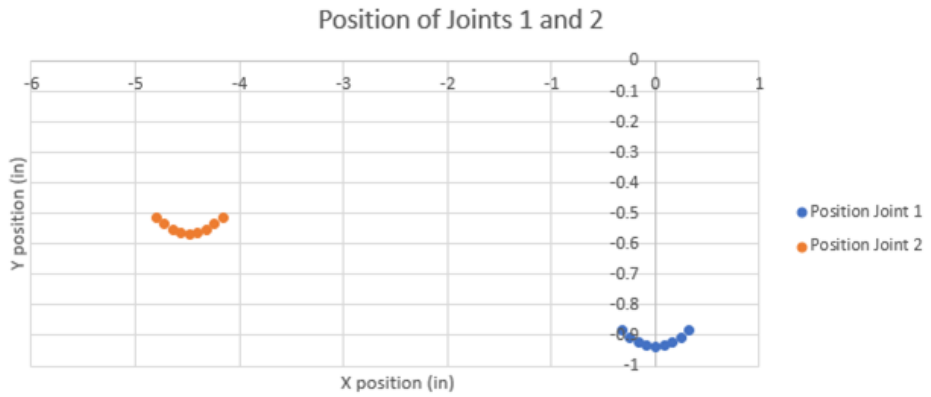

Figure 99: Graph of Position of Joints 1 and 2

Figure 100 below shows the plot of angular displacement v.s time steps for both the input link and the follower link with respect to the origin of the mechanism. The trend lines for each data set show that the rate of change of angular displacement for both the input and follower is the same, meaning that a 17 degree angular displacement at the motor should correspond to a 17 degree angular displacement at the transmission input.

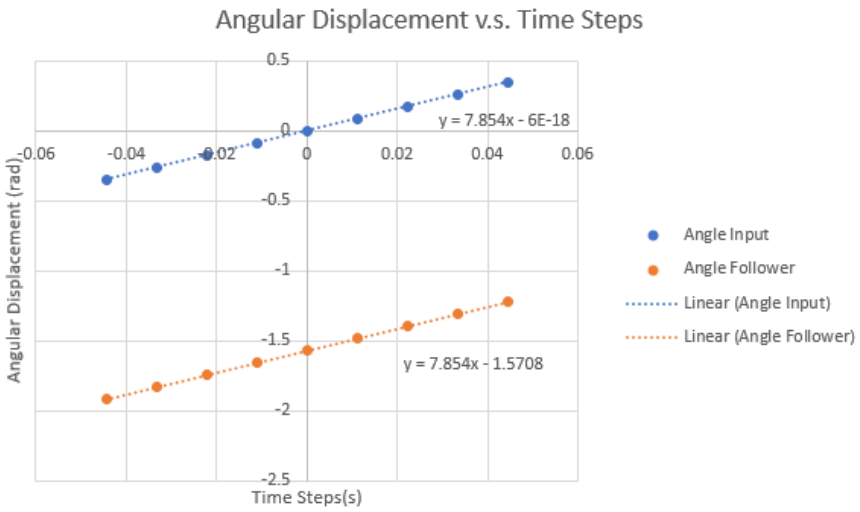

Figure 100: Graph of Angular Displacement

Static and Stress Analysis

Although 16.6 lb-ft does not seem like a considerable amount of torque, the tangential force at the bolt circle of the key hub is about 212.5 lbs, as shown below.

$$F = \frac{16.6\ lb * ft}{\left(\frac{.9375in}{12}\right)} = 212.48\ lbs$$

Commented [42]: table of equations?

According to product specifications available on McMaster-Carr's website, the selected rod ends have a maximum radial load of no less than 1,350 lbs, while these components are nowhere near their failure load, there is not strength data available regarding the turnbuckle style connecting rods, which are manufactured from 6061 aluminum. To verify that they will not be a cause of mechanism failure, the axial stress in each turnbuckle will need to be determined, and compared to the yield strength to determine a safety factor.

Load Determination and Stress Calculations: Shifter Link

The axial load in each link will be determined at the point where the key hub is at full lock in the counterclockwise direction, as this puts each link in tension. The load in each link will be determined independently, assuming that each link will solely counteract the torque produced by the electric motor, although this will not actually be the case as both links will share the load, this represents a worst-case scenario where one link fails.

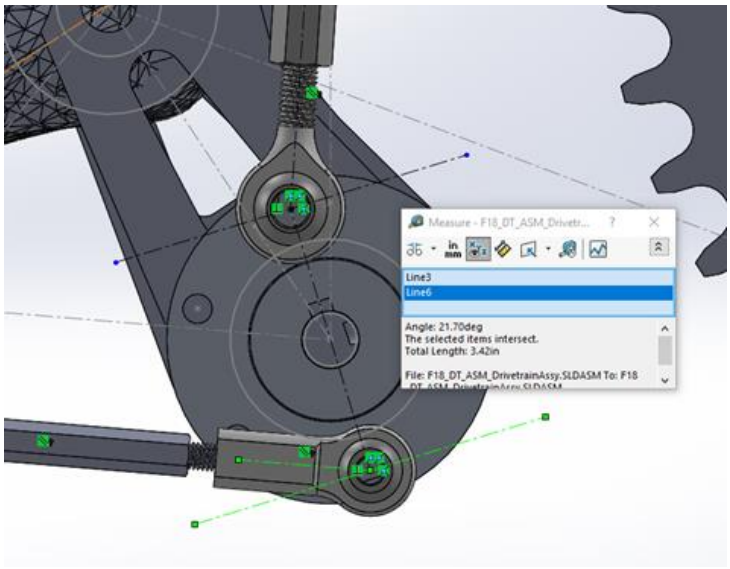

Figure 101: Angle of Shift Linkage

Figure 101 above shows the measured angle between the shift linkage and the tangent line on the bolt circle to be 21.7 degrees. This angle was used in the free body diagram shown below in Figure 102 to determine the axial force in the link. As the link is a two-force member, there is only an axial load, no bending load.

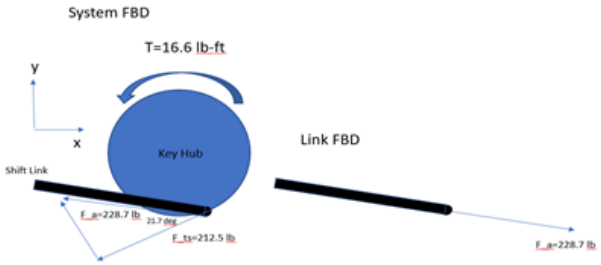

Figure 102: Key Hub Free Body Diagram 1

The axial force in the link, F_a is dependent on the tangential reaction force at the joint, which creates a reaction moment to counteract the torque produced by the motor.

$$F_a = \frac{212.48lb}{\cos(21.7)} = 228.7\ lbs$$

Commented [43]: equation

The turnbuckle for the shift link is externally threaded, assuming the component will not fail from the threads stripping out, it can be modeled as a simple stepped shaft in axial loading that will fail at the cross section where the step occurs. The diameter of the smaller section is the minor diameter of a 10-32 connector, .1508in and the diameter of the larger section is .25in. The nominal axial stress in the smaller cross section is defined as.

$$\sigma_{nom} = \frac{F_a}{\pi * \left(\frac{.1508}{2}\right)^2} = 12{,}805psi$$

Commented [44]: equation

The step up in diameter between the two sections creates a step concentration, which can be determined using the chart shown below in Figure 102, assuming r/d = .1, as there is no measurable radius in the solid model of the part.

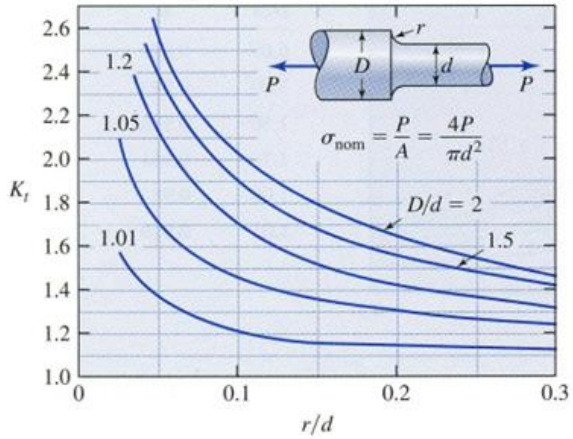

Approximate formula
$K_t \approx B\left(\frac{r}{d}\right)^a$, where:

D/d	B	a
2.00	1.015	−0.300
1.50	1.000	−0.282
1.20	0.963	−0.255
1.05	1.005	−0.171
1.01	0.984	−0.105

Figure 103: Axial Stress

$$\frac{r}{d} = .1$$

$$\frac{D}{d} = \frac{.25}{.1508} = 1.658$$

$$Thus, K_t = \sim 1.9\ and\ \sigma_{axial} = 1.9 * 12805psi = 24330psi$$

As this axial stress is the only stress present in the link, it is also the von Mises effective stress, which, along with the yield strength of 6061 aluminum (39000 psi), can be used to determine a safety factor for the link.

$$N = \frac{39000psi}{24330psi} = 1.6$$

Load Determination and Stress Calculations: Limiting Link

A process like that shown above was also used to determine the axial load present in the limiting link. The angle between the link itself and the tangent line on the bolt circle was measured to be 69.17 degrees, using this value and the free body diagrams shown below in f**igure xx**, the tensile load in the link was found to be 597.6 lbs.

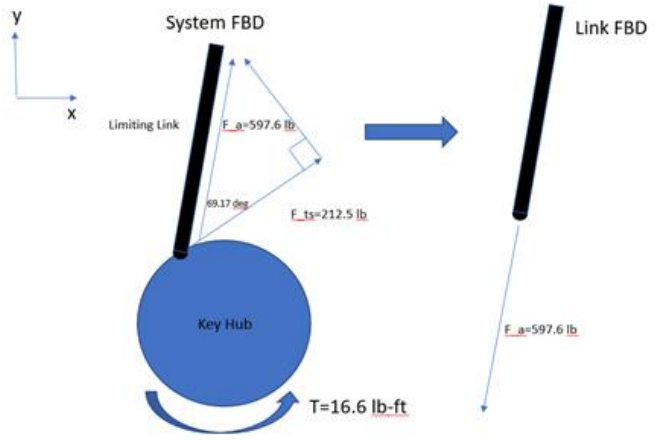

Figure 104: Key Hub Free Body Diagram 2

This turnbuckle is internally threaded and again, assuming it will not fail due to thread pullout, it can be modeled as a hollow rod, with and OD of .376 in and an ID of .25in.

$$\sigma_{nom} = \frac{597.6\ lbs}{\pi * (.188in^2 - .125in^2)} = 9647psi$$

As this turnbuckle is being modeled as a simple rod, there are no geometric features to create stress concentrations, thus sigma nominal is equal to the von Mises effective stress and

$$N = \frac{39000psi}{9647psi} = 4$$

Engine Mount Modification

The final step in validating this subsystem was to re-run the FEA previously done on the engine mounts to verify that the added loads on the rear mounts due to shifting will not cause failure of either mount. We do not expect that the loads from the shifting motor will have any effect on the factor of safety, however it necessary to validate this assumption.

The entire simulation was had already been set up and is explained in a previous section of this report, the only modifications were; the replacement of the rear engine mounts with the newly designed ones that had the provisions for the shifting motor mount, the addition of a 16.6 lb-ft load on the driver side rear engine mount and a vertical load of 2lbs, representing the weight of the electric motor, also applied to the driver side rear motor mount. To get the simulation to run properly, new contact sets needed to be built for the newly added rear engine mounts, the assembly with all applied loads, prior to simulation is shown below in Figure 105.

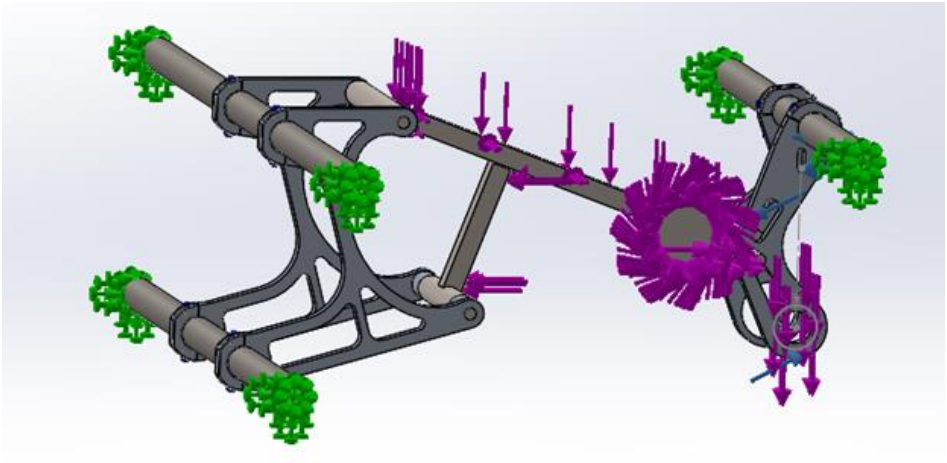

Figure 105: Motor Mounts FEA Setup

As expected, the loads due to the electric motor were so small in comparison to loads produced by the engine/drivetrain that they had little to no effect on the overall FOS for the system. This proven in Figure 106 below, which shows the FOS fringe plot after the simulation was run. Up where the engine mounts meet the frame, the FOS is between 3 and 4, which was expected based on previous simulations, meanwhile, the factor of safety down by the shifting motor is at or above 200.

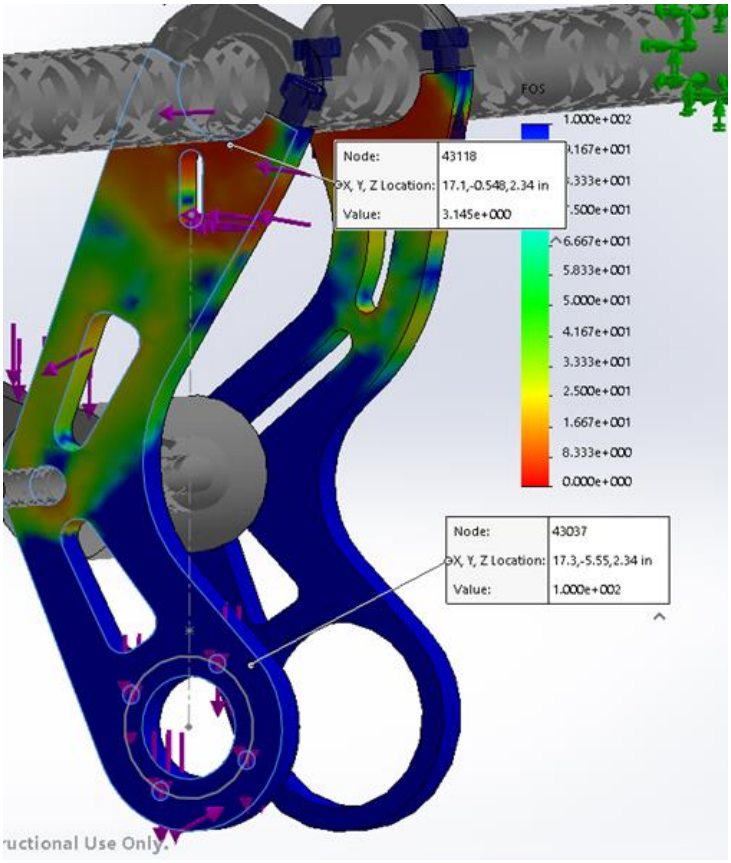

Figure 106: Motor Mounts FEA FOS

Findings

These are preliminary results and will be updated accordingly throughout the rest of the year. Though the intake prototype has not yet been tested, all 3D printed parts have been made thanks to Professor Planchard, and the lower runner segment has been welded as well. Assembly of the intake components has been simple, and due to the self-locating joints used for most part connections, the only difficulty has been in mounting the intake to the engine due to the lack of frame members to mount it to. For physical testing, the restrictor and plenum top have been glued together into a single piece, and the same has been done for the 1x and 5x plenum bottom sections, each with their own runner bellmouth. This has allowed the intake to be assembled in two large sections, making it easy to interchange the two plenum volumes. The joint between the two halves of the plenum will

be sealed by either duct tape or electrical tape during testing, since glue would eliminate the possibility of testing both plenum volumes. The 3D printed components of the intake have all been coated in a layer of epoxy resin to ensure they are airtight, to add additional strength, and to reduce the likelihood of chemical erosion due to any wayward gasoline spray from the fuel injector. A small piece of fibrous gasket paper of approximately 1/16-inch thickness has also been added between the throttle body and restrictor to reduce air leakage since the 3D printed restrictor face does not fit perfectly to the throttle. The joints closed by silicone couplers and hose clamps have functioned well thus far, with no apparent damage to the 3D printed parts and sturdy connections.

The one major difficulty encountered since assembling the prototype intake occurred during the first attempted engine startup. Since the engine had not been tuned yet, a backfire occurred during one of the first attempts to crank the engine, and rather than pulling the intake apart at the taped joint in the plenum, the restrictor was torn out of the plenum top by the force of the explosion. This did not cause any apparent damage to the restrictor, but has cracked the plenum top around the glued joint between it and the restrictor. These cracks may have compromised the structure of the plenum top, and will require application of additional epoxy resin, and potentially fiberglass, to restore it before testing can continue. Luckily, this appears to be the only damage done to the intake during this accident. The team hopes to complete the required repairs as soon as possible so engine testing and tuning can continue.

In C Term, once the prototype intake has been confirmed to function as designed, the team intends to rebuild the intake in a more structurally sound medium, such as fiberglass or carbon fiber. Of particular interest is the replacement of the restrictor with an aluminum section to ensure its dimensions are exactly as designed, since the exact diameter of this component is crucial to compliance with FSAE rules and to the performance of the engine.

Conclusion and Recommendations

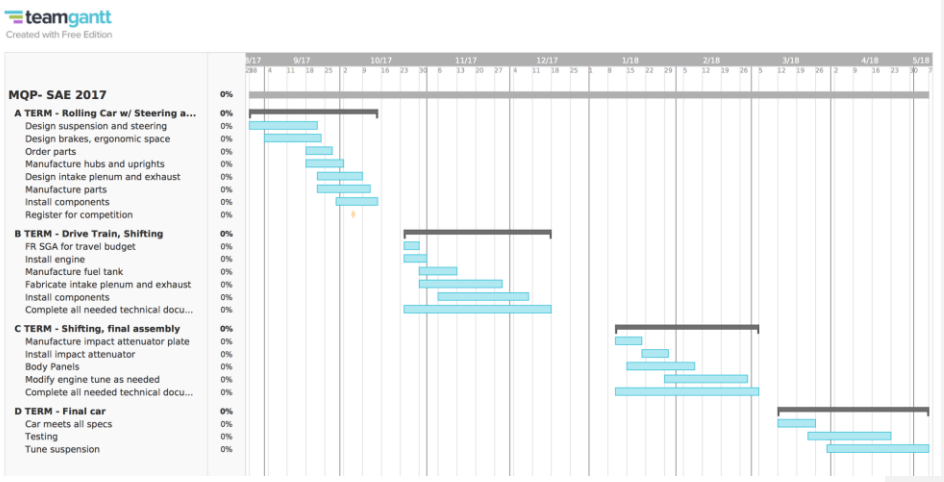

Table 6: Gantt Chart

Shown above, in Table 6, is the Gantt Chart that was used at the beginning of the year. The team's goal for A term was to have a rolling car with steering. This was a very ambitious goal that the team did not believe they would reach but was put in place to make great progress. The goal for B term was to then have a rolling car, with the drivetrain and shifting done. The majority of design work was done during A term. Initial design concepts were ruled out and several designs were finalized. During B term most of the manufacturing was done. The frame was sent to a few welders so the tabs and a-arms could be welded. Due to time constraints and not getting the frame back, the team was unfortunately not able to have a rolling car at the end of B term. However the drivetrain and shifting was finalized and some things that were supposed to be done C term have been started. The team has most of the design work finished and is looking to finish on schedule.

Looking forward in C term the team will validate the designs and make sure they all fit together properly on the car. The rest of the manufacturing will be accomplished and the components will be fitted on the car. Lastly, the car will be tested and optimized.

Appendix

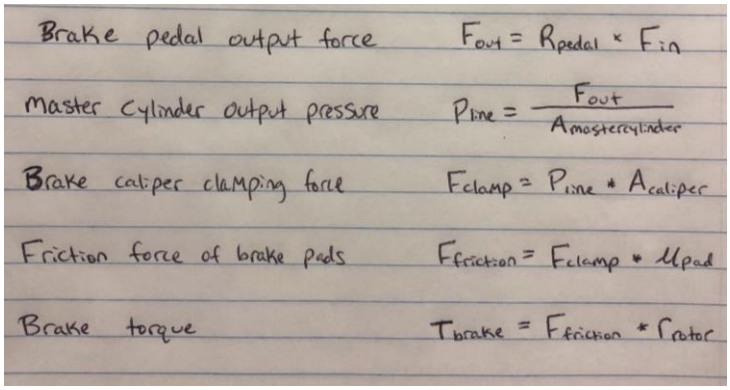

Brake pedal output force	$F_{out} = R_{pedal} \times F_{in}$
master cylinder output pressure	$P_{line} = \frac{F_{out}}{A_{mastercylinder}}$
Brake caliper clamping force	$F_{clamp} = P_{line} * A_{caliper}$
Friction force of brake pads	$F_{friction} = F_{clamp} * \mu_{pad}$
Brake torque	$T_{brake} = F_{friction} * r_{rotor}$

Car with 5/8" front and 13/16" rear master cylinders

Front			Rear	
GS Compact Remote Master Cylinder (5/8 bore)			GS Compact Remote Master Cylinder (13/16 bore)	
DH 4 Dual Hydraulic Caliper			Wilwood SC3 Single Pistons	
Brake Peddle Lever Ratio (lbs)				
pedal force (lbs)	37		pedal force (lbs)	37
Linkage Length (in)	1		Linkage Length (in)	1
Pedal length (in)	5.2		Pedal length (in)	5.2
	192.4			192.4
Master Cylinder Pressure (psi)				
Area Master Cyl (in^2	0.31		Area Master Cyl (in^2	0.52
	620.6451613			370
Line Pressure = at both ends				
Caliper Force (lbs)				
Area Caliper (in^2)	3.54		Area Caliper (in^2)	1.74
	2197.083871			643.8
Clamping Froce (lbs)				
	4394.167742			1287.6
Brake Pad Friction (lbs)				
Friction Coef Pads	0.4		Friction Coef Pads	0.4
	1757.667097			515.04
Rotor Torque (ft*lbs)				
Rotor radius (in)	4		Rotor radius (in)	4
	585.89			171.68

Brake Torque %			Required Torque %	
Front	77.3		Front	81
Rear	22.7	a	Rear	19

Bibliography

1. Ales, M., Mendoza, R., Thomas, M., & Vinokurov, L. (2010). Cal Poly FormulaSAE Engine Development. San Luis Obispo: California Polytechnic State University.
2. Blair, G. P. & Cahoon, M. (2006, September). Best Bell: Design of an Intake Bellmouth. Race Technology Magazine, 34-41.
3. Committee, Formula Sae Rules. "2017-18 Formula SAE® Rules." (n.d.): n. pag. 2 Sept. 2016. Web. 25 Feb. 2017.
4. Fundamentals of Engineering Thermodynamics Moran & Shapiro 5th edition (SI Units)
5. Hamilton, Leonard J., and Jim S. Cowart. "Modeling the Effects of Intake Plenum Volume on the Performance of a Small Naturally Aspirated Restricted Engine." ASME 2010 Internal Combustion Engine Division Fall Technical Conference. American Society of Mechanical Engineers, 2010.
6. Harris, William. "How Car Suspensions Work." HowStuffWorks, HowStuffWorks, 11 May 2005, auto.howstuffworks.com/car-suspension.htm.
7. Kojima, Mike. " The Ultimate Handling Guide Part 8: Understanding Your Caster, King Pin Inclination and Scrub." *MotoIQ,* MotoIQ, 26 Dec, 2011, www.motip.com/MagazineArticles/ID/1982/The-Ultimate-Handling-Guide-Part-8-Understanding-Your-Caster-King-Pin-Inclination-and-Scrub.aspx.
8. Mariucci, V., Selamet, A., & Miazgowicz, K. D. (2007). Effect of Primary Intake Runner Tapers and Bellmouths on the Performance of a Single Cylinder Engine (No. 2007-01-0382). SAE Technical Paper.
9. Miller, Jay K. *Turbo: Real World High-performance Turbocharger Systems*. North Branch, MN: CarTech, 2008. Print.
10. Milliken, Douglas. "Formula SAE Tire Test Consortium ." Milliken Research Associates, Inc, Milliken Research Associates, Inc, 1 Jan. 2001, www.millikenresearch.com/fsaettc.html.
11. Milliken, W.F., Kasprzak, E. M., Milliken, D. L., & Mets, L. D. (1995). *Race car vehicle dynamics*. Warrendale: SAE International
12. Moser, Tyler, et al. "DESIGN AND OPTIMIZATION OF A FSAE VEHICLE." (n.d.): n. page. 28 Apr. 2015. Web. 25 Feb. 2017.
13. Norton, R. L. (2014). *Machine Design an Integrated Approach* (Vol. V). Boston, Mass.: Prentice Hall.
14. Omkar N. Deshpande, and Nitin L. Narappanawar, "Space Advantage Provided by De-Laval Nozzle and Bell Nozzle over Venturi," Lecture Notes in Engineering and Computer Science: Proceedings of The World Congress on Engineering 2015, 1-3 July, 2015, London, U.K., pp1165-1168 http://www.iaeng.org/publication/WCE2015/
15. Sutton Biblarz. Rocket Propulsion Elements 9th ed pg59

Commented [45]: APA best, MLA decent

Commented [46]: citation style?